ALGORITHM DEVELOPMENT IN DENSITY MATRIX RENORMALIZATION GROUP AND CANONICAL TRANSFORMATION THEORY

A Dissertation

Presented to the Faculty of the Graduate School

of Cornell University

in Partial Fulfillment of the Requirements for the Degree of

Doctor of Philosophy

by

Jonathan James Dorando

May 2010

ALGORITHM DEVELOPMENT IN DENSITY MATRIX RENORMALIZATION GROUP AND CANONICAL TRANSFORMATION THEORY

Jonathan James Dorando, Ph.D.

Cornell University 2010

In this thesis, we will describe several extensions of the Density Matrix Renormalization Group (DMRG) and Canonical Transformation Theory (CT).

In the first part we describe a new way to solve for excited states in DMRG. To overcome the limitations of the traditional state-averaging approaches in excited state calculations, where one solves for all states between the ground state and excited state of interest, we have investigated a number of new excited state algorithms. Building on the work of van der Vorst and Sleijpen (SIAM J. Matrix Anal. Appl., **17**, 401 (1996)), we have implemented Harmonic Davidson and State-Averaged Harmonic Davidson algorithms within the context of DMRG. We have assessed their accuracy and stability of convergence in complete active space DMRG calculations on the low-lying excited states in the acenes ranging from naphthalene to pentacene. We find that both algorithms offer increased accuracy over the traditional State-Averaged Davidson approach, and in particular, the State-Averaged Harmonic Davidson algorithm offers an optimal combination of accuracy and stability in convergence.

In the second part, we propose an analytic response theory for DMRG whereby response properties correspond to analytic derivatives of DMRG observables with respect to the applied perturbations. Both static and frequency-dependent response theories are formulated and implemented. We evaluate our pilot implementation by calculating static and frequency-dependent polar-

isabilities of short oligo-di-acetylenes. The analytic response theory is competitive with dynamical DMRG methods and yields significantly improved accuracies when using a small number of density matrix renormalisation group states. Strengths and weaknesses of the analytic approach are discussed.

In the third part, we describe how to calculate density matrices in CT theory. Density matrices are useful not only for computing observables but also for characterizing the nature of individual states. We demonstrate this with a preliminary application of the CT theory to understand the low-lying excited states of oligo-phenylvinylenes.

We finish by presenting the theory and equations for calculating the response (e.g. to an external field) in the CT and DMRG-CT theories.

BIOGRAPHICAL SKETCH

Jonathan Dorando was born in New Brunswick, NJ on January 19, 1983. For the first decade of his life, he grew up in Middlesex, NJ, and later moved to Warren, NJ to finish his education through highschool.

Jon attended college at Carnegie Mellon University in Pittsburgh, Pennsylvania. He completed his B.S. degree with a major in Chemical Physics. For graduate school, Jon came to Cornell to obtain a Ph.D. in Theoretical Chemistry.

This is dedicated to anyone who has read this far into the thesis

ACKNOWLEDGEMENTS

I want to begin by expressing gratitude to everyone I have met here during my past five years here at Cornell.

I want to thank my long-time girlfriend, Christina, for hanging in there with me and giving me support.

Thanks to all my group members, Debashree, Johannes, Haitao, Eric, Jesse, Hitesh, Sandeep, Will, Jun, Takeshi, Claire, and Dominika.

Thanks to all my friends that I have made over the years making Cornell a more enjoyable experience (including Scott, Brenda, Alex, Ben, and many others).

And of course, many thanks to my advisor Garnet Chan.

TABLE OF CONTENTS

LIST OF TABLES

LIST OF FIGURES

CHAPTER 1

INTRODUCTION

We begin with a brief overview of what is in this thesis. Chapter 1 will begin with a brief overview of electronic structure theory and the challenges that are involved. Chapter 2 will provide an introduction to the Density Matrix Renormalization Group (DMRG). Chapter 3 will introduce a new method in DMRG for obtaining excited state energies and consequently excited state properties. Chapter 4 will describe old and new methods to carry out response theory in DMRG. Chapter 5 will present an overview of Canonical Transformation Theory (CT). Chapter 6 will present a method for obtaining the 1- and 2-body reduced density matrices in CT. Chapter 7 will show future directions, which includes developing a response theory in CT.

1.1 Introduction

Quantum chemistry tries to solve the Schrödinger equation. For the purposes of simplicity, we will limit this thesis to the time independent Schrödinger equation. After this simplification, the Schrödinger equation is simply

$$H|\Psi\rangle = E|\Psi\rangle \tag{1.1}$$

where H is the Hamiltonian, E is the energy, and Ψ is the wavefunction. Eqn. 1.1 is deceptively complicated to solve, and this is why there is an entire field of chemistry devoted to solving this equation.

The wavefunction Ψ describes the motion of the electrons, and as such depends on the electron coordinates. The wavefunction also depends on the nuclear motion, but due to the Born-Oppenheimer approximation, which we will describe

later in this section, the wavefunction will not depend explicitly on the nuclear coordinates. The Hamiltonian, H in eqn. 1.1, contains the kinetic and potential energy of a chemical system. The Hamiltonian acting on the wavefunction can be expressed as a function of nuclei and electron positions

$$[-\frac{1}{2}\sum_{i}\nabla_i^2 - \sum_{A}\frac{1}{2M_A}\nabla_A^2 - \sum_{A,i}\frac{Z_A}{r_{Ai}} + \sum_{A>B}\frac{Z_A Z_B}{R_{AB}} + \sum_{i>j}\frac{1}{r_{ij}}]\Psi(\mathbf{r};\mathbf{R}) = H\Psi(\mathbf{r};\mathbf{R}) \tag{1.2}$$

The above equation and subsequent equations are expressed in atomic units, where $\hbar = |e| = \frac{1}{4\pi\epsilon_0} = m_e = 1$. ∇_i^2 and ∇_A^2 are the Laplacian operators with respect to the coordinates of electron i and nuclei A, respectively. M_A is the ratio of the mass of nucleus A to the mass of an electron. Z_A and Z_B are the nuclear charges of the atoms A and B, respectively. r_{ij}, r_{Ai}, and R_{AB} are the distances between electrons i and j, the distances between electron i and nucleus A, and the distances between nuclei A and B, respectively. The first and second term in eqn. 1.2 represent the kinetic energy of the electrons and nuclei, respectively. The third, fourth and fifth terms describe the potential energy of the Coulombic interaction between electron and nucleus, nucleus and nucleus, and electron and electron, respectively. We make a distinction between the nuclear and electron distances with r and R, respectively because we will be utilizing an approximation which is central to quantum chemistry, the Born-Oppenheimer approximation. The Born-Oppenheimer approximation assumes that the electrons of the chemical system are moving with respect to a fixed set of nuclei. Once this approximation is applied we see that eqn. 1.2 appears as

$$[-\frac{1}{2}\sum_{i}\nabla_i^2 - \sum_{A,i}\frac{Z_A}{r_{Ai}} + \sum_{A>B}\frac{Z_A Z_B}{R_{AB}} + \sum_{i>j}\frac{1}{r_{ij}}]\Psi(\mathbf{r}) = E_{el}\Psi(\mathbf{r}) \tag{1.3}$$

In the following sections, we introduce ab-initio quantum chemistry methods, which are used to solve eqn. 1.3.

1.2 Hartree Fock - The Zeroth Order Approximation

Hartree Fock is the basic building block for most ab-initio quantum chemistry methods[1–5]. As this is the case, we will spend this section discussing the theory and short comings of Hartree Fock. Again, to simplify this chapter, we will concentrate on the spin-free version of Hartree Fock, Restricted Hartree Fock (RHF).

Hartree Fock is based a single determinant theory, which means the wavefunction can be described as

$$|HF\rangle = \hat{A}|\phi_1\phi_2\cdots\rangle \tag{1.4}$$

where ϕ is the molecular orbital, and $\hat{A}$ is the antisymmetrization operator. Eqn. 1.4 is used as an approximation to the wavefunction in eqn. 1.1. At this point, we are going to switch to second quantization to make the equations more compact. In second quantization, the Hamiltonian is written as

$$H = \sum_{pq} h_{pq} E^p_q + \frac{1}{2}\sum_{pqrs} g_{pqrs} E^{pq}_{rs} + h_{nuc} \tag{1.5}$$

where h is the one-electron interaction, g is the two-electron interaction, h_{nuc} is the interaction between nuclei, and E is the spin-free creation-destruction operator

$$E^p_q = a^\dagger_{p\alpha} a_{q\alpha} + a^\dagger_{p\beta} a_{q\beta} \tag{1.6}$$

where α, β denote electron spins, and $a^\dagger$, a represent creation and destruction operators.

The Hartree Fock determinant is not an eigenfunction of the Hamiltonian, but of a mean field approximation one electron Hamiltonian known as the Fock

operator, which takes the form

$$H_{HF} = F = \sum_{pq} h_{pq} E_q^p + \sum_{pq} \sum_i (2g_{pqii} - g_{piiq}) E_q^p + h_{nuc} \tag{1.7}$$

where the second term $(2g_{pqii} - g_{piiq})$ is the Fock potential. The first term in the Fock potential represents the average direct Coulombic interaction and the second term represents the effects of exchange.

The Hartree Fock energy is defined as $\langle HF|H|HF\rangle$, and is stationary with respect to the orbitals in Hartree Fock. Hartree Fock is a self-consistent field method (SCF), which means that the Hartree Fock energy and wavefunction can be determined iteratively. The Hartree Fock energy is also size-consistent, which means that the Hartree Fock energy of a system of two non-interacting subsystems is equal to the sum of the energies of the subsystems. The Hartree Fock energy can be expressed as

$$E_{HF} = \langle HF|H|HF\rangle = \sum_{pq} h_{pq}\delta_{pq} + \frac{1}{2} \sum_{pq} \sum_i (2g_{pqii} - g_{piiq})\delta_{pq} + h_{nuc} \tag{1.8}$$

As long as the chemical system can be described using a single Slater determinant, and electron correlation can be neglected then Hartree Fock works well. However, there are many systems where this is not the case. Hartree Fock performs poorly when disassociating a diatomic molecule. Also, Hartree Fock cannot properly predict the low lowing excited states of conjugated polymers. For simple reasons as those just provided, a more accurate method is needed to properly predict these chemical systems.

1.3 Full Configuration Interaction - The Exact Solution

As discussed in section 1.2, Hartree Fock is good for a zeroth order approximation to the wavefunction in an ab-initio quantum chemistry calculation. Now we will take a look at the exact solution to the Schrödinger equation through Full Configuration Interaction (FCI) [1, 6–8]. The Hamiltonian is the same as in eqn. 1.5, but now we will allow the wavefunction to consist of a linear combination of Slater determinants. The wavefunction for FCI is

$$|\Psi\rangle = c_0|HF\rangle + \left(\frac{1}{1!}\right)^2 \sum_{pq} c_q^p |HF_q^p\rangle + \left(\frac{1}{2!}\right)^2 \sum_{pqrs} c_{rs}^{pq} |HF_{rs}^{pq}\rangle + \cdots \tag{1.9}$$

where c are the coefficients for each Slater determinant, and $|HF_q^p\rangle$ denotes a determinant where orbital q has been replaced by orbital p. Eqn. 1.9 is the exact ansatz which solves the Schrödinger equation. Combined with eqn. 1.5 and the variational principle, the exact energy of any chemical system can be obtained with FCI. However, although FCI can be used to obtain the exact energy for a chemical system, the cost scales exponentially with the number of orbitals. This means that even small systems can quickly become intractable as the number of molecular orbitals are increased.

Many of the coefficients c in eqn. 1.9 are either zero or are very close to zero. This will allow us to make approximations to solve the Schrödinger equation, which will be discussed in the next section.

1.4 Dynamic and Static Electron Correlation

So far we have seen in section 1.2, that Hartree Fock theory (HF) was too approximate and gave inaccurate results where electron correlation is significant.

We have also seen in section 1.3, that Full Configuration Interaction (FCI), although exact was an intractable problem except for the very smallest chemical systems.

We can use the Hartree Fock theory as a beginning approximation to the exact wavefunction and apply correction methods on top of it. First we begin by putting each molecular orbital into one of three groups. The first group is the core orbitals. Molecular orbitals in this group are in low energy orbitals and are always largely occupied. The second group is the active orbitals. Molecular orbitals in this group are mid energy orbitals and tend to be the valence space orbitals. The third and final group is the virtual orbitals. Molecular orbitals in this group are high energy orbitals and are largely unoccupied.

The difference in energy between the exact energy and the Hartree Fock energy is known as the correlation energy. The correlation energy can be further broken down into two components, static and dynamic. Static correlation energy is the energy change associated with the correlation in the active space. From eqn. 1.9, this would require solving for the coefficients c that have Slater determinants with different occupancies within the active space. The static correlation energy gives a qualitative picture of a chemical system. To get a quantitative picture of the chemical system, we will also need the dynamic correlation energy. From eqn. 1.9, this would result in solving for the coefficients c in Slater determinants with variable occupancies in the core or virtual space. Although the dynamic correlation tends to be small, it is necessary in combination with the static correlation energy to obtain results comparable to experiment.

At this point, we will provide some examples of higher order methods to obtain the static and dynamic correlation energies. Methods that can provide the static

correlation energy are Complete Active Space Self Consistent Field (CASSCF) [9–11], Density Matrix Renormalization Group (DMRG) [12–17], and Density Matrix Renormalization Group Self Consistent Field (DMRGSCF) [18]. Methods that can provide the dynamic correlation energy are Complete Active Space Perturbation (CASPT2) [19–21], Coupled Cluster (CC) [22–24], Multireference Møller Plesset Perturbation theory (MRMP) [25], Multireference Configuration Interaction (MRCI) [26–29], Multireference Coupled Cluster (MRCC) [30] and Canonical Transformation theory (CT) [31–34].

In this thesis, we will focus on DMRG and DMRGSCF as tools to correct the zeroth order Hartree Fock zeroth order description in the active space and the corresponding static correlation effects. Then we will include the dynamic electron correlation using CT and determine the dynamic correlation effects.

1.5 Scope of the Thesis

In Chapters 2 and 5, we will introduce the basic theory and algorithm behind the Density Matrix Renormalization Group (DMRG) and Canonical Transformation (CT) theory, respectively. Chapter 3 describes a subspace diagonalization algorithm for obtaining the higher energy eigenfunctions of a Hamiltonian. Previous subspace diagonalization methods require that the lower energy eigenfunctions be obtained before the higher energy eigenfunctions. Chapter 4 describes the theory and implementation of the analytical first and second order derivatives in DMRG. Chapter 6 describes the theory and implementation for the 0-, 1- and 2-body density matrices in CT. This will be useful for describing correlations in chemical systems. Chapter 7 is the possible future directions for CT.

Specifically, Chapter 7 describes the theory behind first and second order analytical derivatives for CT.

BIBLIOGRAPHY

[1] T. Helgaker, P. Jørgensen, and J. Olsen, *Molecular Electronic-Structure Theory*, John Wiley & Sons Inc., 2000.

[2] C. C. J. Roothaan, Rev. Mod. Phys. **23**, 69 (1951).

[3] A. Szabo and N. S. Ostlund, *Modern Quantum Chemistry: Introduction to Advanced Electronic Structure Theory*, Dover Publications, Inc., 1989.

[4] R. McWeeny, *Methods of Molecular Quantum Mechanics*, Academic Press Inc., 2nd edition, 1996.

[5] D. B. Cook, *Handbook of Computational Quantum Chemistry*, Oxford University Press, 1998.

[6] S. F. Boys, Proc. Roy. Soc. London. **A201**, 125 (1950).

[7] R. K. Nesbet, Proc. Roy. Soc. London. **A230**, 312 (1955).

[8] B. O. Roos, Chem. Phys. Lett. **15**, 153 (1972).

[9] D. R. Hartree, W. Hartree, and B. Swirles, Phil. Trans. Roy. Soc. (London) **A238**, 229 (1939).

[10] B. O. Roos, P. R. Taylor, and P. E. M. Siegbahn, Chem. Phys. **48**, 157 (1980).

[11] B. O. Roos, The complete active space self-consistent field method and its applications in electronic structure calculation, in *Advances in Chemical Physics; Ab Initio Methods in Quantum Chemistry II*, edited by Wiley, page 399, Chichester, 1987.

[12] S. R. White, Phys. Rev. Lett. **69**, 2863 (1992).

[13] S. R. White, Phys. Rev. B **48**, 10345 (1993).

[14] G. K. L. Chan and M. Head-Gordon, J. Chem. Phys. **116**, 4462 (2002).

[15] G. K. L. Chan and M. Head-Gordon, J. Chem. Phys. **118**, 8551 (2003).

[16] G. K. L. Chan, J. Chem. Phys. **120**, 3172 (2004).

[17] G. K. L. Chan, M. Kállay, and J. Gauss, J. Chem. Phys. **121**, 6110 (2004).

[18] D. Ghosh, J. Hachmann, T. Yanai, and G. K. L. Chan.

[19] K. Andersson, P.-Å.. Malmqvist, B. O. Roos, A. J. Sadlej, and K. Wolinski, J. Phys. Chem. **94**, 5483 (1990).

[20] K. Andersson, P.-Å.. Malmqvist, and B. O. Roos, J. Chem. Phys. **96**, 1218 (1992).

[21] K. Hirao, *Recent Advances in Multireference Methods*, volume 4 of *Recent Advances in Computational Chemistry*, World Scientific Publishing Co. Pte. Ltd., Singapore, 1999.

[22] J. Cizek, J. Chem. Phys. **45**, 4256 (1966).

[23] G. D. Purvis and R. J. Bartlett, J. Chem. Phys. **76**, 1910 (1982).

[24] R. J. Bartlett and M. Musial, Rev. Mod. Phys. **79**, 291 (2007).

[25] K. Hirao, Chem. Phys. Lett. **190**, 374 (1992).

[26] H. F. Schaefer III and F. E. Harris, Phys. Rev. Lett. **21**, 1561 (1968).

[27] R. J. Buenker, S. D. Peyerimhoff, and W. Butscher, Mol. Phys. **35**, 771 (1978).

[28] P. E. M. Siegbahn, J. Chem. Phys. **72**, 1647 (1980).

[29] H.-J. Werner and P. J. Knowles, J. Chem. Phys. **89**, 5803 (1988).

[30] J. Paldus and X. Li, Adv. Chem. Phys. **110**, 1 (1999).

[31] T. Yanai and G. K.-L. Chan, **124**, 194106 (2006).

[32] T. Yanai and G. K.-L. Chan, **127**, 104107 (2007).

[33] E. Neuscamman, T. Yanai, and G. K.-L. Chan, **130**, 124102 (2009).

[34] E. Neuscamman, T. Yanai, and G. K.-L. Chan, **130**, 124102 (2009).

CHAPTER 2

DENSITY MATRIX RENORMALIZATION GROUP (DMRG) - INTRODUCTION

2.1 Introduction

In chapter 1, we discussed static and dynamic correlation energy using Hartree Fock as our starting point. In this chapter, we discuss how to obtain the static correlation effects through Density Matrix Renormalization Group (DMRG). DMRG was originally developed in the physics community by Steven R. White [1, 2]. The quantum chemistry analogue of DMRG was later developed by Chan et al.[3–6]. DMRG has been shown to be quite a powerful tool in ab-initio quantum chemistry for describing static correlation in very large active spaces, which were intractable for methods such as Complete Active Space Configuration Interaction (CASCI) and Complete Active Space Self Consistent Field (CASSCF) [7].

Several reviews of DMRG have been written, which would work well as a supplement to this chapter[8–11].

2.2 Theory

The Full Configuration Interaction (FCI) wavefunction can be written as

$$|\Psi\rangle = \sum_{n_1 n_2 \cdots} \psi^{n_1 n_2 \cdots} |n_1 n_2 \cdots\rangle \tag{2.1}$$

where n_i is the occupation of orbital i and therefore can have a value of 0, 1^α, 1^β, or $2^{\alpha\beta}$. The DMRG wavefunction approximates this expansion as

$$|\Psi_{DMRG}\rangle = \sum_{n_1 n_2 n_3 \cdots} \sum_{i_1 i_2 i_3 \cdots} \psi_{i_1}^{n_1} \psi_{i_1 i_2}^{n_2} \psi_{i_2 i_3}^{n_3} \cdots |n_1 n_2 n_3 \cdots\rangle \tag{2.2}$$

For a fixed set of values of the occupation $n_1 n_2 \cdots$, the object ψ^m are matrices. Thus, the DMRG wavefunction takes the form of a Matrix Product State (MPS)

$$\sum_{i_1 i_2 \cdots} \psi_{i_1}^{n_1} \psi_{i_1 i_2}^{n_2} \cdots = \psi^{n_1} \otimes \psi^{n_2} \otimes \cdots \tag{2.3}$$

where $\otimes$ denotes the matrix product. If we fix the dimensions of each matrix within the DMRG wavefunction, the parameters will only grow polynomially rather than exponentially with respect to the system size as in the case of FCI.

2.3 Algorithm

The algorithm for one-dot DMRG is as follows and is presented pictorially in Figs. 2.1 and 2.2:

1. We split the chemical system into three blocks. We will refer to these pieces as the system, the dot, and the environment. The system will generally consist of at least the first site of the chemical system. A site refers to any single orbital space, where $n = 0, 1^\alpha, 1^\beta, 2^{\alpha\beta}$. The dot will then refer to the single site after the system sites and the environment will consist of all the remaining sites in the chemical system.
2. We then form representations of all the one- and two-body operators from the Hamiltonian that only act on the system, dot, or the environment in the spaces spanned by the system, dot, and environment, respectively.

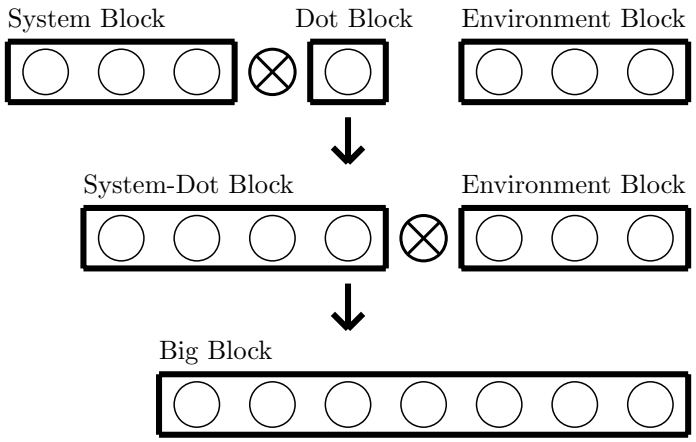

Figure 2.1: A DMRG big block is formed by first forming the tensor product of the system block and the dot block to form the system-dot block. The tensor product of the system-dot block and the environment block forms the big block.

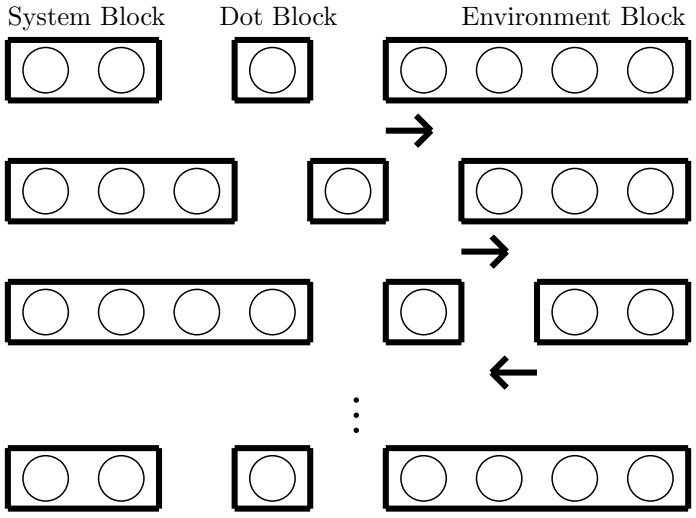

Figure 2.2: A DMRG sweep is performed by growing the system block through decimation and decreasing the environment block. Once the environment is at its minimum size, the DMRG sweep is then performed in the opposite direction.

3. We will "connect" the system and dot, first. We will form representations of the operators that act on both the system and dot, as well as the operators that act on the system and dot alone in the tensor product space of the system and dot. We will refer to this newly "connected" block as the system-dot block.

4. We will now perform a similar step to connect the system-dot block with the environment block. We will refer to this block as the big block. Also, we will form all the operator combinations that act on the system, dot, and environment spaces. This will allow us to form the action of the Hamiltonian on the DMRG wavefunction.

5. Our next objective is to obtain the lowest eigenstate(s) and eigenfunction(s) of the Hamiltonian. This can be achieved by using a subspace method such as Davidson[12], Harmonic Davidson[13], or Lanczos [14].

6. Next, we will form the system reduced density matrix of the system-dot block, using the environment block as our bath. This means that we will trace out the environment using the lowest state(s) from the Hamiltonian. We will then diagonalize this reduced density matrix, and keep M of the eigenstates corresponding to the largest eigenvalues of the reduced density matrix. In the next piece, we will explain why the system reduced density matrix is the key to DMRG.

7. We will then proceed to truncate the system-dot space using the M eigenvectors of the reduced density matrix from the previous step as a transformation matrix. This step is referred to as decimation.

8. The truncated system-dot space from the previous step will now become the space of the new system block, and we will form a new dot block and environment block. We will then repeat steps 3-8 until the environment

has too few sites to form a block. This is called a sweep. Then we will perform a sweep in the opposite direction. We keep performing sweeps until the energy has converged to a preset tolerance. In this way, DMRG is a self consistent method. Once the energy is converged, we can obtain the expectation values of the DMRG state(s).

In the algorithm, we mentioned that using the system reduced density matrix was the key to DMRG. We now intend to explain why this is the case. As the main focus of this thesis is algorithm development, we will provide three different ways of looking into why we truncate the system Hilbert space using the eigenstates corresponding to the largest eigenvalues of the system reduced density matrix as described in the review by Schollwöck[9].

(1) (Expectation values)[15]

We will begin by defining the system reduced density matrix

$$\rho^S = Tr_E(|\Psi\rangle\langle\Psi|) \tag{2.4}$$

where Tr_E refers to tracing out the environment states. The eigenvalues and eigenstates of the system reduced density matrix will have the following properties

$$\rho^S|w_a\rangle = w_a|w_a\rangle \tag{2.5}$$

$$\sum_a w_a = 1 \tag{2.6}$$

$$w_{a-1} \geq w_a \tag{2.7}$$

$$w_a \geq 0 \tag{2.8}$$

where $|w_a\rangle$ are the eigenstates and w_a are the corresponding eigenvalues. The qualitative idea behind using the largest w_a eigenstates is that these eigenstates

are the most important components of the overall eigenstate in the full system and environment. In our first approach to providing insight into the system reduced density matrix (srdm), we will show that in terms of expectation values, specifically the expectation values of operators that act on the system, that these eigenstates retain the most information in the decimation step. To show this let's examine the expectation value of an arbitrary operator acting on the system A

$$E = \frac{\langle\Psi|A|\Psi\rangle}{\langle\Psi|\Psi\rangle} = Tr_S(\rho A) \tag{2.9}$$

where Tr_S refers to a trace over the system. Now let's look at the same equation but in the srdm eigenbasis,

$$Tr_S(\rho A) = \sum_a^{N_S} w_a \langle w_a|A|w_a\rangle \tag{2.10}$$

where the exact expectation value is obtained by summing over all the system states w_a. In DMRG, we truncate the sum to the M states with largest w_a, which we may denote by $Tr_{S_{DMRG}}$. Consequently the error in the DMRG expectation value of A is bounded by

$$|Tr_S(\rho A) - Tr_{S_{DMRG}}(\rho A)| \leq \left(\sum_{a=M}^{N_S} w_a\right) c_A \tag{2.11}$$

where N_S is total number of eigenstates for the system and c_A is a constant.

(2) (Wavefunction)[1, 2]

In this section, we will show that the wavefunction error on truncating the system in the decimation step will be minimized by choosing the eigenstates from the srdm with the largest weights. We start with a wavefunction $|\Psi\rangle$ expressed in the full space of the system (with N_S states) and environment (with N_E states)

$$|\Psi\rangle = \sum_i^{N_S}\sum_j^{N_E} \psi_{ij}|i\rangle|j\rangle, \tag{2.12}$$

where $|i\rangle$ and $|j\rangle$ denote orthonormal sets of system and environment states, respectively. Now, we want to approximate $|\Psi\rangle$ by a wavefunction where we have truncated the system to only M states $|a\rangle$ using the srdm

$$|\Psi_{DMRG}\rangle = \sum_{a}^{M}\sum_{j}^{N_E} a_{aj}|w_a\rangle|j\rangle \tag{2.13}$$

$$|w_a\rangle = \sum_{i} u_{ai}|i\rangle \tag{2.14}$$

where u_{ai} are the coefficients of the eigenvectors of the srdm, and give the relation between the original system states $|i\rangle$ and the truncated states $|a\rangle$.

To determine a_{aj}, we want $|\Psi_{DMRG}\rangle$ to represent $|\Psi\rangle$ as well as possible, i.e. we will minimize

$$|||\Psi_{exact}\rangle - |\Psi_{DMRG}\rangle|| \tag{2.15}$$

Combining eqn. 2.14 and eqn. 2.15, we find

$$|||\Psi_{exact}\rangle - |\Psi_{DMRG}\rangle|| = 1 - 2\sum_{aij}\psi_{ij}a_{aj}u_{ai} + \sum_{aj}a_{aj}^2 \tag{2.16}$$

Differentiating eqn. 2.16 with respect to a_{ij}, and setting the result to zero, gives

$$0 = -\sum_{i}\psi_{ij}u_{ai} + a_{aj} \tag{2.17}$$

This now expresses the DMRG wavefunction coefficients a_{aj} in terms of the original wavefunction coefficients ψ_{ij} and the srdm eigenvectors u_{ai}. Now we remind ourselves of the following definitions of the srdm and its eigenvalues,

$$\rho_{ij} = \sum_{k}\psi_{ik}\psi_{jk} \tag{2.18}$$

$$w_a = \sum_{ij}\sum_{k} u_{ai}\psi_{ik}\psi_{jk}u_{ja} \tag{2.19}$$

Combining eqns. 2.16, 2.17, 2.18, and 2.19, we see that error is a function of the srdm eigenvalues,

$$\epsilon = \sum_{a=M}^{N_S} w_a \leq 1 \tag{2.20}$$

Consequently, the error in the DMRG wavefunction will be minimized using (in eqn. 2.14) the truncated state coefficients u_{aj} corresponding to the eigenvectors $|w_a\rangle$ with the largest eigenvalues w_a.

(3) (Entropy)[16–19]

In this third discussion of the system reduced density matrix (srdm), we will show that the von Neumann entropy of the truncated system is maximized by using the eigenstates of the srdm. Our first step in this demonstration is to perform a singular value decomposition on the exact wavefunction

$$|\Psi\rangle = \sum_{\alpha}^{N} \sqrt{w_a}|w_a^S\rangle|w_a^E\rangle \tag{2.21}$$

$$|w_a^S\rangle = \sum_{i}^{N_S} u_{ia}|i\rangle \tag{2.22}$$

$$|w_a^E\rangle = \sum_{j}^{N_E} v_{ja}|j\rangle \tag{2.23}$$

where u_{ia} and v_{ja} are elements of orthonormal matrices. D "loosely" consists of the eigenvalues of either the environment or the system reduced density matrix. We use the word "loosely", because the system and environment reduced density matrices are obviously of different dimensions, but both matrices have the same number of non-zero eigenvalues. This is why we use the symbol N in eqn. 2.21. N is the number of non-zero eigenvalues of the system and environment reduced density matrices. Now consider the reduced density matrices for the system and environment

$$\rho^S = \sum_a w_a|w_a^S\rangle\langle w_a^S| \tag{2.24}$$

$$\rho^E = \sum_a w_a|w_a^E\rangle\langle w_a^E| \tag{2.25}$$

The von Neumann entropy, which denotes the entanglement of the system in the rest of the world, is defined as follows

$$S = -Tr(\rho \ln_2 \rho) \tag{2.26}$$

Using either eqn. 2.24 or 2.25 for the definition of ρ, we will arrive at the following expression for the von Neumann entropy

$$S = -\sum_a w_a ln_2(w_a) \tag{2.27}$$

Within the truncated DMRG wavefunction, where we retain only M states to describe the system, we see again that by choosing the eigenstates that correspond to the largest eigenvalues of the system reduced density matrix, we will maximize recovery of the von Neumann entropy.

In this section, we have discussed the basic theory behind DMRG and provided three view points for the reader to understand the importance of the reduced density matrix within DMRG. More fundamentally, we have shown how the "density matrix" became part of the name of Density Matrix Renormalization Group.

2.4 Size-consistency of the DMRG wavefunction

To see that DMRG is size consistent, we will revisit the DMRG wavefunction and remind the reader that the DMRG wavefunction can be be rewritten using singular value decomposition

$$|\Psi_{DMRG}\rangle = \sum_{\alpha}^{M} \sqrt{w_a} |w_a^S\rangle |w_a^E\rangle \tag{2.28}$$

A theory is size-consistent if the corresponding wavefunction for a supersystem can be decomposed into the product of wavefunctions for the individual subsystems. For the case of the equations above, we assume that the states that consist of $|i\rangle$ represent subsystem A and the states that consist of $|j\rangle$ represent subsystem B. Further, subsystems A and B do not interact with each other. Now, we form the singular value decomposition as in equation 2.28. As mentioned previously, w_a represents the eigenvalues of the system reduced density matrix. Since these subsystems are non-interacting, there will be only a single eigenvalue of 1, that connects the wavefunction from subsystem A to the wavefunction from subsystem B. In more explicit form, the DMRG wavefunction will have the following form

$$|\Psi_{DMRG}\rangle = |w_a^S\rangle|w_a^E\rangle = \sum_i^{N_S} U_{ia}|i\rangle \sum_j^{N_E} V_{ja}|j\rangle \tag{2.29}$$

2.5 DMRG ordering and orbital construction

In passing, we will briefly mention that there are three subtleties to the DMRG algorithm. First, we will mention that during the first sweep, the environment must be made from an initial guess. Generally, this guess is based on constructing the states of the environment that have a low energy. This guess can affect the DMRG convergence and energy as a bad guess can lead to an improper approximate ground state wavefunction in the initial sweeps, and a corresponding poor quality for the system reduced density matrix. We believe that more research needs to be done to make a proper initial guess environment for DMRG.

A poor guess can be fixed by adding "noise" to DMRG. Noise refers to adding small random numbers to the system reduced density matrix before diagonal-

ization. The reason for doing this, is that the DMRG can get stuck in a local minimum and may not recover, especially with a poor environment guess. This noise allows the DMRG wavefunction to explore sectors of the Hilbert space ("quantum states") that might ordinarily have been lost with a poor environment.

As mentioned only briefly in the introduction of this chapter, DMRG works well with pseudo one-dimensional chemical systems. We will now attempt to explain what is meant by pseudo one-dimensional chemical systems, and more specifically what is called orbital ordering. Let's begin with a simple example, a polyene. A polyene has a carbon backbone, and the valence space of the polyene is linear combinations of the p_z space. In this particular case, we would localize the active space using a method such as Pipek-Mezey localization[20] so that each valence orbital was localized on each carbon atom. We would then order the orbitals from one end to the other along the polyene for DMRG. By localizing, and ordering the orbitals properly for DMRG, the DMRG wavefunction can be very accurate even when retaining very few states.

A polyene is actually one-dimensional in its valence space connectivity. For our next example, we will use anthracene which is actually not one-dimensional but can be ordered in DMRG as to appear pseudo-one dimensional and give the fastest convergence rate. Again, as with polyenes, we will localize the valence orbitals on each carbon atom. When this is completed, we will order the orbitals as show in Fig. 2.3. As can be seen in the figure, the orbitals are ordered so that the distance between orbitals is minimized if the carbon atoms were to be projected along a one dimensional horizontal line.

The two examples mentioned are relatively simple in terms of ordering. In gen-

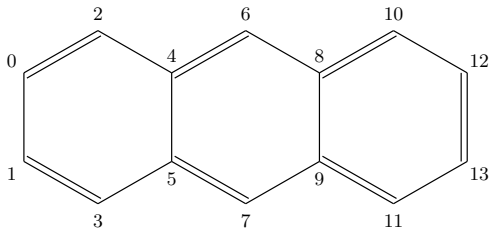

Figure 2.3: Example orbital ordering in DMRG

eral, ordering in DMRG can be difficult if the connectivity of the atoms is more complicated. Additionally, ordering can become difficult if several valence orbitals can be localized on an atom, e.g. the d orbitals in transition metal complexes. Finally, as a practical issue, it is sometimes difficult to construct good valence like orbitals as the starting point for the DMRG calculation, particularly in large basis sets. We believe that more research needs to be done constructing and ordering the active orbitals.

BIBLIOGRAPHY

[1] S. R. White, Phys. Rev. Lett. **69**, 2863 (1992).

[2] S. R. White, Phys. Rev. B **48**, 10345 (1993).

[3] G. K. L. Chan and M. Head-Gordon, J. Chem. Phys. **116**, 4462 (2002).

[4] G. K. L. Chan and M. Head-Gordon, J. Chem. Phys. **118**, 8551 (2003).

[5] G. K. L. Chan, J. Chem. Phys. **120**, 3172 (2004).

[6] G. K. L. Chan, M. Kállay, and J. Gauss, J. Chem. Phys. **121**, 6110 (2004).

[7] J. Hachmann, W. Cardoen, and G. K. L. Chan, J. Chem. Phys. **125**, 144101 (2006).

[8] K. Hallberg, Density matrix renormalization: A review of the method and its applications, in *Theoretical Methods for Strongly Correlated Electrons*, edited by D. Sénéchal, A.-M. Tremblay, and C. Bourbonnais, CRM Series in Mathematical Physics, Springer, New York, 2003.

[9] U. Schollwöck, Rev. Mod. Phys. **77**, 259 (2005).

[10] K. A. Hallberg, Adv. Phys. **55**, 477 (2006).

[11] G. K.-L. Chan et al., An introduction to the density matrix renormalization group ansatz in quantum chemistry, in *Frontiers in Quantum Systems in Chemistry and Physics*, edited by S. Wilson, P. J. Grout, J. Maruani, G. Delgado-Barrio, and P. Piecuch, Progress in Theoretical Chemistry and Physics, Springer, Netherlands, 2008.

[12] E. R. Davidson, J. Comput. Phys. **17**, 87 (1975).

[13] J. J. Dorando, J. Hachmann, and G. K.-L. Chan, J. Chem. Phys. **127**, 084109 (2007).

[14] C. Lanczos, J. of Nat. Bur. of Stand. **45**, 255 (1950).

[15] S. R. White, Phys. Rep. **301**, 187 (1998).

[16] J. Gaite, Mod. Phys. Lett. A **16**, 1109 (2001).

[17] A. Galindo and M. A. Martín-Delgado, Rev. Mod. Phys. **74**, 347 (2002).

[18] T. J. Osborne and M. A. Nielsen, Quantum Inf. Process. **1**, 45 (2002).

[19] E. R. Latorre, J. I. and G. Vidal, Quantum Inf. Comput. **4**, 48 (2004).

[20] J. Pipek and P. Mezey, J. Chem. Phys. **90**, 4916 (1989).

CHAPTER 3

DENSITY MATRIX RENORMALIZATION GROUP - TARGETED EXCITED STATE THEORY[1]

3.1 Introduction

Many excited states possess complicated electronic structure which cannot be described by a single dominant electronic configuration. For such states, a reliable description requires a multireference quantum chemistry method.

Recently, the Density Matrix Renormalization Group (DMRG) has emerged as a new tool for multireference quantum chemistry problems [2–8]. When applied to bond-breaking, it achieves a balanced description across potential energy curves due to its reference-free nature [9–11]. Reduced-scaling DMRG algorithms have also been developed and applied to large multireference problems in quasi-one-dimensional systems such as conjugated polyenes and acenes [12, 13].

The DMRG ansatz can be written as a linear expansion in terms of many-body functions which are subsequently optimised with respect to internal non-linear degrees of freedom $\{\mathbf{R}\}$,

$$|\Psi\rangle = \sum_{lr} \psi_{lr} \, |lr\,(\{\mathbf{R}\})\rangle \tag{3.1}$$

Note that if we choose the expansion functions $|lr\rangle$ to be Slater determinants and the internal degrees of freedom $\{\mathbf{R}\}$ to be their constituent orbitals, the above ansatz describes the Complete-Active-Space Self-Consistent-Field (CASSCF)

[1]Parts of this chapter were published in JCP August 28, 2007[1]

wavefunction [14]. In the DMRG, the expansion functions are instead complicated many-body basis states and the non-linear degrees of freedom are renormalisation matrices, which allows for a particularly compact and efficient expansion [15].

To obtain excited states in the DMRG we usually use the iterative Davidson algorithm to solve for eigenvectors $|\Psi_i\rangle = \psi^i_{lr}|lr\rangle$ ranging from the ground-state to the excited state of interest [16]. The non-linear parameters $\{\mathbf{R}\}$ for these states are subsequently optimised for a density matrix that is averaged over all the states $|\Psi_i\rangle$. State-averaging is necessary to improve the stability of the non-linear optimisation and to prevent root-flipping, which occurs when the approximate wavefunction leaves the convergence basin of the target excited state and enters that of a different excited state [17–21].

The drawbacks of this conventional approach, which we shall refer to as the State-Averaged Davidson (SA-D) algorithm, become clear if one is interested in higher regions of the spectrum because it becomes infeasible, both in terms of computational cost and accuracy, to solve for and adequately represent all the lower-lying eigenvectors in the state-averaged DMRG basis. Consequently, it is desirable to explore alternative algorithms that directly yield individual or a few excited state wavefunctions at a time. Any such an algorithm should also retain the stability of the SA-D algorithm during non-linear optimisation, so as to be able to rapidly converge to the desired target excited state(s) without root-flipping.

Iterative methods for linear algebra that work with shifted and inverted operators such as $(\omega - H)^{-1}$ have long been used in numerical analysis to obtain the interior (i.e. excited state) eigenvalues of matrices [22, 23]. Sleijpen and van der

Vorst proposed an efficient modification that used a shifted and inverted operator to directly calculate *harmonic Ritz* approximations to excited eigenvalues and eigenvectors [24]. We shall refer to this variant as the *Harmonic Davidson* (HD) algorithm to distinguish it from the original algorithm above. Aside from a demonstration for the one-electron Kohn-Sham equation in Ref. [25], we are not aware of the application of this technique elsewhere in quantum chemistry.

The purpose of this work is to investigate the Harmonic Davidson algorithm as a means to directly target individual excited states and regions of the spectrum within the DMRG. One area in which the current application to quantum chemistry differs from previous numerical applications is the presence of a subsequent nonlinear optimisation step for the wavefunction. We investigate how combining the Harmonic Davidson procedure with state-averaging over nearby states in the spectrum (State-Averaged Harmonic Davidson, or SA-HD) can be used to confer stability in this non-linear optimisation. While we have focused on the DMRG method here, our findings are relevant to excited state algorithms for other quantum chemistry methods whose ansatz contains both linear and non-linear parameters, such as in the CASSCF method.

The structure of this paper is as follows. In Sec. 3.2, we briefly review the DMRG method and the Davidson and Harmonic Davidson algorithms. In Sec. 3.3, we present DMRG calculations on the excited states of acenes from naphthalene to pentacene using both direct targeting with the Harmonic Davidson algorithm (in both state-averaged and non-state-averaged forms) as well as with the traditional (state-averaged) Davidson approach. We also compare our excited state spectrum with that obtained from Equation of Motion Coupled Cluster theory. We summarise our findings in Sec. 3.4.

3.2 Theory

3.2.1 DMRG

The quantum chemistry DMRG algorithm used in this work has been described fully elsewhere [12, 26]. As a detailed understanding is not necessary here, we shall restrict ourselves to only the essentials. As described above, the DMRG wavefunction may be written in the form (3.1). The DMRG sweep algorithm then provides an iterative method through which the many-body basis functions $|l\rangle, |r\rangle$ may be optimised with respect to a set of internal non-linear parameters $\mathbf{R}$. For each orbital in the problem we can associate an $\mathbf{R}$ matrix, which describes a many-body renormalisation transformation involving the orbital (i.e. not simply an orbital rotation). In a sweep to optimize the $|l\rangle$ states (an analogous procedure holds for the $|r\rangle$ states), $\mathbf{R}$ matrices are determined from the M eigenvectors of the many-particle reduced density matrix with the largest eigenvalues. In the ground-state case, the density matrix that determines the $|l\rangle$ states is obtained by tracing out the $|r\rangle$ states from the wavefunction, viz

$$\Gamma_{ll'} = \sum_r \psi_{lr}\psi_{l'r} \tag{3.2}$$

$$\Gamma_{ll'}R_{l'm} = \gamma_l R_{lm}, \;\; m = 1, \ldots, M \tag{3.3}$$

M is referred to as the size of the DMRG many-body basis, and as M increases, the DMRG wavefunction becomes exact. For excited state calculations, it is usual to employ state-averaging to increase the stability of the non-linear optimisation. This consists of using an averaged reduced density matrix in eq. (3.2)

$$\Gamma_{ll'} = \sum_r w_i \psi^i_{lr}\psi^i_{l'r} \tag{3.4}$$

where typically we choose equal weights for all the states of interest.

3.2.2 The Davidson Algorithm

The Davidson algorithm provides an efficient iterative solver for the large number of linear coefficients in the expansion of the ground-state DMRG wavefunction (3.1) [27, 28]. $|\Psi\rangle$ is expressed in an auxiliary basis $\{\eta_i\}$ (generated by the Davidson iterations)

$$|\Psi\rangle = \sum_i c_i |\eta_i\rangle \tag{3.5}$$

$$|\eta_i\rangle = \eta_{lr}^i |lr\rangle \tag{3.6}$$

The coefficients c_i are determined by left-projection with $\langle\eta_j|$

$$\sum_i \langle\eta_j|H - E|\eta_i\rangle c_i = 0 \tag{3.7}$$

where E is the approximate expectation value $\langle\psi|H|\psi\rangle/\langle\psi|\psi\rangle$. Each iteration of the Davidson algorithm, generates a new basis function $|\eta\rangle$ from the current trial solution $|\psi\rangle$ via

$$|\eta\rangle = (\mathrm{diag}(H) - E)^{-1}(H - E)|\psi\rangle \tag{3.8}$$

which is then orthogonalised against and added to the subspace $\{\eta_i\}$.

To obtain excited state eigenvectors, the simple generalization known as the block Davidson or Davidson-Liu algorithm [29, 30] is typically used. Here a residual vector is generated for each of the states from the ground-state up to the target excited state. Solution of the subspace eigenvalue equation (3.7) then yields successive approximations to all eigenstates up to the excited state of

interest. In the subsequent non-linear optimisation of the excited state in the DMRG algorithm, the eigenvectors obtained from the block Davidson algorithm (i.e. from the ground-state to the target eigenvector of interest) are all averaged together in the density matrix (3.4). We shall refer to this combined procedure as the State-Averaged Davidson, or SA-D algorithm.

From the above, we see that the primary drawbacks of the traditional SA-D approach are (i) computational cost - we must solve for all the states between the ground-state and excited state of interest, and (ii) decreased accuracy - since a single set of non-linear parameters must now represent multiple states rather than a single state.

3.2.3 The Harmonic Davidson algorithm

To avoid the need to solve for the states below the excited state of interest as in the Davidson algorithm above, classic shift and invert methods map the target excited state of the Hamiltonian H onto the ground-state of a shifted and inverted operator Ω

$$\Omega = H_{\omega}^{-1} = (\omega - H)^{-1} \tag{3.9}$$

The Harmonic Davidson algorithm introduced by Sleijpen and van der Vorst [24] (see also Ref. [23] for a clear review) extends the Davidson algorithm to work with the operator Ω without the need to explicitly compute the operator inverse in eqn. (3.9). Each iteration generates a basis $\{\eta_i\}$, but now we expand the target excited state $|\Psi\rangle$ in $\{H_w\eta_i\}$

$$|\Psi\rangle = \sum_i c_i |H_\omega \eta_i\rangle \tag{3.10}$$

Left projection with $\langle \eta_i H_\omega |$ yields a generalized eigenvalue problem

$$\begin{aligned} \langle \eta_j H_\omega | (H_\omega^{-1} - E_\omega^{-1}) | H_\omega \eta_i \rangle c_i = 0 \\ \Rightarrow \sum_i [\langle \eta_j | H_w | \eta_i \rangle_i - E_\omega^{-1} \langle \eta_j H_\omega | H_\omega \eta_i \rangle] c_i = 0 \end{aligned} \tag{3.11}$$

where E_ω^{-1} is the current approximation to $(\omega - E)^{-1}$. E_ω is known as a harmonic Ritz approximation to the corresponding eigenvalue of H_ω. From (3.11), we see that solving the eigenvalue equation for H_ω^{-1} in the subspace $\{H_\omega \eta_i\}$ is equivalent to solving the eigenvalue equation for the non-inverted operator H_ω where the trial solution is expanded in the basis $\{|\eta_i\rangle\}$, and the coefficients are obtained by right projection using a *different* space $\{\langle \eta_j H_\omega |\}$. This suggests that subspace $\{\eta_i\}$ for eqn. (3.11) can also be generated from the trial solution $|\psi\rangle$ through a Davidson-type iteration

$$|\eta\rangle = (\text{diag}(H_\omega) - E'_\omega)^{-1} (H_\omega - E'_\omega) |\psi\rangle \tag{3.12}$$

where here E'_ω refers to the expectation value $\langle \psi | H_\omega \psi \rangle / \langle \psi | \psi \rangle$, which is distinct from E_ω appearing in eqn. (3.11).

While we could obtain the excited state eigenvalues and eigenvectors directly from the generalized eigenvalue problem (3.11), in practice it is numerically more stable to consider a slightly different form. By Schmidt orthogonalization, we can construct an orthogonal decomposition $\{\tilde{\eta}_i\}$ of $\{H_\omega \eta_i\}$ such that $\langle \tilde{\eta}_j H_\omega | H_\omega \tilde{\eta}_i \rangle = \delta_{ji}$. Re-expressing the eigenvalue problem in this basis gives

$$\sum_i (\langle \tilde{\eta}_j | H_\omega | \tilde{\eta}_i \rangle - E_\omega^{-1} \delta_{ji}) c_i = 0 \tag{3.13}$$

From eqn. (3.13) we see that implementing the Harmonic Davidson algorithm requires only minor alterations to the traditional Davidson routine relating to the change in the subspace from $\{\eta_i\}$ to $\{\tilde{\eta}_i\}$. In essence, there are only two

additional steps: the subspace functions are first multiplied by H_ω, and second, they are Schmidt orthogonalized to yield $\{\tilde{\eta}_i\}$.

In our later DMRG calculations, we will refer to the use of the above iterative procedure to solve for the linear coefficients together with the non-linear optimisation of the many-body basis functions $|l\rangle, |r\rangle$ without state-averaging, collectively, as the Harmonic Davidson algorithm (HD).

While the operator H_ω has the target excited state of interest as its ground-state eigenvector, stable convergence is not guaranteed in the non-linear optimisation. However, the formulation of the excited state problem as a ground-state minimization, albeit with a different operator Ω, illustrates that root-flipping is really no different from the poor convergence that may be found in difficult ground-state DMRG calculations. Consequently, the same procedures may be used to eliminate the convergence difficulty: either we can increase the size M of the DMRG basis or we can employ a state-average over the competing states. While we do not know *a priori* which states will cause convergence difficulties, it is reasonable to assume that they must lie energetically near our state of interest. We have thus implemented two types of State-Averaged Harmonic Davidson (SA-HD) algorithms. In the first (referred to as simply SA-HD) we average over the first n excited states of Ω. These correspond to the n excited states that lie immediately above our target excited state in the spectrum of H. In the second, we average over the n states which lie closest (on either side) to the target excited state in the H spectrum. We refer to this variant algorithm as SA-HDa.

The second variant (SA-HDa) is particularly suited to an alternative way of using the shift ω. Rather than choosing a shift to target a specific excited state, we

Table 3.1: RHF, CCSD, and DMRG(500) total energies of the acenes. All energies are in hartrees.

Molecule	E_{RHF}	CCSD	DMRG(500)
$C_{10}H_8$	-378.66597	-378.85130	-378.85360
$C_{14}H_{10}$	-529.44420	-529.70634	-529.71032
$C_{18}H_{12}$	-680.21823	-680.56059	-680.56538
$C_{22}H_{14}$	-830.99045	-831.41614	-831.42016

can instead choose to find the excited states around a given shift. If stable convergence is not achieved, we simply then increase the number of states used in the SA-HDa average until convergence is recovered. In this way, we can patch together the spectrum piece by piece by using successively higher shifts.

3.3 Application to Acenes

We have investigated the low-lying states of the acene series ranging from naphthalene (2-acene) to pentacene (5-acene). In the following subsections, we describe the details of the computations (Sec. 3.3.1), examine the excitation energies using the State-Averaged, Harmonic Davidson, and State-Averaged Harmonic Davidson DMRG algorithms (Sec. 3.3.2), and finally use the (near-exact) DMRG results to assess the accuracy of the excitation spectrum obtained from Equation-of-Motion Coupled Cluster theory (EOM-CC) (Sec. 3.3.3).

3.3.1 Computational Details

We used a model geometry for the acenes with C_{2v} symmetry. The C-H bond lengths were 1.090 Å. Along the legs of the acene ladder, the alternate C-C bond lengths were 1.410 Å and 1.405 Å, respectively. Along the rungs of the acene ladder, the C-C bond length was 1.465 Å. An example geometry for naphthalene is shown in Fig. 3.1.

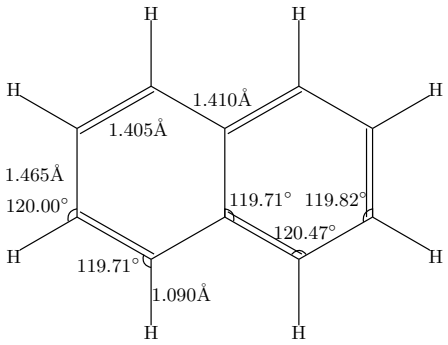

Figure 3.1: Naphthalene model geometry.

All calculations used the STO-3G (Slater-Type-Orbitals fitted to 3 Gaussians minimal basis set, consisting of 2s1p functions on C and 1s functions on H [31]. We obtained the atomic orbital integrals and Restricted Hartree-Fock (RHF) orbitals from the PSI3.2 package [32]. The RHF energies are given in Table 3.1. For the excited state calculations, we used a π-active space consisting of one p_z orbital per carbon i.e. n-acene would have a $(4n + 2, 4n + 2)$ active space. In the DMRG calculations, we further symmetrically orthonormalized the p_z orbitals with respect to the overlap S. This gave a local orthonormal basis which yields faster convergence in the DMRG calculations. The remaining non-active orbitals from the RHF calculations were kept frozen in all calculations.

We calculated excitation energies with the State-Averaged Davidson (SA-D),

Harmonic Davidson (HD), and State-Averaged Harmonic Davidson (SA-HD) algorithms described in Sec. 3.2. Our calculations used the local quadratic-scaling DMRG algorithm described in Ref. [12]. We employed a screening threshold of 10^{-8} Hartrees (E_h) with no spatial symmetry. The ordering of the orbitals for anthracene is shown in Fig. 3.2 and the other acenes were ordered similarly. In all of our sweeps, we added a small amount of random noise ($10^{-6} - 10^{-8}$) to the density matrix so that we would not lose important quantum numbers [26, 33]. In the current algorithm it is difficult to converge DMRG energies beyond the intrinsic accuracy associated with the finite number M of DMRG basis states. Thus DMRG energies were converged to within 1 milli-Hartree (mE_h) ($M = 50$), 0.5 mE_h ($M = 100$), 0.5 mE_h ($M = 250$), or 0.1 mE_h ($M = 500$), respectively. We note that our largest M DMRG excitation energies are essentially exact (within the one-particle basis) to all reported digits. This is possible for the large active spaces used here because of the compact parametrisation afforded by the DMRG wavefunction.

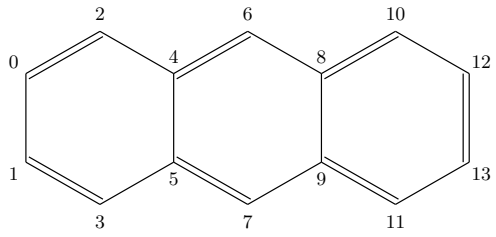

Figure 3.2: The orbital ordering used for anthracene.

In the HD and SA-HD calculations, the shift ω for a specific root was obtained as follows. To begin, we guessed an initial shift (typically based on our previous SA calculations). In the case where the shift was too low or too high, the next guess for ω was obtained from the DMRG (block) iteration, where an undesired state first appeared as the ground state of the Harmonic Davidson procedure.

The shift ω was then taken to lie on the correct side of the desired state in this iteration. In this simple manner, we found that we could obtain a suitable shift for a given root with at most two to three guesses.

To determine the symmetries of the excitations in the DMRG calculations we used the following method. Firstly, spin symmetries were obtained from the expectation value of S^2. To obtain the spatial symmetries, we first assumed that the ground-state Ψ_0 was of A_1 symmetry (as in experiment). For the excited states, we examined "dipole" type matrix elements $\langle\Psi_0|n_0^\alpha + n_0^\beta - n_1^\alpha - n_1^\beta|\Psi_i\rangle$ (essentially a dipole transition element along the short-axis of the acene; 0 and 1 refer to atom labels in Fig. 3.2.) For singlet excited states a non-vanishing dipole then implied B_2 symmetry, while a vanishing dipole implied A_1 symmetry. For the triplet excited states, all such matrix elements vanish. However, we could still determine the spatial symmetry through the expectation value $\langle\Psi_0|n_0^\alpha - n_1^\alpha|\Psi_i\rangle$ since $n_0^\alpha - n_1^\alpha$ does not preserve spin symmetry and creates a residual expectation value from which one can determine the spatial symmetry of the excited state.

To obtain the orbital character of the excitations, we calculated transition one-particle density matrices $\langle\Psi_0|a_i^\dagger a_j|\Psi_i\rangle$, where Ψ_i denotes the ith excited state and identified the largest matrix elements.

We further calculated the excitation spectrum (in the same π-active space as the DMRG calculations) with the Equation-Of-Motion Coupled Cluster Singles and Doubles method (EOM-CCSD) [34] using the DALTON package[35].

3.3.2 Comparison of Excited-state algorithms for DMRG by SA, HD, and SA-HD

The ground state DMRG energies for the acenes are given in Table 3.1. Tables 3.2, 3.3, 3.4, and 3.5 contain the first seven $\pi - \pi^*$ excitation energies for each acene, while Fig. 3.3 displays them in graphical form. Under C_{2v} symmetry, the only two possible representations of the $\pi - \pi^*$ excited states are $^{1,3}A_1$ and $^{1,3}B_2$. Experimentally, there are three well-documented singlet bands that appear in the visible spectrum [36, 37]. The α-band and β-band correspond to a polarization along the long axis and the p-band corresponds to a transverse polarization. We observed the α-transition as the lowest singlet excitation in each acene. Neither the p-band nor the β-band appeared within the first eight states of each acene. Instead, for the case of naphthalene, the p-band emerged at 8.42 eV (state 19). The p-band normally appears lower in the spectrum, but the absence of dynamic $\sigma - \pi$ correlations is responsible for its artificially high excitation energy here. This is consistent with previous studies of acenes using Complete-Active-Space Self-Consistent-Field (CASSCF) and Complete-Active-Space Moller-Plesset second order perturbation theory (CASMP2) theory [38–40]. Triplet excitations are somewhat harder to measure experimentally. We observe that the triplet excitation energies decrease in energy more rapidly with system size than the singlet excitations. Thus while in naphthalene and anthracene there is one triplet level between the first two singlet excitations, in naphthacene and pentacene there are two.

Table 3.2: DMRG excitation energies for naphthalene ($C_{10}H_8$) obtained with the SA-D, HD and SA-HD algorithms. All energies are in eV. State 0 refers to the ground-state, and SA[m-n] refers to a state-average over all states from the mth to nth excited state. Numbers in parentheses give the number of DMRG states M. The "Exact (HD(500))" numbers are the (near-exact) excitation energies, while other entries give the errors from this result. The "Excitation" row gives the character of the excitation where 1 denotes HOMO, 2 denotes HOMO-1, $1'$ denotes LUMO, $2'$ denotes LUMO+1 and so on. The last column gives the mean improvement in the excitation energy over the SA [0-7] D result with the same M. n.c. denotes no convergence.

Method	State								Mean
	1^1A_1	1^3B_2	2^1A_1	1^3A_1	2^3B_2	3^3B_2	2^3A_1	3^1A_1	Improvement
Excitation		$1 \to 1'$ $2 \to 2'$	$2 \to 1'$ $1 \to 2'$	$2 \to 1'$ $1 \to 2'$	$2 \to 2'$ $1 \to 1'$	$3 \to 1'$ $1 \to 3'$	$4 \to 1'$ $1 \to 4'$	$3 \to 2'$ $2 \to 3'$	

Table 3.2 (Continued)

Method	State								Mean
	1^1A_1	1^3B_2	2^1A_1	1^3A_1	2^3B_2	3^3B_2	2^3A_1	3^1A_1	Improvement
Excitation		$1 \to 1'$ $2 \to 2'$	$2 \to 1'$ $1 \to 2'$	$2 \to 1'$ $1 \to 2'$	$2 \to 2'$ $1 \to 1'$	$3 \to 1'$ $1 \to 3'$	$4 \to 1'$ $1 \to 4'$	$3 \to 2'$ $2 \to 3'$	
Exact (HD(500))	0.00	2.86	4.08	4.34	4.63	4.70	5.51	5.87	
SA [0-7] D (50)	0.13	0.09	0.21	0.46	0.18	0.15	0.26	0.19	
SA [0-3] D (50)	0.11	0.17	0.18	0.34					0.02
SA [3-7] HD (50)				0.46	0.17	0.18	0.24	0.25	−0.01
HD (50)	0.04	0.05	0.08	n.c.	n.c.	n.c.	n.c.	0.08	0.09
SA [2-3] HD (50)			0.22	0.25					0.10
SA [0-7] D (100)	0.01	0.02	0.02	0.03	0.02	0.02	0.02	0.02	
SA [0-3] D (100)	0.01	0.01	0.01	0.02					0.01
SA [3-7] HD (100)				0.03	0.02	0.02	0.02	0.02	0.00
HD (100)	0.00	0.01	0.01	0.01	0.01	n.c	0.01	0.01	0.01
SA [0-7] D (250)	0.00	0.00	0.00	0.00	0.00	0.00	0.00	0.02	

Table 3.2 (Continued)

Method	State								Mean
	1^1A_1	1^3B_2	2^1A_1	1^3A_1	2^3B_2	3^3B_2	2^3A_1	3^1A_1	Improvement
Excitation		$1 \rightarrow 1'$ $2 \rightarrow 2'$	$2 \rightarrow 1'$ $1 \rightarrow 2'$	$2 \rightarrow 1'$ $1 \rightarrow 2'$	$2 \rightarrow 2'$ $1 \rightarrow 1'$	$3 \rightarrow 1'$ $1 \rightarrow 3'$	$4 \rightarrow 1'$ $1 \rightarrow 4'$	$3 \rightarrow 2'$ $2 \rightarrow 3'$	
SA [0-3] D (250)	0.00	0.00	0.00	0.00					0.00
SA [3-7] HD (250)				0.00	0.00	0.00	0.00	0.00	0.00
HD (250)	0.00	0.00	0.00	0.00	0.00	0.00	0.00	0.00	0.00
SA [0-7] D (500)	0.00	0.00	0.00	0.00	0.00	0.00	0.00	0.00	
SA [0-3] D (500)	0.00	0.00	0.00	0.00					0.00
SA [3-7] HD (500)				0.00	0.00	0.00	0.00	0.00	0.00

Table 3.3: DMRG excitation energies for anthracene ($C_{14}H_{10}$). Refer to table 3.2 for details.

Method	State								Mean
	1^1A_1	1^3B_2	2^1A_1	2^3B_2	1^3A_1	3^3B_2	2^3A_1	3^1A_1	Improvement
Excitation		$1 \rightarrow 1'$ $2 \rightarrow 2'$ $3 \rightarrow 3'$	$2 \rightarrow 1'$ $1 \rightarrow 2'$	$3 \rightarrow 1'$ $1 \rightarrow 3'$	$2 \rightarrow 1'$ $1 \rightarrow 2'$	$2 \rightarrow 2'$	$4 \rightarrow 1'$ $1 \rightarrow 4'$	$2 \rightarrow 3'$ $3 \rightarrow 2'$	
Exact(HD(500))	0.00	2.08	3.57	3.71	3.85	4.46	4.73	4.80	
SA [0-7] D (50)	0.40	0.45	0.75	0.65	1.28	0.77	0.82	0.91	
SA [0-3] D (50)	0.29	0.24	0.46	0.41					0.21
SA [3-7] HD (50)				0.73	0.58	0.60	0.47	0.69	0.27
HD (50)	0.12	0.13	0.40	n.c.	n.c.	n.c.	n.c.	n.c.	0.32
SA [2-3] HD (50)			0.49	0.41					0.25
SA [0-7] D (100)	0.12	0.12	0.15	0.15	0.25	0.23	0.18	0.19	
SA [0-3] D (100)	0.07	0.07	0.10	0.09					0.05

Table 3.3 (Continued)

Method	State								Mean
	1^1A_1	1^3B_2	2^1A_1	2^3B_2	1^3A_1	3^3B_2	2^3A_1	3^1A_1	Improvement
Excitation		$1 \rightarrow 1'$ $2 \rightarrow 2'$ $3 \rightarrow 3'$	$2 \rightarrow 1'$ $1 \rightarrow 2'$	$3 \rightarrow 1'$ $1 \rightarrow 3'$	$2 \rightarrow 1'$ $1 \rightarrow 2'$	$2 \rightarrow 2'$	$4 \rightarrow 1'$ $1 \rightarrow 4'$	$2 \rightarrow 3'$ $3 \rightarrow 2'$	
SA [3-7] HD (100)				0.15	0.20	0.20	0.16	0.28	0.00
HD (100)	0.01	0.03	0.05	0.04	n.c.	n.c.	n.c.	n.c.	0.10
SA [5-6] HD (100)						0.13	0.22		0.03
SA [6-7] HD (100)							0.14	0.12	0.09
SA [0-7] D (250)	0.01	0.01	0.01	0.02	0.03	0.02	0.02	0.02	
SA [0-3] D (250)	0.00	0.00	0.01	0.01					0.01
SA [3-7] HD (250)				0.02	0.03	0.02	0.02	0.09	−0.01
HD (250)	0.00	0.00	0.00	0.00	0.00	0.00	0.00	0.00	0.02
SA [0-7] D (500)	0.00	0.00	0.00	0.00	0.00	0.00	0.00	0.00	
SA [0-3] D (500)	0.00	0.00	0.00	0.00					0.00

Table 3.3 (Continued)

Method	State								Mean
	1^1A_1	1^3B_2	2^1A_1	2^3B_2	1^3A_1	3^3B_2	2^3A_1	3^1A_1	Improvement
Excitation		$1 \rightarrow 1'$ $2 \rightarrow 2'$ $3 \rightarrow 3'$	$2 \rightarrow 1'$ $1 \rightarrow 2'$	$3 \rightarrow 1'$ $1 \rightarrow 3'$	$2 \rightarrow 1'$ $1 \rightarrow 2'$	$2 \rightarrow 2'$	$4 \rightarrow 1'$ $1 \rightarrow 4'$	$2 \rightarrow 3'$ $3 \rightarrow 2'$	
SA [3-7] HD (500)				0.00	0.00	0.00	0.00	0.00	0.00

Table 3.4: DMRG excitation energies for naphthacene ($C_{18}H_{12}$). Refer to table 3.2 for details.

Method	State								Mean
	1^1A_1	1^3B_2	2^3B_2	2^1A_1	1^3A_1	3^3B_2	4^3B_2	1^1B_2	Improvement
Excitation		$1 \to 1'$ $3 \to 3'$	$3 \to 1'$ $1 \to 3'$	$2 \to 1'$ $1 \to 2'$	$2 \to 1'$ $1 \to 2'$	$3 \to 2'$ $2 \to 3'$	$5 \to 1'$ $1 \to 5'$	$4 \to 1'$ $1 \to 4'$	
Exact(HD(500))	0.00	1.52	2.95	3.27	3.50	3.93	4.02	4.23	
SA [0-7] D (50)	0.71	0.81	1.07	1.33	1.75	1.45	1.51	1.70	
SA [0-3] D (50)	0.50	0.48	0.66	0.92					0.34
SA [2-7] HD (50)			0.20	1.04	1.25	1.39	1.34	1.34	0.38
SA [3-7] HD (50)				n.c.	n.c.	n.c.	n.c.	n.c.	0.00
HD (50)	0.20	0.27	n.c.	n.c.	n.c.	n.c.	n.c.	n.c.	0.52
SA [1-2] HD (50)		1.43	0.95						−0.25
SA [2-3] HD (50)			0.67	0.84					0.45
SA [0-7] D (100)	0.27	0.28	0.32	0.40	0.58	0.47	0.41	0.50	

Table 3.4 (Continued)

Method	State								Mean
	1^1A_1	1^3B_2	2^3B_2	2^1A_1	1^3A_1	3^3B_2	4^3B_2	1^1B_2	Improvement
Excitation		$1 \rightarrow 1'$ $3 \rightarrow 3'$	$3 \rightarrow 1'$ $1 \rightarrow 3'$	$2 \rightarrow 1'$ $1 \rightarrow 2'$	$2 \rightarrow 1'$ $1 \rightarrow 2'$	$3 \rightarrow 2'$ $2 \rightarrow 3'$	$5 \rightarrow 1'$ $1 \rightarrow 5'$	$4 \rightarrow 1'$ $1 \rightarrow 4'$	
SA [0-3] D (100)	0.12	0.14	0.16	0.20					0.16
SA [2-7] HD (100)			0.33	0.40	0.57	0.45	0.39	0.54	0.00
SA [3-7] HD (100)				n.c.	n.c.	n.c.	n.c.	n.c.	0.00
HD (100)	0.03	0.06	0.08	0.11	n.c.	n.c.	n.c.	n.c.	0.25
SA [0-7] D (250)	0.03	0.04	0.04	0.06	0.08	0.08	0.06	0.07	
SA [0-3] D (250)	0.01	0.01	0.02	0.03					0.03
SA [3-7] HD (250)				0.05	0.07	0.07	0.06	0.09	0.00
HD (250)	0.00	0.00	0.00	n.c.	n.c.	0.02	0.01	0.01	0.05
SA [0-7] D (500)	0.00	0.00	0.00	0.01	0.01	0.01	0.01	0.01	
SA [0-3] D (500)	0.00	0.00	0.00	0.00					0.00
SA [3-7] HD (500)				0.01	0.01	0.01	0.01	0.01	0.00

Table 3.5: DMRG excitation energies for pentacene ($C_{22}H_{14}$). Refer to table 3.2 for details.

Method	State								Mean
	1^1A_1	1^3B_2	2^3B_2	2^1A_1	1^3A_1	3^3B_2	4^3B_2	1^1B_2	Improvement
Excitation		$1 \to 1'$ $2 \to 2'$	$2 \to 1'$ $1 \to 2'$	$3 \to 1'$ $1 \to 3'$	$3 \to 1'$ $1 \to 3'$	$3 \to 2'$ $2 \to 3'$	$4 \to 1'$ $1 \to 4'$ $2 \to 2'$	$1 \to 5'$ $5 \to 1'$	
Exact(HD(500))	0.00	1.15	2.39	3.10	3.15	3.30	3.43	3.88	
SA [0-7] D (50)	1.10	1.55	1.79	1.86	2.31	2.29	2.26	2.38	
SA [0-3] D (50)	0.72	0.72	0.98	1.24					0.66
SA [2-7] HD (50)			1.23	1.62	1.88	1.75	1.97	1.95	0.41
SA [3-7] HD (50)				n.c.	n.c.	n.c.	n.c.	n.c.	0.00
HD (50)	0.29	0.40	n.c.	n.c.	n.c.	n.c.	n.c.	n.c.	0.98
SA [2-3] HD (50)			0.68	1.21					0.88
SA [0-7] D (100)	0.44	0.48	0.52	0.70	0.87	0.80	0.82	0.87	

Table 3.5 (Continued)

Method	State								Mean
	1^1A_1	1^3B_2	2^3B_2	2^1A_1	1^3A_1	3^3B_2	4^3B_2	1^1B_2	Improvement
Excitation		$1 \rightarrow 1'$ $2 \rightarrow 2'$	$2 \rightarrow 1'$ $1 \rightarrow 2'$	$3 \rightarrow 1'$ $1 \rightarrow 3'$	$3 \rightarrow 1'$ $1 \rightarrow 3'$	$3 \rightarrow 2'$ $2 \rightarrow 3'$	$4 \rightarrow 1'$ $1 \rightarrow 4'$ $2 \rightarrow 2'$	$1 \rightarrow 5'$ $5 \rightarrow 1'$	
SA [0-3] D (100)	0.31	0.33	0.34	0.38					0.20
SA [2-7] HD (100)			0.47	0.56	0.75	0.67	0.56	0.69	0.15
SA [3-7] HD (100)				n.c.	n.c.	n.c.	n.c.	n.c.	0.00
HD (100)	0.04	0.09	0.14	n.c.	n.c.	n.c.	n.c.	n.c.	0.39
SA [0-7] D (250)	0.06	0.08	0.10	0.12	0.15	0.16	0.12	0.15	
SA [0-3] D (250)	0.02	0.02	0.03	0.04					0.06
SA [3-7] HD (250)				0.09	0.10	0.12	0.10	0.12	0.03
HD (250)	0.00	0.01	0.01	0.02	n.c.	n.c.	n.c.	n.c.	0.08
SA [0-7] D (500)	0.00	0.01	0.01	0.01	0.02	0.02	0.02	0.02	
SA [0-3] D (500)	0.00	0.00	0.00	0.00					0.01

Table 3.5 (Continued)

Method	State								Mean
	1^1A_1	1^3B_2	2^3B_2	2^1A_1	1^3A_1	3^3B_2	4^3B_2	1^1B_2	Improvement
Excitation		$1 \rightarrow 1'$ $2 \rightarrow 2'$	$2 \rightarrow 1'$ $1 \rightarrow 2'$	$3 \rightarrow 1'$ $1 \rightarrow 3'$	$3 \rightarrow 1'$ $1 \rightarrow 3'$	$3 \rightarrow 2'$ $2 \rightarrow 3'$	$4 \rightarrow 1'$ $1 \rightarrow 4'$ $2 \rightarrow 2'$	$1 \rightarrow 5'$ $5 \rightarrow 1'$	
SA [3-7] HD (500)				0.01	0.01	0.02	0.02	0.02	0.00

Table 3.6: DMRG excitation energies for the higher excited states of naphthalene ($C_{10}H_8$). Refer to table 3.2 for details.

Method	State						Mean
	2^3A_1	3^1A_1	4^3B_2	3^3A_1	1^1B_2	4^1A_1	Improvement
Excitation	$4 \rightarrow 1'$ $1 \rightarrow 4'$	$3 \rightarrow 2'$ $2 \rightarrow 3'$	$4 \rightarrow 2'$ $2 \rightarrow 4'$	$2 \rightarrow 3'$ $3 \rightarrow 2'$	$1 \rightarrow 3'$ $3 \rightarrow 1'$ $4 \rightarrow 2'$ $2 \rightarrow 4'$	$4 \rightarrow 1'$ $1 \rightarrow 4'$	
Exact(HD(500))	5.51	5.87	6.28	6.48	6.84	6.84	
SA [0-11] D (50)	0.29	0.21	0.19	0.45	0.32	0.43	
SA [6-11] HDa (50)	0.29	0.20	0.17	0.46	0.35	0.43	0.00
HD (50)	n.c	0.08	n.c	n.c	n.c	n.c	0.13
SA [0-11] D (100)	0.03	0.03	0.03	0.03	0.05	0.06	
SA [6-11] HDa (100)	0.03	0.02	0.03	0.03	0.05	0.06	0.00
HD (100)	0.01	0.01	0.01	0.01	0.02	n.c	0.02

Table 3.6 (Continued)

Method	State						Mean
	2^3A_1	3^1A_1	4^3B_2	3^3A_1	1^1B_2	4^1A_1	Improvement
Excitation	$4 \rightarrow 1'$ $1 \rightarrow 4'$	$3 \rightarrow 2'$ $2 \rightarrow 3'$	$4 \rightarrow 2'$ $2 \rightarrow 4'$	$2 \rightarrow 3'$ $3 \rightarrow 2'$	$1 \rightarrow 3'$ $3 \rightarrow 1'$ $4 \rightarrow 2'$ $2 \rightarrow 4'$	$4 \rightarrow 1'$ $1 \rightarrow 4'$	
SA [10-11] HDa (100)					0.04	0.04	0.02
SA [0-11] D (250)	0.00	0.00	0.00	0.00	0.00	0.00	
SA [6-11] HDa (250)	0.00	0.00	0.00	0.00	0.00	0.00	0.00
HD (250)	0.00	0.00	0.00	0.00	0.00	n.c	0.00
SA [10-11] HDa (250)					0.00	0.00	0.00
SA [0-11] D (500)	0.00	0.00	0.00	0.00	0.00	0.00	
SA [6-11] HDa (500)	0.00	0.00	0.00	0.00	0.00	0.00	0.00

Comparing the accuracies of the SA-D, HD, and SA-HD calculations we observe that as expected, (other than by the size of the DMRG basis M), the accuracy in the excitation energies is determined primarily by the number of eigenvectors in the state-average. Consequently the traditional SA-D algorithm yielded the lowest accuracy (as it averages over all states between the ground state and excited state of interest) while the HD calculations were correspondingly the most accurate since they targeted a single state at a time. The accuracy of the SA-HD calculations lay somewhere in between depending on the number of states used in the average. In all cases, the differences between the various algorithms was most marked for the smaller sizes M of the DMRG basis, as for larger M all the wavefunctions become essentially exact. We would expect the differences to become more pronounced in larger systems, where we are unable to use a sufficiently large M to reach exactness.

Regarding the stabilities of the various algorithms, we found that there were no difficulties in converging the DMRG sweeps to the correct states with the SA-D algorithm. The HD algorithm on the other hand exhibited the expected convergence difficulties characteristic of root-flipping for certain higher excited states. As previously discussed, the stability of the HD algorithm would increase with the size of the DMRG many-body basis M. In naphthacene, we required $M \geq 250$ to converge states 5-7 with the HD algorithm, while in pentacene, we required $M = 500$ to converge states 4-7. While the HD algorithm exhibited root-flipping, it was ameliorated with respect to simple eigenvector following (defined as following the n^{th} eigenvector in the block Davidson algorithm in successive DMRG iterations) because of the use of the shift ω. For example, with $M = 100$, the third excited state of naphthalene could not be converged with simple eigenvector following, but could be converged without

difficulty using the HD algorithm.

Including a sufficient number of states in the SA-HD algorithm restored the stability of the convergence. Certain "competing" states were particularly important for the state average, especially for smaller M. For all the acenes, the second and third excited states were examples of such states. Thus while the state averages SA[2-3] HD and SA[2-7] HD converged without difficulty, calculations using SA[3-7] HD did not, at least for smaller M.

As mentioned previously, rather than choosing a shift to target specific excited states, we could take the different approach of trying to find the excited states around the frequency of a given shift ω. In this way, we could piece together a complete spectrum by performing, say, SA-HD or SA-HDa calculations with successively higher shifts. To demonstrate this, we computed the excitation energies for states 6-11 for naphthalene using the SA-HDa algorithm with a shift chosen slightly above the state 7 excitation energy as estimated from the previous SA-HD [4-7] calculation. These are shown in table 3.6.

3.3.3 Comparison of DMRG and EOM-CC excitation energies in the acenes

The ground state EOM-CCSD energies for the acenes are summarized in Table 3.1. We used our near-exact DMRG(500) excitation energies to examine the accuracy of the EOM-CC method in acenes. The EOM-CCSD and the DMRG symmetries and excitation energies are shown in Fig. 3.3. For the larger acenes, the EOM-CCSD excited states are in a qualitatively different order as compared to

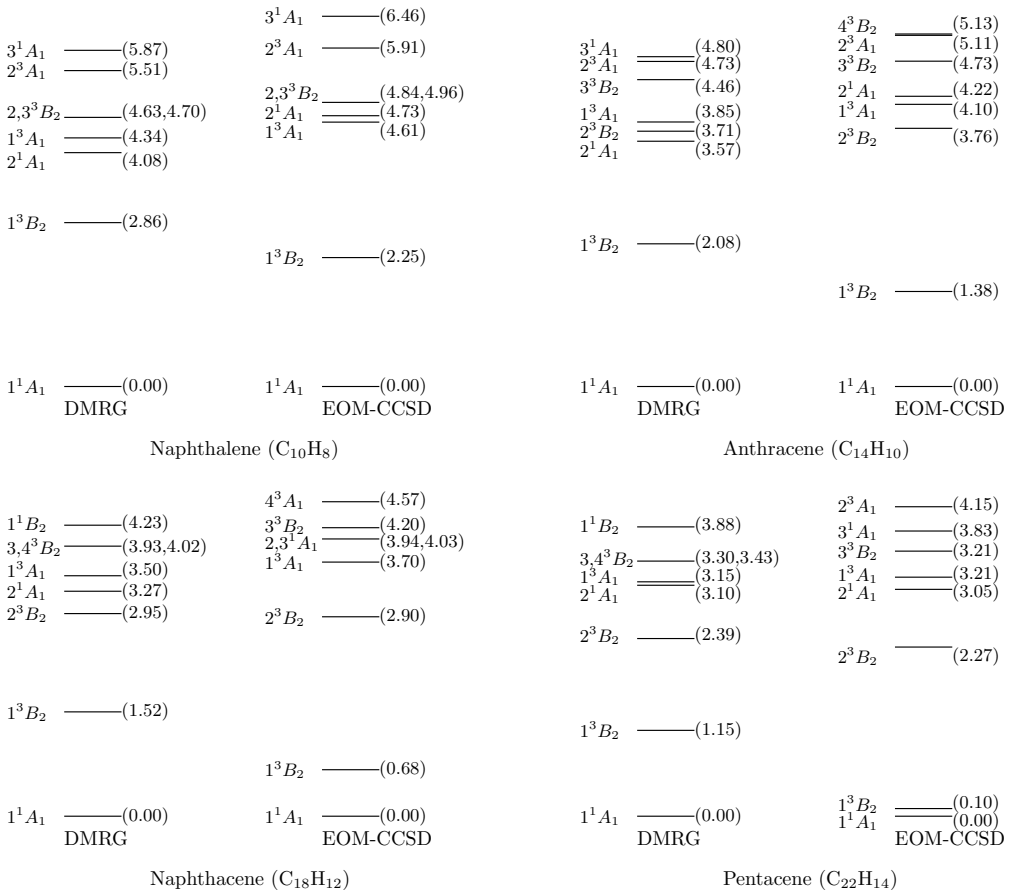

Figure 3.3: Comparison of DMRG and EOM-CCSD excitation energies for acenes. All energies in eV.

DMRG. Similarly, EOM-CCSD erroneously predicts a very small singlet-triplet gap for the longer acenes. This points to the necessity of including relatively high order correlation effects to accurately describe excitations in the acenes.

3.4 Conclusions

To overcome the computational and accuracy limitations of the traditional State-Averaged Davidson Algorithm, which requires both solving for and represent-

ing all states between the ground state and excited state of interest, we have investigated a number of new excited state algorithms within the context of the Density Matrix Renormalization Group (DMRG). In the *Harmonic Davidson* (HD) algorithm, using a shifted and inverted operator enabled us to directly solve for the excited state of interest. In the *State-Averaged Harmonic Davidson* (SA-HD) algorithm, we combined the HD method with an average over nearby excited states, to confer greater stability and overcome problems of root-flipping in the non-linear optimisation of the wavefunction.

To assess the accuracy, stability, and computational cost of these new methods we calculated the low-lying excited states in the acenes ranging from naphthalene to pentacene. We found that as expected, in addition to the size of the DMRG basis M used, the accuracy was primarily determined by the number of states used in the state average. Thus the State-Averaged Davidson approach gave the least accuracy, the Harmonic Davidson algorithm, the highest, and the State-Averaged Harmonic Davidson lay in between depending on how many nearby states were included. The State-Averaged Harmonic Davidson algorithm converged smoothly without root-flipping so long as nearby "competing" states were included in the average.

We also argued that through the shift ω in the Harmonic Davidson algorithms we could piece together a complete excitation spectrum by targeting different regions with successively higher shifts. This we demonstrated by calculating some higher lying excited states in naphthalene.

Within the basis used, our DMRG excitation energies are near-exact and we have used them to assess the accuracy of the EOM-CCSD method in the acenes. We found that the EOM-CCSD excitation spectrum was qualitatively different

from that of the DMRG for the larger acenes, which demonstrates the necessity of including higher-order correlations to properly describe the electronic spectrum of conjugated quasi-one-dimensional molecules.

Finally, we observe that the Harmonic Davidson algorithms studied here are quite general methods and are not limited to the Density Matrix Renormalisation Group. Thus they may be useful also to target excited states in other multi-reference theories, such as Complete Active Space Self-Consistent-Field theory.

BIBLIOGRAPHY

[1] Dorando, J.J. and Hachmann, J. and Chan, Garnet Kin-Lic, J. Chem. Phys. **127**, 84109 (2007).

[2] D. Yaron, E. E. Moore, Z. Shuai, and J. Brédas, J. Chem. Phys. **108**, 7451 (1998).

[3] S. R. White and R. L. Martin, J. Chem. Phys. **110**, 4127 (1999).

[4] Ö. Legeza, J. Röder, and B. A. Hess, Phys. Rev. B **67**, 125114 (2003).

[5] G. Fano, F. Ortolani, and L. Ziosi, J. Chem. Phys. **108**, 9246 (1998).

[6] Z. Shuai, J. L. Brédas, S. K. Pati, and S. Ramasesha, Proc. of SPIE **3145**, 293 (1997).

[7] G. K.-L. Chan and M. Head-Gordon, J. Chem. Phys. **116**, 4462 (2002).

[8] K. Hallberg, Advances in Physics **55**, 477 (2006).

[9] Ö. Legeza, J. Röder, and B. A. Hess, Mol. Phys. **101**, 2019 (2003).

[10] G. Moritz, A. Wolf, and M. Reiher, J. Chem. Phys. **123**, 184105 (2005).

[11] G. K.-L. Chan, M. Kállay, and J. Gauss, J. Chem. Phys. **121**, 6110 (2004).

[12] J. Hachmann, W. Cardoen, and G. K.-L. Chan, J. Chem. Phys. **125**, 144101 (2006).

[13] J. Hachmann, J. J. Dorando, M. Avilés, and G. K.-L. Chan, J. Chem. Phys. **127**, 134309 (2007).

[14] B. O. Roos, Adv. Chem. Phys. **69**, 399 (1987).

[15] U. Schollwöck, Rev. Mod. Phys. **77**, 259 (2005).

[16] K. Hallberg, Density matrix renormalization: A review of the method and its applications, in *Theoretical Methods for Strongly Correlated Electrons*, edited by D. Senechal, A.-M. Tremblay, and C. Bourbonnais, CRM Series in Mathematical Physics, New York, 2003, Springer.

[17] K. K. Docken and J. Hinze, J. Chem. Phys. **57**, 4928 (1972).

[18] Y. G. Khait, A. I. Panin, and A. S. Averyanov, Int. J. Quantum Chem. **54**, 329 (1995).

[19] P. J. Knowles and H. J. Werner, Theor. Chim. Acta **4**, 95 (1992).

[20] M. R. Hoffmann, C. D. Sherill, M. L. Leininger, and H. F. Schaefer, Chem. Phys. Lett. **355**, 183 (2002).

[21] E. Cancès, H. Galicher, and M. Lewin, J. Comp. Phys. **212**, 73 (2006).

[22] R. B. Morgan, Lin. Alg. Appl. **154-156**, 289 (1991).

[23] Z. Bai, J. Demmel, J. Dongarra, A. Ruhe, and H. van der Vorst, *Templates for the solution of algebraic eigenvalue problems: a practical guide*, SIAM, Philadelphia, PA, 2000.

[24] G. L. G. Sleijpen and H. A. van der Vorst, SIAM J. Matrix Anal. Appl. **17**, 401 (1996).

[25] A. Tackett and M. D. Ventra, Phys. Rev. B **66**, 245104 (2002).

[26] G. K.-L. Chan, J. Chem. Phys. **120**, 3172 (2004).

[27] M. Crouzeix, B. Philippe, and M. Sadkane, J. Sci. Comput. **15**, 62 (1994).

[28] Y. Saad, *Numerical Methods for Large Eigenvalue Problems*, Manchester University Press, Manchester, U.K., 1993.

[29] E. R. Davidson, J. Comput. Phys. **17**, 87 (1975).

[30] J. Olsen, P. Jørgensen, and J. Simons, Chem. Phys. Lett. **169**, 463 (1990).

[31] W. J. Hehre, R. F. Stewart, and J. A. Pople, J. Chem. Phys. **51**, 2657 (1969).

[32] T. D. Crawford et al., PSI 3.2 (2003), see www.psicode.org.

[33] A. O. Mitrushenkov, R. Linguerri, P. Palmieri, and G. Fano, J. Chem. Phys. **119**, 4148 (2003).

[34] R. J. Bartlett and M. Musiał, Rev. Mod. Phys. **79**, 291 (2007).

[35] C. Angeli et al., DALTON, a molecular electronic structure program, release 2.0 (2005), see www.kjemi.uio.no/software/dalton/.

[36] E. S. Kadantsev, M. J. Stott, and A. Rubio, J. Chem. Phys. **124**, 134901 (2006).

[37] H. H. Heinze, A. Görling, and N. Rösch, J. Chem. Phys. **113**, 2088 (2000).

[38] H. Nakatsuji, M. Komori, and O. Kitao, Chem. Phys. Lett. **142**, 446 (1987).

[39] Y. Kawashima, T. Hashimoto, H. Nakano, and K. Hirao, Theor. Chim. Acta **102**, 49 (1999).

[40] T. Hashimoto, H. Nakano, and K. Hirao, J. Chem. Phys. **104**, 6244 (1996).

CHAPTER 4

DENSITY MATRIX RENORMALIZATION GROUP - RESPONSE THEORY[1]

4.1 Introduction

The density matrix renormalisation group method [2] is now established as a powerful tool for "difficult" electronic structure problems in physics and chemistry [3–6]. In molecular systems, it has been used to describe multireference correlation in medium-sized active spaces (20-30 active orbitals) for small molecules with complex bonding [7–10], as well as a local multireference correlation method in extended long-chain molecules, e.g. to describe excited states in conjugated molecules, using large active spaces of up to 100 active orbitals [11].

Response properties, which represent the change in an observable as a function of an applied perturbation, are of interest in many physical and chemical applications. For example, geometry optimisation and vibrational frequencies both require the response of the energy with respect to changes in the nuclear coordinates, quantities usually known as nuclear derivatives. Nuclear derivatives are examples of static response properties because the perturbation does not depend on time. It is also common to consider frequency-dependent (i.e dynamical) response properties where the applied perturbation is a function of time. The most common time-dependent perturbations are fluctuating electric and/or magnetic fields. In extended systems, the frequency dependence of the response gives insight into the elementary excitations of the system and this can be used characterise the nature of the electronic ground-state [12].

[1]Parts of this chapter were published in JCP May 13, 2008[1]

In many electronic structure methods, response properties are obtained by so-called "analytic" techniques. Analytic response theories of this kind at linear and higher orders have been developed and implemented for most electronic structure methods, including Hartree-Fock [13], density functional [14], coupled cluster [15], multi-configurational self-consistent [16], and Moller-Plesset perturbation theories [17]. A review of the formal theory and some of these developments may be found in Ref. [18]. The name "analytic" is used because the response properties evaluated (e.g. the perturbed energies) correspond strictly to derivatives of the ground-state energies or quasi-energies [18–20] evaluated in the presence of the perturbation, using the same level of approximation for the (quasi-)energy with and without the perturbation.

In contrast, response properties in the density matrix renormalisation group have typically been obtained using a quite different approach that appears natural within the DMRG. In the DMRG, the wavefunction is expanded in a set of many-electron states that are adapted to the state of interest. To obtain a response property, one can choose to solve response equations using basis states that are adapted not only to the zeroth order state but also to the calculation of the state's response. These response methods, which have proven very useful in the calculation of dynamical response in DMRG model Hamiltonian calculations, go by the name of Lanczos-vector DMRG [21], correction-vector DMRG [22, 23], and dynamical DMRG [24]. More recently, explicit real-time propagation of the DMRG equations has also been used to obtain high-frequency response properties [25]. A recent review of all these DMRG response methods can be found in Ref. [26].

In the current work we return to an analytic formulation of response theory

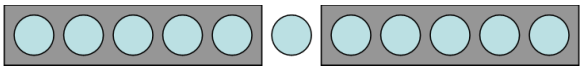

Figure 4.1: One-site DMRG block configuration. $\mathbf{L}^n$ tensors are associated with the left block, $\mathbf{R}^n$ tensors with the right block, and the middle site is site p in Eq. 4.1.

within the density matrix renormalisation group, in a way that parallels the description of response properties in other electronic structure methods. We use as our starting point the wavefunction based (matrix-product state) formulation of the DMRG [3, 6, 27, 28]. As we shall see, the analytic response approach has a number of strengths and weaknesses compared to earlier DMRG response methods. To understand these strengths and weaknesses better, we perform a series of benchmark static and frequency-dependent polarisability calculations on oligo-diacetylenes that compare the behaviour of the earlier dynamical DMRG method with our analytic response DMRG approach. Using our data we examine the scaling of the polarisability as a function of the number of monomer units.

4.2 Time-independent and time-dependent density matrix renormalization group equations

The density matrix renormalisation group works with a variational ansatz for the wavefunction Ψ. The simplest ansatz to analyse is the "one-site" form of the DMRG wavefunction [5, 28, 29]. For the block-configuration depicted in Fig.

4.1, the wavefunction takes the form

$$|\Psi\rangle = \sum_{\{n\}} \mathbf{L}^{n_1} \dots \mathbf{L}^{n_{p-1}} \mathbf{C}^{n_p} \mathbf{R}^{n_{p+1}} \dots \mathbf{R}^{n_k} |n_1 \dots n_k\rangle \tag{4.1}$$

The $\mathbf{L}^n$ and $\mathbf{R}^n$ renormalisation tensors satisfy the orthogonality conditions

$$\sum_n \mathbf{L}^{n\dagger} \mathbf{L}^n = \mathbf{1} \tag{4.2}$$

$$\sum_n \mathbf{R}^n \mathbf{R}^{n\dagger} = \mathbf{1} \tag{4.3}$$

and formally define the sequence of renormalisation transformations to obtain basis states $\{l\}$, $\{r\}$ for the left and right blocks in Fig. 4.1. (Note that in Eqs. (4.2), (4.3) we have dropped the sub-indices on n as these conditions are not specific to any given site. We will use a similar convention throughout to avoid a proliferation of unnecessary indices). The coefficient tensor $\mathbf{C}^n$ gives the expansion coefficients of the wavefunction in the superblock basis $\{l\} \otimes \{n_p\} \otimes \{r\}$. When viewed as a flattened vector $\mathbf{c}$ it satisfies the normalisation condition $\mathbf{c}^\dagger \mathbf{c} = 1$.

The DMRG energy is minimised when the tensors satisfy certain equations. For the coefficient vector, this is a time-independent effective Schrödinger equation

$$\mathbf{H}\mathbf{c} = E\mathbf{c} \tag{4.4}$$

where the effective renormalised superblock Hamiltonian $\mathbf{H}$ satisfies $E = \langle\Psi|H|\Psi\rangle = \mathbf{c}^\dagger \mathbf{H} \mathbf{c}$. The renormalisation tensors at each position are defined from the coefficient tensor at the same position, i.e. $\mathbf{C}^n$ defines $\mathbf{L}^n$ and $\mathbf{R}^n$, via intermediate left and right density matrices. To obtain the left density matrix $\mathbf{D}_L$, we view the tensor $\mathbf{C}^n$ as a matrix $\mathbf{C}$ indexed by $(ln), r$, where l is the row index of $\mathbf{C}^n$, then $\mathbf{D}_L = \mathbf{C}\mathbf{C}^\dagger$. The right density matrix $\mathbf{D}_R$ is defined in a similar way, we view the tensor $\mathbf{C}^n$ as a matrix $\mathbf{C}$ indexed by $l, (nr)$, where r is the column

index of $\mathbf{C}^n$, and $\mathbf{D}_R = \mathbf{C}^\dagger\mathbf{C}$. The renormalisation tensors $\mathbf{L}^n$, $\mathbf{R}^n$, when viewed as matrices $\mathbf{L}, \mathbf{R}$ in the appropriate way, are obtained from the M eigenvectors (with largest weights) of the the density matrix $\mathbf{D}_L$ and $\mathbf{D}_R$ respectively i.e.

$$\mathbf{D}_L\mathbf{L} = \mathbf{L}(\sigma_1 \ldots \sigma_M)_{\text{diag}}, \;\; \sigma_1 \geq \sigma_2 \ldots \geq \sigma_M, \; (\mathbf{L}_{(ln)i} = \mathbf{L}^n_{li}) \tag{4.5}$$

$$\mathbf{D}_R\mathbf{R} = \mathbf{R}(\sigma_1 \ldots \sigma_M)_{\text{diag}}, \;\; \sigma_1 \geq \sigma_2 \ldots \geq \sigma_M, \; (\mathbf{R}_{(rn)i} = \mathbf{R}^n_{ir}) \tag{4.6}$$

More explicitly, writing the eigenvectors of the left and right density matrices as $\mathbf{l}^i$, $\mathbf{r}^i$,

$$\mathbf{D}_L\mathbf{l}^i = \mathbf{l}^i\sigma_i, \;\; \sigma_1 \geq \sigma_2 \geq \sigma_3 \ldots \tag{4.7}$$

$$\mathbf{D}_R\mathbf{r}^i = \mathbf{r}^i\sigma_i, \;\; \sigma_1 \geq \sigma_2 \geq \sigma_3 \ldots \tag{4.8}$$

$\mathbf{L}^n$, $\mathbf{R}^n$ are constructed by assigning the elements of the eigenvectors to the tensors in the following way

$$\mathbf{L}^n_{ji} = \mathbf{l}^i_{(nj)}, \;\; i = 1 \ldots M \tag{4.9}$$

$$\mathbf{R}^n_{ij} = \mathbf{r}^i_{(nj)}, \;\; i = 1 \ldots M \tag{4.10}$$

In Ref. [30], we showed that satisfying the solution conditions Eqs. (4.4), (4.5), (4.6) for $\mathbf{C}^n, \mathbf{L}^n, \mathbf{R}^n$ is formally equivalent to minimising the DMRG energy subject to normalisation and the orthogonality constraints (4.2), (4.3). We can formally extend the DMRG theory to time-dependent scenarios by making stationary the Dirac-Frenkel action $\langle\Psi|i\partial/\partial t - H|\Psi\rangle$ [13] subject to the same normalisation and orthogonality constraints. (Interestingly, the Dirac-Frenkel action has recently been independently rederived in the DMRG context in Ref. [31]). For the coefficient vector the time-evolution is then given by an effective time-dependent Schrödinger equation

$$i\partial_t\mathbf{c} = \mathbf{H}\mathbf{c} \tag{4.11}$$

The corresponding $\mathbf{L}^n$ and $\mathbf{R}^n$ remain defined by Eqs. (4.5), (4.6).

4.3 Coupled-perturbed density matrix renormalization group response equations

We now consider the effect of an external perturbation. We start with a time-independent perturbation V. In the superblock basis $\{l\}\otimes\{n_p\}\otimes\{r\}$, this yields the effective perturbation $\mathbf{V}$ which satisfies $\langle\Psi|V|\Psi\rangle = \mathbf{c}^\dagger\mathbf{V}\mathbf{c}$.

In response to this perturbation, the $\mathbf{L}^n, \mathbf{C}^n, \mathbf{R}^n$ tensors each can be expanded in orders of $|V|$, giving

$$\mathbf{L}^n = \mathbf{L}^{n[0]} + \mathbf{L}^{n[1]} + \ldots \tag{4.12}$$

$$\mathbf{C}^n = \mathbf{C}^{n[0]} + \mathbf{C}^{n[1]} + \ldots \tag{4.13}$$

$$\mathbf{R}^n = \mathbf{R}^{n[0]} + \mathbf{R}^{n[1]} + \ldots \tag{4.14}$$

Thus the first-order DMRG wavefunction for the block-configuration in Fig. 4.1 takes the general form

$$|\Psi^{[1]}\rangle = \sum_{\{n\}} \big[(\mathbf{L}^{n_1[1]}\ldots\mathbf{C}^{n_p[0]}\ldots\mathbf{R}^{n_k[0]}) + \ldots + (\mathbf{L}^{n_1[0]}\ldots\mathbf{C}^{n_p[1]}\ldots\mathbf{R}^{n_k[0]}) + \ldots + (\mathbf{L}^{n_1[0]}\ldots\mathbf{C}^{n_p[0]}\ldots\mathbf{R}^{n_k[1]})\big]\,|n_1 n_2\ldots n_k\rangle \tag{4.15}$$

We now derive the response equations satisfied by each of the quantities $\mathbf{L}^{n[1]}, \mathbf{C}^{n[1]}, \mathbf{R}^{n[1]}$. These are obtained by the perturbation expansion of the solution conditions (4.4), (4.5), (4.6). For the coefficient vector, this yields

$$(\mathbf{H}^{[0]} + \mathbf{\Delta H}^{[1]} + \mathbf{V}^{[1]} + \ldots)(\mathbf{c}^{[0]} + \mathbf{c}^{[1]} + \ldots) = (E^{[0]} + E^{[1]} + \ldots)(\mathbf{c}^{[0]} + \mathbf{c}^{[1]} + \ldots) \tag{4.16}$$

Note the first-order change in the Hamiltonian $\mathbf{\Delta H}^{[1]}$. This arises because the effective Hamiltonian in the superblock basis $\mathbf{H}$ depends on the renormalisation

tensors $\mathbf{L}^n, \mathbf{R}^n$ (which define the renormalised basis) and so first-order changes in those tensors lead to a first-order change in the effective Hamiltonian. (The construction of $\mathbf{\Delta H}^{[1]}$ is described later in Sec. 4.4). Gathering first-order terms and enforcing intermediate normalisation through the projector $\mathbf{Q} = \mathbf{1} - \mathbf{c}^{[0]}\mathbf{c}^{[0]\dagger}$ gives

$$(\mathbf{H}^{[0]} - E^{[0]}\mathbf{1})\mathbf{c}^{[1]} = -\mathbf{Q}(\mathbf{\Delta H}^{[1]} + \mathbf{V}^{[1]})\mathbf{c}^{[0]} \tag{4.17}$$

Because $\mathbf{\Delta H}^{[1]}$ depends on the first-order wavefunction through its dependence on the $\mathbf{L}^n, \mathbf{R}^n$ tensors, Eq. (4.17) must be solved self-consistently. It is therefore a coupled-perturbed response equation, analogous to the coupled-perturbed orbital equations that arise in the Hartree-Fock theory of response.

The first-order coefficients $\mathbf{C}^{n[1]}$ define first-order renormalisation tensors at the same site $\mathbf{L}^{n[1]}, \mathbf{R}^{n[1]}$. Viewing $\mathbf{C}^{n[0]}, \mathbf{C}^{n[1]}$ as a matrices in the appropriate fashion, we obtain first-order left and right density matrices

$$\mathbf{D}_L^{[1]} = \mathbf{C}^{[0]}\mathbf{C}^{[1]\dagger} + \mathbf{C}^{[1]}\mathbf{C}^{[0]\dagger}, \ (\mathbf{C}_{(nl),r} = \mathbf{C}^n_{lr}) \tag{4.18}$$

$$\mathbf{D}_R^{[1]} = \mathbf{C}^{[0]\dagger}\mathbf{C}^{[1]} + \mathbf{C}^{[1]\dagger}\mathbf{C}^{[0]}, \ (\mathbf{C}_{l,(nr)} = \mathbf{C}^n_{lr}) \tag{4.19}$$

In response to the change in the density matrices, the eigenvectors have a perturbation expansion

$$\mathbf{l}^i = \mathbf{l}^{i[0]} + \mathbf{l}^{i[1]} + \ldots \tag{4.20}$$

$$\mathbf{r}^i = \mathbf{r}^{i[0]} + \mathbf{r}^{i[1]} + \ldots \tag{4.21}$$

and we can set up corresponding response equations

$$(\mathbf{D}_L^{[0]} - \sigma_i\mathbf{1})\mathbf{l}^{i[1]} = -\mathbf{Q}_L\mathbf{D}_L^{[1]}\mathbf{l}^{i[0]} \tag{4.22}$$

$$(\mathbf{D}_R^{[0]} - \sigma_i\mathbf{1})\mathbf{r}^{i[1]} = -\mathbf{Q}_R\mathbf{D}_R^{[1]}\mathbf{r}^{i[0]} \tag{4.23}$$

where $\mathbf{Q}_L, \mathbf{Q}_R$ project out the span of $\mathbf{D}_L, \mathbf{D}_R$ respectively, i.e. $\mathbf{Q}_L = \mathbf{1} - \sum_{i=1}^{M} \mathbf{l}^{i[0]}\mathbf{l}^{i[0]\dagger}, \mathbf{Q}_R = \mathbf{1} - \sum_{i=1}^{M} \mathbf{r}^{i[0]}\mathbf{r}^{i[0]\dagger}$. We assign the elements of each of the M perturbed vectors $\mathbf{l}^{i[1]}, \mathbf{r}^{i[1]}$ according to Eq. (4.9), (4.10), to define $\mathbf{L}^{n[1]}, \mathbf{R}^{n[1]}$. The response equations for a time-dependent perturbation may be obtained in an analogous way as above. We consider for simplicity a perturbation with a single Fourier component,

$$V(t) = Ve^{i\omega t} + V^* e^{-i\omega t} \tag{4.24}$$

We expand the $\mathbf{L}^n, \mathbf{C}^n, \mathbf{R}^n$ tensors in terms of orders of $|V|$,

$$\mathbf{L}^n(t) = (\mathbf{L}^{n[0]} + \mathbf{L}^{n[1]}(t) + \ldots)e^{-iE^{[0]}t} \tag{4.25}$$

$$\mathbf{C}^n(t) = (\mathbf{C}^{n[0]} + \mathbf{C}^{n[1]}(t) + \ldots)e^{-iE^{[0]}t} \tag{4.26}$$

$$\mathbf{R}^n(t) = (\mathbf{R}^{n[0]} + \mathbf{R}^{n[1]}(t) + \ldots)e^{-iE^{[0]}t} \tag{4.27}$$

For the coefficient vector, we substitute this expansion into the effective time-dependent Schrödinger equation (4.11) and identify terms with frequencies ω, $-\omega$, giving

$$(\mathbf{H}^{[0]} - (E^{[0]} + \omega)\mathbf{1})\mathbf{c}^{[1]}(\omega) = -\mathbf{Q}(\mathbf{\Delta H}^{[1]}(\omega) + \mathbf{V}^{[1]})\mathbf{c}^{[0]} \tag{4.28}$$

$$(\mathbf{H}^{[0]} - (E^{[0]} - \omega)\mathbf{1})\mathbf{c}^{[1]}(-\omega) = -\mathbf{Q}(\mathbf{\Delta H}^{[1]}(-\omega) + \mathbf{V}^{[1]*})\mathbf{c}^{[0]} \tag{4.29}$$

where $\mathbf{Q}$ is the projector defined in Eq. (4.17). The first-order frequency perturbed wavefunctions then define first-order perturbed density matrices $\mathbf{D}_L(\omega), \mathbf{D}_L(-\omega), \mathbf{D}_R(\omega), \mathbf{D}_R(-\omega)$, which can be used to obtain $\mathbf{L}^{n[1]}(\omega), \mathbf{L}^{n[1]}(-\omega), \mathbf{R}^{n[1]}(\omega), \mathbf{R}^{n[1]}(-\omega)$ through Eqs. (4.22), (4.23).

4.3.1 Response properties

Once we obtain the first-order response of the DMRG wavefunction we can evaluate response properties of interest. We take as our example here the dipole-dipole response function or polarisability. For a uniform static electric field $\mathcal{E}_i$, the dipole moment is expanded as

$$\mu_i = \mu_i^{[0]} + \sum_j \alpha_{ij}\mathcal{E}_j + \ldots, \quad i, j \ldots \in x, y, z \tag{4.30}$$

which defines the static polarisability α_{ij} as the first-order change in the dipole moment. Within the DMRG response theory, the polarisability is therefore obtained as

$$\alpha_{ij} = \mathbf{c}^{[0]\dagger}\mu_i^{[0]}\mathbf{c}_j^{[1]} + \mathbf{c}_j^{[1]\dagger}\mu_i^{[0]}\mathbf{c}^{[0]} + \mathbf{c}^{[0]\dagger}\mu_{i(j)}^{[1]}\mathbf{c}^{[0]} \tag{4.31}$$

Here μ_i is the effective dipole operator in the superblock basis, and $\mathbf{c}_j^{[1]}$ is the first-order wavefunction in response to an electric field in the j direction. Note the additional contribution $\mu_{i(j)}^{[1]}$. This is the change in the effective dipole operator μ_i due to the response of the $\mathbf{L}^n$, $\mathbf{R}^n$ tensors to an applied field in the j direction. This quantity is constructed in a similar way to the effective Hamiltonian $\mathbf{\Delta H}^{[1]}$.

For a frequency dependent electric field $\mathcal{E}_i(t)$, we expand the dipole moment as

$$\mu_i(t) = \mu_i^{[0]} + \sum_j \int d\omega e^{-i\omega t}\alpha_{ij}(\omega)\mathcal{E}_j(\omega) + \ldots \quad i, j \ldots \in x, y, z \tag{4.32}$$

where $\alpha_{ij}(\omega)$ and $\mathcal{E}_j(\omega)$ are the ω frequency components of the frequency dependent polarisability and electric field. $\alpha_{ij}(\omega)$ contains two contributions, one from the $e^{i\omega t}$ component of the applied perturbation, one from the $e^{-i\omega t}$ component.

The final expression for $\alpha_{ij}(\omega)$ therefore reads as

$$\alpha_{ij}(\omega) = G_{ij}(\omega) + G_{ij}(-\omega) \tag{4.33}$$

$$G_{ij}(\omega) = \mathbf{c}^{[0]\dagger}\mu_i^{[0]}\mathbf{c}_j^{[1]}(\omega) + \mathbf{c}_j^{[1]\dagger}(\omega)\mu_i^{[0]}\mathbf{c}^{[0]} + \mathbf{c}^{[0]\dagger}\mu_{i(j)}^{[1]}(\omega)\mathbf{c}^{[0]} \tag{4.34}$$

$G_{ij}(\omega)$ and $G_{ij}(\omega)$ are obtained from two separate response calculations, solving Eq. (4.28), (4.29) respectively.

4.3.2 Comparison to other DMRG response theories

So far we have derived a DMRG theory of response that was based on expanding the solution conditions satisfied by the DMRG wavefunction in terms of the applied perturbation. This corresponds to an *analytic* theory of response in the following way. Consider a time-independent perturbation for simplicity. Let us consider minimising the energy of the DMRG wavefunction, for some fixed number of states M, with respect to the full Hamiltonian (with the perturbation) $H = H^{[0]} + \lambda V^{[1]}$ where λ is used to scale the strength of the perturbation. This gives a wavefunction $\Psi(\lambda)$ and an energy $E(\lambda)$. The first-order wavefunction $\Psi^{[1]}$, and corresponding first-, second-, and third-order energies calculated with the analytic DMRG response theory correspond exactly to the following derivatives

$$\Psi^{[1]} = \left.\frac{\partial \Psi(\lambda)}{\partial \lambda}\right|_{\lambda=0} \tag{4.35}$$

$$E^{[1]} = \left.\frac{\partial E(\lambda)}{\partial \lambda}\right|_{\lambda=0} \tag{4.36}$$

$$E^{[2]} = \left.\frac{\partial^2 E(\lambda)}{\partial \lambda^2}\right|_{\lambda=0} \tag{4.37}$$

$$E^{[3]} = \left.\frac{\partial^3 E(\lambda)}{\partial \lambda^3}\right|_{\lambda=0} \tag{4.38}$$

Analogous statements for time-dependent perturbations can be made by considering an appropriate quasi-energy [18–20].

The analytic approach to DMRG response does not represent the only way to obtain response within the DMRG. Existing DMRG response methods use various related *adaptive basis* approaches, commonly in two categories, the Lanczos vector method [21], and the dynamical density matrix renormalisation group [24]. The dynamical density matrix renormalisation group is established as the most accurate approach to response properties and we shall focus on it here. (Note the dynamical density matrix renormalisation group and correction vector methods [22, 23, 26] are essentially the same but differ in the algorithm used to solve the response equations. In fact, if the response quantities are evaluated using a quadratic functional of the correction vector such as Eq. (4.48), it is possible to obtain quadratic errors with the correction vector method without the explicit minimisation as used in the dynamical DMRG).

In the dynamical DMRG the ansatz for the zeroth and first-order wavefunction are both modified relative to the unperturbed DMRG wavefunction, i.e.

$$|\Psi^{[0]}\rangle = \sum_{\{n\}} \tilde{\mathbf{L}}^{n_1[0]} \dots \tilde{\mathbf{C}}^{n_p[0]} \dots \tilde{\mathbf{R}}^{n_k[0]} |n_1 n_2 \dots n_k\rangle \tag{4.39}$$

$$|\Psi^{[1]}\rangle = \sum_{\{n\}} \tilde{\mathbf{L}}^{n_1[0]} \dots \tilde{\mathbf{C}}^{n_p[1]} \dots \tilde{\mathbf{R}}^{n_k[0]} |n_1 n_2 \dots n_k\rangle \tag{4.40}$$

The tildes indicate that the $\tilde{\mathbf{L}}^n$, $\tilde{\mathbf{C}}^n$, $\tilde{\mathbf{R}}^n$ tensors appearing in Eqs. (4.39), even for the zeroth order wavefunction, do not correspond to the same tensors obtained in a DMRG calculation without the perturbation. The zeroth and first-order coefficient vectors are obtained from the effective Schrödinger equation (4.4) and an uncoupled response equation, e.g.

$$(\mathbf{H}^{[0]} - (E^{[0]} + \omega)\mathbf{1})\mathbf{c}^{[1]}(\omega) = -\mathbf{Q}\mathbf{V}^{[1]}\mathbf{c}^{[0]} \tag{4.41}$$

The dynamical DMRG ansatz is able to capture the response of the $\mathbf{L}^n$ and $\mathbf{R}^n$ tensors in an average way, because it uses $\tilde{\mathbf{L}}^n$, $\tilde{\mathbf{R}}^n$ that are different from those in the unperturbed DMRG calculation. Specifically, the left and right renormalisation tensors at each block configuration are obtained as eigenvectors of *modified* left and right density matrices, where the density matrices corresponding to $\mathbf{c}^{[0]}, \mathbf{c}^{[1]}, \mathbf{v} = \mathbf{V}^{[1]}\mathbf{c}^{[0]}$ are all averaged together i.e. for $\mathbf{D}_L$

$$\mathbf{D}_L = \alpha \mathbf{C}^{[0]}\mathbf{C}^{[0]\dagger} + \beta \mathbf{C}^{[1]}\mathbf{C}^{[1]\dagger} + \gamma(\mathbf{V}\mathbf{c}^{[0]})(\mathbf{V}\mathbf{c}^{[0]})^\dagger \tag{4.42}$$

where $\alpha + \beta + \gamma = 1$ and in the last term we are interpreting the perturbation multiplied by the zeroth order wavefunction $\mathbf{V}^{[1]}\mathbf{c}^{[0]}$ as a matrix in the same way as $\mathbf{c}^{[0]}$ is interpreted as a matrix. (Note that the above is for real frequencies; when considering complex frequencies, one typically separates the imaginary and real contributions of the response vector [24]). Because the density matrix contains information on the perturbation and the response, the DMRG basis is "adapted" to the perturbation being considered. While this is very simple to implement within a standard DMRG algorithm and has proven very successful, one drawback relative to the analytic response approach is that a single set of DMRG basis states is being used to represent several quantities, including both the zeroth order and response vectors. For this reason, we can expect some loss of accuracy with this method for small M calculations relative to the analytic response method.

4.4 Implementation

We have implemented the analytic DMRG response theory as described above. This consists of three parts: solving the coupled-perturbed equation (4.17) for

the first-order coefficient vector $\mathbf{c}^{[1]}$, solving for the first-order renormalisation tensors $\mathbf{L}^{n[1]}$, $\mathbf{R}^{n[1]}$ (4.5), (4.6), and constructing the first-order effective Hamiltonian $\mathbf{\Delta H}^{[1]}$ and necessary intermediates, as well as other first-order operators needed for properties (e.g. $\mu^{[1]}_{i(j)}$ in Eq. 4.31). The first two parts are quite straightforward: we solve the coupled-perturbed equation (4.17) using a Krylov subspace iterative solver with preconditioning, and to obtain the first-order renormalisation tensors (4.22), (4.23) we use explicit Rayleigh-Schrödinger expressions for the first-order density matrix eigenvectors

$$\mathbf{l}^{i[1]} = \sum_{j=M+1} -\frac{\mathbf{l}^{j[0]\dagger}\mathbf{D}_L^{[1]}\mathbf{l}^{i[0]}}{\sigma_j^{[0]} - \sigma_i^{[0]}}\mathbf{l}^{j[0]} \tag{4.43}$$

$$\mathbf{r}^{i[1]} = \sum_{j=M+1} -\frac{\mathbf{r}^{j[0]\dagger}\mathbf{D}_R^{[1]}\mathbf{r}^{i[0]}}{\sigma_j^{[0]} - \sigma_i^{[0]}}\mathbf{r}^{j[0]} \tag{4.44}$$

In practice small denominators can arise in the perturbation expression Eq. (4.44); for stability we set contributions from any denominators below a certain threshold (e.g. 10^{-12}) to zero.

We now focus on the implementation to obtain $\mathbf{\Delta H}^{[1]}$ and related quantities such as $\mu^{[1]}_{i(j)}$. We recall that the effective Hamiltonian $\mathbf{H}^{[0]}$ is expressed as a tensor product of operators on the left and right blocks (we consider the single-site $\bullet$ in the block configuration Fig. 4.1 to be part of the left block for simplicity)

$$\mathbf{H} = \sum_{ij} w_{ij}\mathbf{O}_L^i \otimes \mathbf{O}_R^j \tag{4.45}$$

where $\mathbf{O}_L$ acts only the left block and $\mathbf{O}_R$ acts only on the right block, and we assume that $\otimes$ takes into account the appropriate parity factors associated with the fermion character of the operators (see e.g. Ref. [3, 5]). The first-order Hamiltonian is constructed from the response of the operators $\mathbf{O}_L, \mathbf{O}_R$, through

$$\mathbf{\Delta H}^{[1]} = \sum_{ij} w_{ij}(\mathbf{O}_L^{i[0]}\mathbf{O}_R^{j[1]} + \mathbf{O}_L^{i[1]}\mathbf{O}_R^{j[0]}) \tag{4.46}$$

We therefore need to calculate the first-order operators $\mathbf{O}_L^{[1]}$, $\mathbf{O}_R^{[1]}$. These are built up sequentially through the blocking steps in the sweep much like the zeroth order operators. The renormalisation transformation $\mathcal{R}$ of the first-order operator at a given block configuration in a left→right sweep, is given by

$$\mathcal{R}[\underline{\mathbf{O}}_L^{[1]}] = \mathbf{L}^{[0]\dagger}\underline{\mathbf{O}}_L^{[1]}\mathbf{L}^{[0]} + \mathbf{L}^{[1]\dagger}\underline{\mathbf{O}}_L^{[0]}\mathbf{L}^{[0]} + \mathbf{L}^{[0]\dagger}\underline{\mathbf{O}}_L^{[0]}\mathbf{L}^{[1]} \tag{4.47}$$

where we have used the underline to indicate that the operators refer to blocked operators (i.e. for the left block plus the single-site), and the renormalisation tensors are interpreted as matrices $\mathbf{L}$ as described in Eq. (4.5). At the beginning of the left→right sweep, $\mathbf{O}_L^{[1]} = 0$ for all such operators. Analogous expressions hold for the right→left sweep and the operators $\mathbf{O}_R$.

The full sweep algorithm for the DMRG analytic response can be summarised as follows:

1. Converge a standard DMRG algorithm for the state of interest and store all intermediate zeroth-order operators $\mathbf{O}_L^{[0]}$, $\mathbf{O}_R^{[0]}$ and tensors $\mathbf{L}^{n[0]}$, $\mathbf{C}^{n[0]}$, $\mathbf{R}^{n[0]}$.
2. Set all $\mathbf{O}_L^{[1]}, \mathbf{O}_R^{[1]} = 0$
3. Start a sweep (left→right)
    - Set all $\mathbf{O}_L^{[1]}$ to 0
    - At each block configuration:
    - Solve coupled perturbed response equation, Eq. (4.17). $\mathbf{\Delta H}^{[1]}$ is constructed using current best guesses for $\mathbf{O}_L^{[1]}$, $\mathbf{O}_R^{[1]}$
    - Solve for perturbed density matrix eigenvectors and $\mathbf{L}^{n[1]}$, Eq. (4.22)
    - Update all $\mathbf{O}_L^{[1]}$ using Eq. (4.47)

4. Start a sweep (right→left), analogous to (left→right) sweep
5. Loop to 3. until convergence.
6. Evaluate response properties (e.g. as in Sec. 4.3.1)

We note that the cost of a single sweep for the analytic response has the same order of computational and storage cost as an ordinary sweep in the DMRG calculation, which, for the *ab-initio* Hamiltonian is $O(M^3k^3) + O(M^2k^4)$ computation, $O(M^2k^2)$ memory, and $O(M^2k^3)$ disk, where k is the number of correlated orbitals. The memory cost is roughly twice that for the calculation of the energy because of storage of the first-order operators as well as the zeroth-order operators.

We have assumed in the above that the coupled-perturbed equations of the analytic DMRG response theory, i.e. Eqs. (4.17), (4.29) can be solved through a simple self-consistency cycle. In practice, however, we should expect convergence problems to occur when the first-order wavefunction $\mathbf{c}^{[1]}$ is large compared to $\mathbf{c}^{[0]}$, as this will lead to a large first-order effective Hamiltonian $\mathbf{\Delta H}^{[1]}$ and a feedback effect in the response equations (4.17), (4.29). This scenario arises near the poles of the response, and indeed we find this to be the case (see below).

4.5 Static and frequency-dependent polarizabilities of oligo-di-acetylenes

As an initial test of the analytic DMRG response theory and implementation, we have calculated static and frequency-dependent longitudinal polarisabilities of

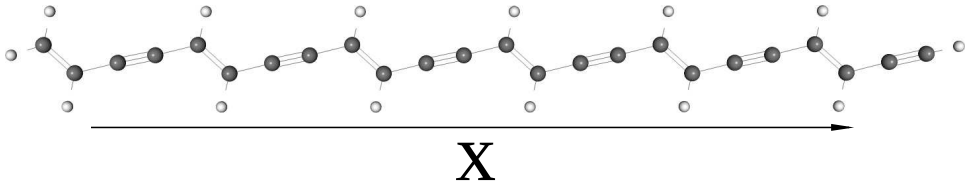

Figure 4.2: Oligo-di-acetylenes, with the long-axis moment of inertia aligned with the x-coordinate. This is the axis along which the polarisabilities are evaluated.

several oligo-di-acetylenes using the analytic DMRG response theory, the dynamical DMRG method, and the linear-response coupled cluster method. Long oligo-di-acetylenes are of interest due to their large third-order non-linear polarisability [32]. While we will calculate only the linear polarisability here, the same analytic derivative techniques can in principle be extended to higher order polarisabilities and non-linear optical response.

We carried out calculations on short all-trans oligo-di-acetylenes (ODAs), 2-ODA C_8H_6, 4-ODA $C_{16}H_{10}$, 6-ODA $C_{24}H_{14}$. Optimised geometries were obtained at the density functional theory B3LYP [33, 34] level in a correlation consistent Dunning double-zeta (cc-pVDZ) basis [35]. Subsequent Hartree-Fock, DMRG, and coupled cluster (CC) calculations were carried out in a minimal STO-6G Gaussian basis [35, 36]. We realise that this basis is too small for the quantitative calculation of polarisabilities, but it has been chosen to enable a preliminary study. Also, we note that qualitative trends in polarisabilities can be captured using rather small basis sets of split-valence quality [32]. The Hartree-Fock calculations were used to determine molecular orbitals with σ and π character. All σ orbitals were kept frozen in the DMRG response calculations, and the π orbitals were localised. Calculated polarisabilities refer to the α_{xx} component, where the x-axis is aligned with the long moment of inertia axis of the

molecules (see Fig. 4.2). The DMRG response calculations used an active space of p_z orbitals only, corresponding to an (8e, 8orb) active space for 2-ODA, a (16e, 16orb) active space for 4-ODA, and a (24e, 24orb) active space for 6-ODA. For the analytic response DMRG calculations using M states we first converged a ground-state DMRG calculation with M states using the one-site algorithm, and used this as the starting point for the response calculation.

In addition to the analytic response DMRG calculations, we carried out calculations using the dynamical DMRG method for comparison. The dynamical DMRG polarisabilities were obtained by solving the linear response equation in the dynamical DMRG basis $(\omega\mathbf{1} - \mathbf{H}^{[0]})\mathbf{c}^{[1]})_i = \mathbf{Q}\mu_i\mathbf{c}^{[0]}$ just as in the correction vector method, but the resulting polarisabilities were evaluated using the quadratic functional

$$G_{ij} = \mathbf{c}_i^{[1]\dagger}(\omega\mathbf{1} - \mathbf{H}^{[0]})\mathbf{c}_j^{[1]} + \mathbf{c}^{[0]\dagger}\mu_i\mathbf{c}_j^{[1]} + \mathbf{c}_j^{[1]\dagger}\mu_i\mathbf{c}^{[0]}j \tag{4.48}$$

which ensures that the obtained polarisability is quadratic in the error in $\mathbf{c}^{[1]}$ [37, 38], which is the hallmark of the dynamical DMRG approach. For comparison, we also computed linear-response restricted coupled cluster polarisabilities at the singles and doubles level [15], both at the all electron level, and within the p_z active space only, using the PSI3 [39] package.

We note one issue that arises with the response DMRG calculations in our initial implementation as opposed to ordinary ground-state DMRG calculations. In ground-state DMRG calculations with the one-site algorithm, we are generally able to converge the DMRG energy from sweep to sweep to very high accuracy, e.g. nanoHartrees. However, in our initial response implementation, we were not able to converge the calculated polarisabilities to similar accuracy. Typically the forward and backwards sweeps would converge to somewhat dif-

ferent results, and even between consecutive forwards (or backwards) sweeps, the polarisability would oscillate somewhat. This was true both for the dynamical DMRG and the analytic response DMRG calculations. The oscillation can be quite severe, particularly for small M calculations and for higher frequencies that are nearer to a pole (e.g. at frequency $\omega = 0.2$ a.u.) and reflects the greater sensitivity of the response calculation to the discarded states in the density matrix. In our results, we report the average polarisability of the last 4 sweeps, together with twice the standard deviation. These results are reported in table 4.1.

Table 4.1: Static and frequency dependent polarisabilities in a.u. of oligo-diacetylenes, with 2, 4, 6 monomers (2-ODA, 4-ODA, 6-ODA). D stands for dynamical DMRG, A stands for analytic response theory. ω is the frequency (in a.u.), M refers to the number of states in the DMRG wavefunction. **The numbers in brackets do not represent intrinsic truncation error from finite** M but represent the numerical convergence of the DMRG sweep, since the forwards and backwards sweeps typically converge to slightly different results. The bracketed number is twice the standard deviation (2σ) in the last 4 forward and backwards sweeps. See text for further discussion.

		2-ODA		4-ODA		6-ODA	
ω	M	D	A	D (2σ)	A (2σ)	D (2σ)	A (2σ)
0.00	25	52.77	52.89	144.16 (0.03)	145.21 (0.04)	354.28 (17.96)	243.65 (0.06)
	50	52.89	52.89	146.07 (0.01)	145.74 (0.09)	246.04 (0.02)	245.06 (0.07)
	250	52.88	52.88	145.75 (0.01)	145.80 (0.01)	245.20 (0.00)	245.27 (0.03)
	1000	n.a.	n.a.	145.77 (0.01)	145.81 (0.00)	245.13 (0.10)	245.14 (0.02)
	LR-CCSD	53.38		148.15		249.67	

Table 4.1 (Continued)

		2-ODA		4-ODA		6-ODA	
ω	M	D	A	D (2σ)	A (2σ)	D (2σ)	A (2σ)
0.05	25	53.98	53.96	148.46 (0.02)	149.80 (0.04)	449.82 (35.15)	252.00 (0.14)
	50	54.07	54.07	150.64 (0.01)	150.26 (0.07)	254.61 (0.02)	253.62 (0.13)
	250	54.06	54.07	150.37 (0.00)	150.39 (0.04)	253.87 (0.00)	253.92 (0.02)
	LR-CCSD	54.62		153.19		259.40	
0.10	25	57.83	57.57	163.62 (0.03)	165.42 (0.13)	462.00 (22.55)	282.05 (0.25)
	50	57.99	57.99	166.46 (0.02)	166.11 (0.05)	284.81 (0.03)	283.96 (0.22)
	250	57.99	58.00	166.19 (0.00)	166.23 (0.02)	284.30 (0.00)	284.26 (0.21)
	LR-CCSD	58.72		170.76		294.16	
0.15	25	65.85	64.97	195.14 (0.07)	201.06 (0.17)	557.18 (114.72)	353.66 (0.57)
	50	66.07	66.06	202.51 (0.03)	202.24 (0.09)	357.02 (0.05)	356.37 (0.20)
	250	66.05	66.08	202.45 (0.00)	202.49 (0.04)	357.26 (0.00)	357.10 (0.10)
	LR-CCSD	67.22		212.20		381.68	
0.20	25	82.03	79.89	279.06 (0.35)	294.06 (0.89)	520.61 (84.68)	564.50 (1.38)
	50	82.57	82.54	296.86 (0.62)	295.83 (1.67)	564.25 (16.84)	566.94 (0.89)

Table 4.1 (Continued)

		2-ODA		4-ODA		6-ODA	
ω	M	D	A	D (2σ)	A (2σ)	D (2σ)	A (2σ)
	250	82.56	82.60	296.71 (0.55)	296.44 (0.06)	571.44 (0.71)	571.63 (1.73)
	LR-CCSD	84.83		328.71		682.10	

From table 4.1 we make the following observations about the relative performance of the analytic DMRG response method relative to the dynamical DMRG method that has been commonly used. For small M (e.g. M=25) the analytic DMRG response method is clearly superior. Whereas the dynamical DMRG method produces poor polarisabilities for M=25, in error by more than 50% in some cases, the analytic DMRG polarisabilities are quite reasonable at M=25 and typically in error by less than 1%. This is consistent with our discussion in section 4.3.2 where we argue the the dynamical DMRG method suffers from using the same set of DMRG basis states to represent both the zeroth order DMRG vector as well as the response and perturbation vectors. Thus, for small M there simply are not enough DMRG states to yield a meaningful result in the dynamical DMRG. Both methods converge as M increases. For the most accurate calculations (M=250), although both methods perform well, the dynamical DMRG polarisabilities appear slightly better than the analytic DMRG polarisabilities. However, this appears to be related to the instabilities in the convergence of the analytic DMRG response sweeps; whereas the oscillations in the dynamical DMRG sweeps vanish for larger M, they still remain for the analytic DMRG sweeps. From the 2σ values, we see that currently we can only conclude that the analytic and dynamical DMRG response methods are comparable for larger M.

Observing the trends in the polarisabilities, we see that the polarisabilities increase as the applied frequency increases which is what one would expect since we are approaching the first excitonic ^1B_u pole. We are not able to converge our response calculations very close to a pole because of the large norm in $\mathbf{c}^{[1]}$. The standard solution to this is to include a small imaginary broadening in ω. However, a straightforward incorporation of broadening leads to complex operators

in the analytic theory which we have not yet implemented.

It is often the case that one wishes to determine an entire spectrum, i.e. some response property for a very large range of ω. While in the dynamical DMRG this is usually performed by scanning through ω (with some small imaginary component) and performing a response calculation for each frequency, it may be more appropriate in the analytic response approach to adopt a different strategy. The coupled-perturbed response equations may be viewed as a linear eigenvalue problem for the excitation energies (i.e. poles) and may be solved in this way, in the same way that the time-dependent Hartree-Fock or time-dependent density functional equations are solved as an eigenvalue problem to obtain excitation energies. Once a sufficient number of poles are obtained, the spectrum can then be reconstructed analytically.

Comparing the DMRG polarisabilities and the coupled cluster polarisabilities, we see that the coupled cluster polarisabilities are generally quite good even at the singles and doubles level. (They appear to consistently overestimate the polarisability by only a few percent). This is not surprising since by virtue of the one-electron nature of the dipole operator, the linear polarisability only samples states with single-excitation character relative to the ground-state. Such excited states are well captured by CCSD theory. However, earlier studies indicate that the overall spectrum in conjugated systems (including e.g. doubly excited and triplet excited states) is poorly reproduced by coupled cluster theory [40], and so we would expect much larger discrepancies between the CC and DMRG description of third-order non-linear optical response.

In Fig. 4.3 we plot the static active space and total polarisabilities ($\omega = 0$) per monomer calculated using the analytic DMRG response theory as a function of

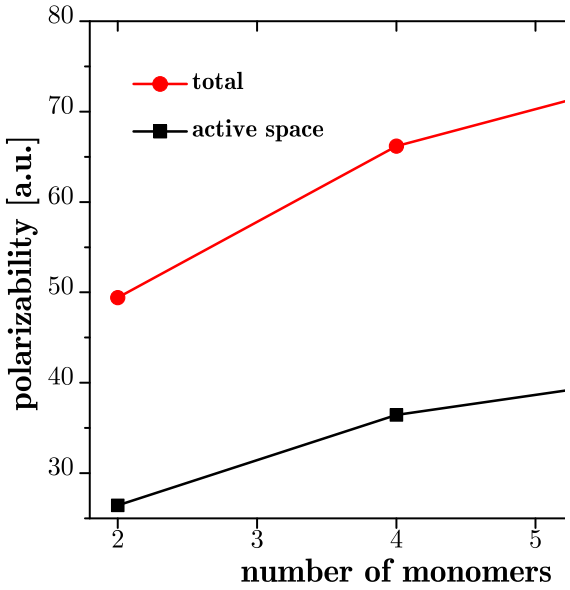

Figure 4.3: Scaling of total and active space polarisabilities per monomer.

the number of di-acetylene monomers in the calculation. The total polarisability for the DMRG calculations is obtained using the core-correction from the linear-response coupled cluster calculations i.e.

$$\alpha^{\text{tot}}_{\text{DMRG}} = \alpha^{\text{tot}}_{CC} - \alpha^{\text{act}}_{CC} + \alpha^{\text{act}}_{DMRG} \tag{4.49}$$

We see a slow saturation of the polarisability per monomer as a function of the chain length, although the polarisability is not yet fully saturated at the 6-ODA level. While larger basis set calculations and calculations on longer chains are necessary to obtain a definitive conclusion, we note that our results are consistent with early semi-empirical calculations which indicate an onset of saturation between 2-ODA and 3-ODA [41].

4.6 Conclusions

In the current work we have described an analytic approach to the calculation of response quantities in the density matrix renormalisation group. The analytic response method is familiar from other electronic structure theories but has not so far been developed within the density matrix renormalization group. The analytic response implementation does not change the computational cost of the ground-state DMRG calculation by more than a constant factor. Compared to the popular dynamical density matrix renormalisation group approach we find that the analytic response method produces considerably more accurate response quantities when using a small number of DMRG states, without any greater computational cost. While it is simpler within the dynamical DMRG to implement higher-order response properties and complex frequencies, based on our investigations, the improved accuracy of the analytic response approach may justify the additional implementation effort. In future work, we will explore both higher-order response quantities and determination of complete spectra using the analytic DMRG response approach.

BIBLIOGRAPHY

[1] J. Dorando, J. Hachmann, and G. K.-L. Chan, J. Chem. Phys. **130**, 184111 (2009).

[2] S. R. White, Phys. Rev. Lett. **69**, 2863 (1992).

[3] U. Schollwöck, Rev. Mod. Phys. **77**, 259 (2005).

[4] S. R. White and R. L. Martin, J. Chem. Phys. **110**, 4127 (1999).

[5] G. K.-L. Chan and M. Head-Gordon, J. Chem. Phys. **116**, 4462 (2002).

[6] D. Ghosh, J. Hachmann, T. Yanai, and G. K.-L. Chan, J. Chem. Phys. **128**, 144117 (2008).

[7] K. H. Marti, I. M. Ondik, G. Moritz, and M. Reiher, J. Chem. Phys. **128**, 014104 (2008).

[8] G. K.-L. Chan, M. Kállay, and J. Gauss, J. Chem. Phys. **121**, 6110 (2004).

[9] Y. Kurashige and T. Yanai, J. Chem. Phys. (2008), submitted.

[10] D. Zgid and M. Nooijen, J. Chem. Phys. **128**, 144116 (2008).

[11] J. Hachmann, J. J. Dorando, M. Avilés, and G. K.-L. Chan, J. Chem. Phys. **127**, 134309 (2007).

[12] G. Kotliar et al., Rev. Mod. Phys. **78**, 865 (2006).

[13] R. McWeeny and B. T. Sutcliffe, *Methods of Molecular Quantum Mechanics*, Academic, New York, 1969.

[14] C. Jamorski, M. E. Casida, and D. R. Salahub, J. Chem. Phys. **104**, 5134 (1996).

[15] H. Koch, H. J. A. Jensen, P. Jørgensen, and T. Helgaker, J. Chem. Phys. **93**, 3345 (1990).

[16] J. Olsen and P. Jørgensen, J. Chem. Phys. **82**, 3235 (1985).

[17] T. Kobayashi, K. Sasagane, F. Aiga, and K. Yamaguchi, J. Chem. Phys. **110**, 11720 (1999).

[18] J. Olsen and P. Jørgensen, (1995).

[19] J. E. Rice and N. C. Handy, J. Chem. Phys. **94**, 4959 (1991).

[20] K. Sasagane, F. Aiga, and R. Itoh, J. Chem. Phys. **99**, 3738 (1993).

[21] K. A. Hallberg, Phys. Rev. B **52**, 9827 (1995).

[22] S. S. Ramasesha, S. K. Pati, H. R. Krishnamurthy, Z. Shuai, and J. L. Brédas, Phys. Rev. B **54**, 7598 (1996).

[23] T. D. Kühner and S. R. White, Phys. Rev. B **60**, 335 (1999).

[24] E. Jeckelmann, Phys. Rev. B **66**, 45114 (2002).

[25] S. R. White and I. Affleck, Phys. Rev. B **77**, 134437 (2008).

[26] E. Jeckelmann, (2008), cond-mat.str-el/0808.2620.

[27] S. Rommer and S. Östlund, Phys. Rev. B **55**, 2164 (1997).

[28] D. Zgid and M. Nooijen, J. Chem. Phys. **128**, 144115 (2008).

[29] S.R.White, Phys. Rev. B. **72**, 180403 (2005).

[30] G. K.-L. Chan, Phys. Chem. Chem. Phys. **10**, 3454 (2008).

[31] K. Ueda, C. Jin, N. Shibata, Y. Hieida, and T. Nishino, (2006), cond-mat.stat-mech/0612480.

[32] J. L. Bredas, C. Adant, P. Tackx, A. Persoons, and B. M. Pierce, Chem. Rev. **94**, 243 (1994).

[33] A. D. Becke, J.Chem.Phys. **98**, 5648 (1993).

[34] C. Lee, W. Yang, and R. Parr, Phys. Rev. B **37**, 785 (1988).

[35] K. L. Schuchardt et al., J. Chem. Inf. Model. **47**, 1045 (2007).

[36] W. J. Hehre, R. F. Stewart, and J. A. Pople, J. Chem. Phys. **51**, 2657 (1969).

[37] H. Koch and R. J. Harrison, J. Chem. Phys. **95**, 7479 (1991).

[38] H. Sellers, Int. J. Quantum Chem. **30**, 433 (1986).

[39] T. D. Crawford et al., PSI 3.2 (2003), see www.psicode.org.

[40] J. J. Dorando, J. Hachmann, and G. K.-L. Chan, J. Chem. Phys. **127**, 084109 (2007).

[41] B. Kirtman, Int. J. Quantum Chem. **36** (1989).

CHAPTER 5

CANONICAL TRANSFORMATION THEORY (CT) - INTRODUCTION

5.1 Introduction

In the previous chapters, we have discussed Density Matrix Renormalization Group (DMRG), which is an excellent alternative approximation to Configuration Interaction (CI) approaches to obtaining the static correlation energy. This gives a very good idea qualitatively of what is happening in a chemical system, but we need a way to obtain the remaining dynamic correlation energy so that we can get a quantitative description of the chemical system for direct comparison of our theoretical results to experiment.

There are several theories already available for describing dynamic correlation given a "multireference" state (i.e., the statically correlated starting point). These theories broadly fall into three categories, multireference perturbation theory, multireference configuration interaction, and multireference coupled cluster. Examples of multireference perturbation theory include complete active space perturbation theory (CASPT) [1], multireference Møller-Plesset (MRMP) [2], and n-electron valence perturbation theory (NEVPT) [3, 4]. Multireference perturbation theory has a high computational scaling of at least $O(n^7)$ where n is the number of orbitals. Multireference configuration interaction theories can either be applied directly or in conjunction with size consistency corrections[5–9]. Typical computational scaling of this category of multireference theory is $O(n^{10})$ and $O(e^n)$. The final category of multireference theories consists of variations of multireference coupled cluster (MRCC) theory. These theories tend to have computational scalings even higher than MRCI theories, and have not yet

been applied to a real system.

Based on the current discussion, there are many multireference theories, but as of yet there are no satisfactory methods for describing dynamic correlation in multireference systems. We believe that CT will address the faults that underlie the current multireference systems. Coupled Cluster (CC) theory is considered one of the best methods for describing dynamic correlation for single reference states[10]. As such, CT was created to mimic many of the good aspects contained in Coupled Cluster Singles Doubles (CCSD) theory, the most common variety of CC theory.

CT has the following properties in common with CCSD:

1. CT is size-consistent
2. CT has a computational scaling of $O(n^6)$
3. CT uses an exponential operator ansatz, and therefore reduces to an approximated CCSD for a single reference state

Based on this analysis we believe that CT will become the best method for describing dynamic correlation. Besides this brief introduction to CT there are many more detailed reviews describing CT and dynamic correlation[11–16].

5.2 Theory

To obtain the dynamic correlation energy, we will first split the orbital space into two spaces. The space that contains the multireference orbitals (which were obtained from a static correlation theory such as DMRG) will be defined as the

active space, and the space that includes the core and virtual orbitals will be defined as the external orbitals. Much as Coupled Cluster Theory (CC) works with an effective Hamiltonian, CT will also do the same

$$\overline{H} = e^{-A} H e^{A} \tag{5.1}$$

where A is a unitary transformation rather than the customary similarity transformation found in CC. This implies $A^{\dagger} = -A$. Here A is defined as

$$\begin{aligned} A &= A_i^a \hat{o}_i^a + A_{ij}^{ab} \hat{o}_{ij}^{ab} + A_{ij}^{ak} \hat{o}_{ij}^{ak} + \cdots && (5.2)\\ \hat{o}_i^a &= a_i^a - a_a^i && (5.3)\\ \hat{o}_{ij}^{ab} &= a_{ij}^{ab} - a_{ab}^{ij} && (5.4)\\ \hat{o}_{ij}^{ak} &= a_{ij}^{ak} - a_{ak}^{ij} && (5.5)\\ &\vdots \end{aligned}$$

where $abc\cdots$ represent the external orbitals, $ijk\cdots$ represent the active orbitals, and $a_i^a = a_a^{\dagger} a_i$. All the 2-body operators in A have no more than three active orbital indices.

Our next step will be to form the Baker-Campbell-Hausdorff (BCH) expansion of the effective Hamiltonian in eqn. 5.1

$$\overline{H} = H + [H, A] + \frac{1}{2}[[H, A], A] + \cdots \tag{5.6}$$

Eqn. 5.6 contains 0-, to n-body operators. Each commutation generates successively more complicated operators and terms. In chapter 1, we mentioned that the dynamic correlation energy is relatively small compared to the static correlation energy. We can expect the contribution of complex n-body effects to be insignificant. We will approximate the effective Hamiltonian with 0-, 1-, and 2-body operators

$$\overline{H}_{1,2} = H + [H, A]_{1,2} + \frac{1}{2}[[H, A]_{1,2}, A]_{1,2} + \cdots \tag{5.7}$$

where $_{1,2}$ denotes the retention of only 0-, 1-, and 2-body operators. Now we will explain how to arrive at this approximation. Let's first recall how normal ordered 1-, 2-, and 3-body operators are defined with respect to a Fermi vacuum

$$\tilde{a}^p_s = a^p_s - \delta^p_s n_s \tag{5.8}$$

$$\begin{aligned}\tilde{a}^{pq}_{st} &= a^{pq}_{st} - \delta^p_s n_s a^q_t - \delta^q_t n_t a^p_s + \delta^p_t n_t a^q_s \\ &\quad +\delta^q_s n_s a^p_t + \delta^{pq}_{st} n_p n_q\end{aligned} \tag{5.9}$$

$$\begin{aligned}\tilde{a}^{pqr}_{stu} &= a^{pqr}_{stu} - \delta^p_s n_p a^{qr}_{tu} + \delta^q_s n_q a^{pt}_{ru} + \delta^r_s n_r a^{qp}_{tu} \\ &\quad +\delta^p_t n_p a^{qr}_{su} - \delta^q_t n_q a^{pr}_{su} + \delta^r_t n_r a^{pq}_{su} + \delta^p_u n_p a^{qr}_{ts} \\ &\quad +\delta^q_u n_q a^{pr}_{st} - \delta^r_u n_r a^{pq}_{st} + \delta^{pq}_{st} n_p n_q a^r_u + \delta^{pr}_{su} n_p n_r a^q_t \\ &\quad +\delta^{qr}_{tu} n_q n_r a^p_s - \delta^{pq}_{su} n_p n_q a^r_t - \delta^{pq}_{tu} n_p n_q a^r_s - \delta^{pr}_{st} n_p n_r a^q_u \\ &\quad -\delta^{pr}_{tu} n_p n_r a^q_s - \delta^{qr}_{st} n_q n_r a^p_u - \delta^{qr}_{su} n_q n_r a^p_t - \delta^{pqr}_{stu} n_p n_q n_r\end{aligned} \tag{5.10}$$

where the tilde above the operator refers to the operators formed from the particle and hole creation and destruction operators of the Fermi vacuum. We would approximate our 3-body operator in eqn. 5.10, by neglecting the 3-body operator on the right hand side. Unfortunately, all the operators are operating on a multireference state, not a Fermi vacuum, and we therefore need a new set of operators that are normal ordered with respect to the multireference states encountered in CT. Mukherjee and Kutzelnigg[17, 18] have generalized the above equations for multireference states, keeping the normal ordering with respect to the multireference states

$$a^p_s = \tilde{a}^p_s + \gamma^p_s \tag{5.11}$$

$$a^{pq}_{st} = \tilde{a}^{pq}_{st} - 4(\gamma^p_s \wedge \tilde{a}^q_t) + \gamma^{pq}_{st} \tag{5.12}$$

$$a^{pqr}_{stu} = \tilde{a}^{pqr}_{stu} + 9(\gamma^p_s \wedge \tilde{a}^{qr}_{tu}) + 9(\gamma^{pq}_{st} \wedge \tilde{a}^r_u) + \gamma^{pqr}_{stu} \tag{5.13}$$

where $\wedge$ represent the anti-symmetric permutation of the indices with a normalization factor of $\frac{1}{p^2}$ and $\gamma^p_q, \gamma^{pq}_{rs}$ represent 1-, and 2-body density matrices. p

is the original rank of the operator (or the total number of indices). We will use the above equations for the operators in the effective Hamiltonian. For CT, we will neglect $\tilde{a}^{pqr}_{stu}$, and we will approximate the 3-body reduced density matrix in eqn. 5.13. Now we will examine the 1-,2-, and 3-body reduced density matrices. Similar to decomposing the 3-body operators, we can also reduce the 3-body density matrices through cumulant decomposition[19–21]

$$\gamma^{p}_{s} = \lambda^{p}_{s} \tag{5.14}$$

$$\gamma^{pq}_{st} = \lambda^{pq}_{st} + \gamma^{p}_{s}\gamma^{q}_{t} - \gamma^{p}_{t}\gamma^{q}_{s} \tag{5.15}$$

$$\begin{aligned}\gamma^{pqr}_{stu} = {} & \lambda^{pqr}_{stu} + \gamma^{p}_{s}\lambda^{qr}_{tu} - \gamma^{p}_{t}\lambda^{qr}_{su} + \gamma^{p}_{u}\lambda^{qr}_{su} \\ & -\gamma^{q}_{s}\lambda^{pr}_{tu} + \gamma^{q}_{t}\lambda^{pr}_{su} - \gamma^{q}_{u}\lambda^{pr}_{st} + \gamma^{r}_{s}\lambda^{pq}_{tu} \\ & -\gamma^{r}_{t}\lambda^{pq}_{su} + \gamma^{r}_{u}\lambda^{pq}_{st} + \gamma^{p}_{s}\gamma^{q}_{t}\gamma^{r}_{u} - \gamma^{p}_{s}\gamma^{r}_{t}\gamma^{q}_{u} \\ & +\gamma^{1}_{s}\gamma^{r}_{t}\gamma^{p}_{u} - \gamma^{1}_{s}\gamma^{p}_{t}\gamma^{r}_{u} + \gamma^{r}_{s}\gamma^{p}_{t}\gamma^{q}_{u} - \gamma^{r}_{s}\gamma^{q}_{t}\gamma^{p}_{u}\end{aligned} \tag{5.16}$$

where λ are the cumulants. We will neglect the 3-body cumulant, and substitute eqns. 5.14, and 5.15 into eqn. 5.16, to obtain the approximation to the 3-body reduced density matrix using only the 1- and 2-body density matrices

$$\gamma^{pqr}_{stu} = 9(\gamma^{p}_{s} \wedge \gamma^{qr}_{tu}) - 12(\gamma^{p}_{s} \wedge \gamma^{q}_{t} \wedge \gamma^{r}_{u}) \tag{5.17}$$

Beginning with eqn. 5.13, we will use eqns. 5.11, 5.12, and 5.17 to substitute for $\tilde{a}^{r}_{u}$, $\tilde{a}^{qr}_{tu}$, and γ^{pqr}_{stu}, respectively, to obtain the approximated 3-body operator used in CT

$$a^{pqr}_{stu} = 9(\gamma^{p}_{s} \wedge a^{qr}_{tu}) - 36(\gamma^{p}_{s} \wedge \gamma^{q}_{t} \wedge a^{r}_{s}) + 9(\gamma^{pq}_{st} \wedge a^{r}_{u}) + 24(\gamma^{p}_{s} \wedge \gamma^{q}_{t} \wedge \gamma^{r}_{u}) - 9(\gamma^{pq}_{st} \wedge \gamma^{r}_{u}) \tag{5.18}$$

The above equation is the central approximation needed to form the effective Hamiltonian in eqn. 5.7.

The only unknowns at this point are the amplitudes A that define the canonical

transformation e^A. We solve for the amplitudes based on the following equations

$$\begin{aligned} 0 &= \langle\Psi|[\overline{H}_{1,2}, \hat{o}_i^a]_{1,2}|\Psi\rangle && (5.19) \\ 0 &= \langle\Psi|[\overline{H}_{1,2}, \hat{o}_{ij}^{ab}]_{1,2}|\Psi\rangle && (5.20) \\ 0 &= \langle\Psi|[\overline{H}_{1,2}, \hat{o}_{ij}^{ak}]_{1,2}|\Psi\rangle && (5.21) \\ &\vdots \end{aligned}$$

As closing to theory segment of CT, there are two things to note. First, CT is a non-variational theory, which means that the energy obtained from the effective Hamiltonian is not always above the minimum energy. Second, CT has a computational cost of $O(a^2e^4)$, where a is the number of active orbitals and e is the number of external orbitals. The CT computational cost is comparable to single reference Coupled Cluster theory.

5.3 CT convergence

In this section, we will discuss the one issue that plagues CT. In the previous section, we discussed that the amplitudes A are obtained by solving eqns. 5.19-5.21. Due to approximations of the effective Hamiltonian, these equations have numerical instabilities. Specifically, the Jacobian that is used to solve these equations has small eigenvalues. This is related to the problem of small denominators, or "intruder states" in Perturbation Theory (PT). There has been research devoted to eliminating these intruder states, but more research in needed. In this section, we will briefly describe two methods that have been developed to eliminate intruder states. Both of these methods restrict the variational freedom

in A

$$\hat{o}_i = \sum_j C_{ij} a_j \tag{5.22}$$

where $\hat{o}_i$ represents all the operators in eqns. 5.3-5.6, and C is a coefficient matrix yet to be defined. $\hat{o}_i$ are linear combinations of the original excitation/de-excitation operators, a_j.

The first method involves using the overlap matrix. This method is the most intuitive method, and the most common method for dealing with basis sets that are over-complete. The overlap matrix in CT is defined as

$$S_{ij} = \langle \Psi | a_i a_j | \Psi \rangle \tag{5.23}$$

We then diagonalize the matrix S to obtain a set of eigenvalues and eigenvectors. Using a cutoff, we eliminate the small values of overlap matrix and form the $S^{-\frac{1}{2}}$ matrix. The first method is referred to as the overlap matrix truncation, and as such the coefficients of the C matrix are the coefficients of the $S^{-\frac{1}{2}}$ matrix. The major drawback of this method is that it is not so easy to choose a cutoff for the small eigenvalues of the overlap matrix. For some systems, this cutoff is obvious, because the spectrum of the eigenvalue of the overlap matrix will have a gap in the spectrum that distinguishes the large eigenvalues from the small or intruder state eigenvalues. But, as this author has experienced (in the case of dioxetanes), there are cases where the overlap matrix has a continuous spectrum and choosing a threshold is not an easy matter.

More recently, there has been a better method developed for eliminating intruder states called strong contraction. This procedure is described in detail in Neuscamman et al. [15].

BIBLIOGRAPHY

[1] K. Andersson, P.-Å. Malmqvist, B. O. Roos, A. J. Sadlej, and K. Wolinski, J. Phys. Chem. **94**, 5483 (1990).

[2] K. Hirao, Chem. Phys. Lett. **190**, 374 (1992).

[3] C. Angeli, R. Cimiraglia, S. Evangelisti, T. Leininger, and J.-P. Malrieu, J. Chem. Phys. **114**, 10252 (2001).

[4] C. Angeli, R. Cimiraglia, and J.-P. Malrieu, J. Chem. Phys. **117**, 9138 (2002).

[5] R. J. Buenker and S. D. Peyerimhoff, Theor. Chim. Acta **35**, 33 (1974).

[6] P. E. M. Siegbahn, J. Chem. Phys. **72**, 1647 (1980).

[7] H.-J. Werner and P. J. Knowles, J. Chem. Phys. **89**, 5803 (1988).

[8] R. J. Gdanitz and R. Ahlrichs, Chem. Phys. Lett. **143**, 413 (1988).

[9] P. G. Szalay and R. J. Bartlett, Chem. Phys. Lett. **214**, 481 (1993).

[10] R. J. Bartlett and M. Musial, Rev. Mod. Phys. **79**, 291 (2007).

[11] T. Yanai and G. K.-L. Chan, J. Chem. Phys. **124**, 194106 (2006).

[12] T. Yanai and G. K.-L. Chan, J. Chem. Phys. **127**, 104107 (2007).

[13] E. Neuscamman, T. Yanai, and G. K.-L. Chan, J. Chem. Phys. **130**, 124102 (2009).

[14] E. Neuscamman, T. Yanai, and G. K.-L. Chan, J. Chem. Phys. **130**, 124102 (2009).

[15] E. Neuscamman, T. Yanai, and G. K.-L. Chan, J. Chem. Phys. (2009), submitted.

[16] E. Neuscamman, T. Yanai, and G. K.-L. Chan, J. Chem. Phys. (2009), submitted.

[17] W. Kutzelnigg and D. Mukherjee, J. Chem. Phys. **107**, 432 (1997).

[18] D. Mukherjee, **274**, 561 (1997).

[19] F. Colmenero and C. Valdemoro, Chem. Phys. Lett. **47**, 979 (1993).

[20] W. Kutzelnigg and D. Mukherjee, J. Chem. Phys. **110**, 2800 (1999).

[21] H. Nakastsuji and K. Yasuda, Phys. Rev. Lett. **76**, 1039 (1996).

CHAPTER 6

CANONICAL TRANSFORMATION THEORY DENSITY MATRICES

6.1 Introduction

Density matrices are very useful because they remove extraneous information that is present in the wavefunction. For example, whereas a quantum state is described by an N-particle wavefunction, expectation values of most physical operators can be obtained from the one- and two-particle density matrices alone, which are much simpler quantities.

In addition to determining the expectation values of physical operators, density matrices tell us much about the nature of the states from which they are derived. This is important when working with DMRG based descriptions, because the wavefunction is represented in a very compact form and obtaining detailed N-particle information on the state is difficult. For example, whereas the standard way to identify the character of an excited state is to examine the dominant determinants in the wavefunction, the re-expansion of the DMRG wavefunction back into a determinantal representation is not practical. Instead, we need to identify the character of excited states using the appropriate density matrices that either measure the occupancies of the orbitals in the excited states, or measure the change in the occupancies between the ground-state and the excited state.

The procedure to obtain density matrices in the DMRG was described in Ref. [1]. In the current chapter, we describe how we can obtain the corresponding density matrices when the dynamic correlation is included as well, in the CT

theory. We first describe the general theory, then we describe the application of this technique to understand the low-lying excited states in *trans*-stilbene and oligo-phenylvinylene using the joint CT-DMRG theory.

6.2 Unrelaxed density matrices in CT theory

6.2.1 Definition

Given a normalized wavefunction Ψ, one- and two-particle density matrix elements γ^p_q, γ^{pq}_{rs} may be defined as

$$\gamma^p_q = \langle \Psi | a^p_q | \Psi \rangle \tag{6.1}$$

$$\gamma^{pq}_{rs} = \langle \Psi | a^{pq}_{rs} | \Psi \rangle \tag{6.2}$$

Such density matrices are sometimes called *unrelaxed*, as they are defined as an expectation value rather than as derivatives of the Lagrangian with respect to the one- and two-particle integrals, the two definitions being different if the energy is not obtained in a variational way (e.g. as in coupled cluster theory). While it is possible to obtain relaxed density matrices in CT theory, we will here be concerned with unrelaxed quantities only.

In CT theory, $\Psi = e^A |\Psi_0\rangle$ (5.1) and expectation values of this wavefunction are computed not exactly, but approximately, using an operator decomposition (see Sec. 5.2). Consequently, the natural definition of the CT one- and two-particle density matrices is not precisely via the expectation values (6.1), (6.2), but rather via expectation values computed using an operator decomposition.

First, denote the density matrices of the reference state Ψ_0, $\gamma_q^{p[0]}$, $\gamma_{rs}^{pq[0]}$, defined as

$$\gamma_q^{p[0]} = \langle \Psi_0 | a_q^p | \Psi_0 \rangle \tag{6.3}$$

$$\gamma_{rs}^{pq[0]} = \langle \Psi_0 | a_{rs}^{pq} | \Psi_0 \rangle \tag{6.4}$$

where the superscript $[0]$ does not denote perturbation order, but rather the power of A appearing in the definition. The CT density matrices are then defined by the operator decomposed BCH expansions

$$\gamma_q^p = \langle \Psi_0 | (e^{-A} a_q^p e^A)_{\text{op. decomp}} | \Psi_0 \rangle \tag{6.5}$$

$$= \langle \Psi_0 | a_q^p + [a_q^p, A]_{1,2} + \frac{1}{2}[[a_q^p, A]_{1,2}, A]_{1,2} + \ldots | \Psi_0 \rangle \tag{6.6}$$

$$\gamma_{rs}^{pq} = \langle \Psi_0 | a_{rs}^{pq} + [a_{rs}^{pq}, A]_{1,2} + \frac{1}{2}[[a_{rs}^{pq}, A]_{1,2}, A]_{1,2} + \ldots | \Psi_0 \rangle \tag{6.7}$$

Defined in this way, traces of the transformed density matrices with untransformed integrals match those of the reference density matrices with transformed integrals. Writing the one- and two-particle integrals of the untransformed and effective (transformed) Hamiltonian in CT theory (5.7) as $h_q^{p[0]}$, $v_{rs}^{pq[0]}$, and $\bar{h}_q^p$, $\bar{v}_{rs}^{pq}$ respectively, this means

$$\sum_{pq} \bar{h}_q^p \gamma_q^{p[0]} = \sum_{pq} h_q^{p[0]} \gamma_q^p \tag{6.8}$$

$$\sum_{pqrs} \bar{v}_{rs}^{pq} \gamma_{rs}^{pq[0]} = \sum_{pqrs} v_{rs}^{pq[0]} \gamma_{rs}^{pq} \tag{6.9}$$

6.2.2 Evaluation

CT density matrices defined by the expansions (6.6), (6.7) can be evaluated recursively, similarly to the evaluation of the effective Hamiltonian in CT theory. Let us first establish notation, while recalling the construction of the CT effective Hamiltonian. We denote generic zero-, one- or two-particle operator strings

(const, a_q^p, a_{rs}^{pq}, say) by the generic symbol o. The untransformed Hamiltonian is then $H = \sum_i h_i o_i$ while the effective (transformed) Hamiltonian is defined by its expansion

$$\bar{H} = H + [H, A]_{1,2} + \frac{1}{2}[[H, A]_{1,2}, A]_{1,2} + \dots \tag{6.10}$$

$$= \sum_i (h_i^{[0]} + h_i^{[1]} + h_i^{[2]} + \dots) o_i \tag{6.11}$$

where the superscripts denote powers of A in the definition.

In each commutator, terms like $[o_i, A]$ appear. In general, because o_i and A contain up to two-particle operators,

$$[o_i, A] = \text{const} + \text{1-particle op.} + \text{2-particle op.} + \text{3-particle op.} \tag{6.12}$$

The Mukherjee-Kutzelnigg operator decomposition used in CT theory reduces the 3-particle operators to linear combinations of zero, one-, and two-particle operators. Consequently, (6.12) becomes

$$[o_i, A]_{1,2} = \sum_j x_{ij} o_j \tag{6.13}$$

Taking the first commutator $[H, A]_{1,2}$ as an example, we see

$$\sum_i h_i^{[1]} o_i = [H, A]_{1,2} \tag{6.14}$$

$$= \sum_i h_i^{[0]} [o_i, A]_{1,2} \tag{6.15}$$

$$= \sum_{ij} h_i^{[0]} x_{ij} o_j \tag{6.16}$$

$$h_i^{[1]} = h_i^{[0]} x_{ij} \tag{6.17}$$

and in general, the Hamiltonian coefficients in (6.11) are obtained recursively,

$$h_i^{[n]} = \frac{1}{n} h_i^{[n-1]} x_{ij} \tag{6.18}$$

An analogous evaluation procedure holds for the density matrix elements. The expectation value of o_i is a zero-, one- or two-particle density matrix element, denoted generically by γ_i. The reference state density matrix elements $\gamma_i^{[0]}$ are given by

$$\gamma_i^{[0]} = \langle \Psi_0 | o_i | \Psi_0 \rangle \tag{6.19}$$

Now examine the contribution to the density matrix element $\gamma_i^{[0]}$ of the first commutator of (6.6), (6.7). We find

$$\begin{aligned} \gamma_i^{[1]} &= \langle \Psi_0 | [o_i, A]_{1,2} | \Psi_0 \rangle \\ &= \sum_j x_{ij} \langle \Psi_0 | o_j | \Psi_0 \rangle \qquad (6.20) \\ &= \sum_j x_{ij} \gamma_j^{[0]} \qquad (6.21) \end{aligned}$$

Similarly for the second commutator, we see that

$$\begin{aligned} \gamma_i^{[2]} &= \frac{1}{2} \langle \Psi_0 | [[o_i, A]_{1,2}, A]_{1,2} | \Psi_0 \rangle \\ &= \frac{1}{2} \sum_j x_{ij} \langle \Psi_0 | [o_j, A]_{1,2} | \Psi_0 \rangle \qquad (6.22) \\ &= \frac{1}{2} \sum_j x_{ij} \gamma_j^{[1]} \qquad (6.23) \end{aligned}$$

Consequently, we have the general recurrence, analogous to that for the effective Hamiltonian (6.18)

$$\gamma_i^{[n]} = \frac{1}{n} \sum_j x_{ij} \gamma_j^{[n-1]} \tag{6.24}$$

Because of the similarity between the density matrix and effective Hamiltonian construction, the leading order cost of evaluating the one- and two-body density matrices is $O(n_{act}^2 n_{ext}^4)$. This is the same as that for the energy evaluation in the CT theory.

6.3 *trans*-stilbene and oligo-phenylvinylenes

The oligomers of the phenylvinylene family (here abbreviated as PPV-n) contain a large number of important compounds important in photochemistry. The simplest, PPV-1 or *trans*-stilbene (Fig. 6.1) is often studied as the prototype system in which to understand photo-induced *cis-trans* isomerisation. The polymer, poly-phenyvinylene or PPV, is the parent compound of some of the earliest light-emitting polymers.

Surprisingly, the electronic structure of the low-lying excited states of the PPV's, even in *trans*-stilbene, is still a matter for some debate. In the ideal planar geometry, PPV's display C_{2h} symmetry and the π valence-excitations give rise to states of A_g and B_u symmetry. The ground-state has A_g symmetry, consequently excitations to B_u states are one-photon allowed.

Recent theoretical and experimental investigations of the low-lying states of *trans*-stilbene disagree on the ordering of the low-lying B_u and A_g states [2–7]. In this molecule, there are several candidate low-lying states. In the case of the B_u states, there is $B_u(HL)$, the HOMO→LUMO excitation excited on absorption, but in addition, there is also a low-lying B_u state ($B_u(W)$ of mixed HOMO-1→LUMO, HOMO→LUMO+1 character, that is weakly absorbing. In the case of the A_g states, there is a singly excited A_g state, denoted $A_g(S)$, as well as a doubly excited state $A_g(D)$ of HOMO^2 →LUMO^2 character, that is believed to be important for photoisomerisation.

CASPT2 studies by Molino *et al* [2] initially found that the weak transition $B_u(W)$ lay below the HOMO→LUMO transition, although experimental studies detected no such state. Later studies by the same group argued that the two

states were strongly mixed, which would lead to the $B_u(HL)$ being the lowest state, although the corresponding intensity borrowing would also give two bands in the absorption [3]. However, additional experiments only observed a single band [4]. The mystery appeared to be recently resolved in favor of experiment by theoretical studies using a different variant of multireference perturbation theory (NEVPT2) [5], SAC-CI [7], as well as TD-DFT calculations [6], which all reproduce the experimental ordering of B_u states. However, all these theories produce differing pictures of the A_g states. CASPT2 calculations predict that the excited A_g state is $A_g(S)$ which is at a similar position to the lowest B_u state in the theory, with $A_g(D)$ lying at a significantly higher energy [2]. SAC-CI finds the $A_g(D)$ state to be lowest in energy while the TD-DFT calculation find that $A_g(S)$ is the lowest state, although the position of the state appears to be much higher than in CASPT2, and above that of the B_u state [6, 7].

Finally, moving to longer PPVs, as described by Saha et al [7] no theory appears to give a reasonable description of the chain-length dependence of the lowest B_u excitation energy.

The challenge of describing these states can be traced to the need to properly balance the description of nondynamic and dynamic correlation. For example, dynamic correlation leads to significant lowering of the $B_u(HL)$ state, while nondynamic correlation is important to properly describe the doubly excited $A_g(D)$ state. Since the theoretical methods employed to date typically sacrifice the accurate treatment of one type of correlation (e.g. CASPT2 has an accurate treatment of nondynamic correlation, but a low-level treatment of dynamic correlation, while SAC-CI has the reverse traits) we hoped to shed new insight into these problems by employing our joint CT-DMRG theory, which includes a

high-level treatment of both kinds of correlation effects.

6.4 Computational Details

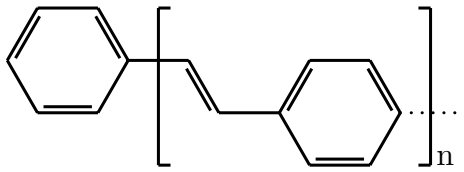

Figure 6.1: polyphenylene vinylene oligomer (PPV-n). n is the number of units. For *trans*-stilbene, n=1.

The geometry for PPV-1 (trans-stilbene) and PPV-2 is shown in fig. 6.1. PPV-1 and PPV-2 were placed in the xy plane and a C_{2h} symmetry was used. The geometries were obtained using Density Functional Theory (DFT) with a PBE0 functional and a 6-31+G(d,p) basis set. The optimization was performed using Gaussian[8]. After the optimization was completed, a Hartree Fock (HF) SCF calculation with an ANO basis of double zeta quality (H - (2s), C - (3s,2p,1d)) (derived from the ANO-RCC basis[9]) was performed on the optimized geometry to obtain the HF molecular orbitals for input into the DMRG calculation. For PPV-1, an additional HF SCF calculation with an ANO basis of near triple zeta quality (H - (2s1p), C - (4s,3p,1d)) was performed. The HF calculation was conducted using PSI3[10]. The energies for the DFT optimization and the subsequent HF calculation are displayed in Table 6.1.

The π_z valence space was chosen for the active space of PPV-1 and PPV-2. This equated to an active space of (14,14) and (22,22) for PPV-1 and PPV-2, respectively. Each molecular active space consisted equally of A_u and B_g HF molecular orbitals. The active space were then localized in their respective symmetries us-

Table 6.1: DFT optimization, and HF total energies of PPV-1 and PPV-2 at the DFT equilibrium geometry. All energies are in Hartrees.

Molecule	DFT	HF
PPV-1 (ANO-DZ)	-540.09214	-537.21938
PPV-1 (ANO-TZ)	-540.09214	-537.29238
PPV-2	-848.20403	-843.70492

ing the Pipek-Mezey localization method[11] to obtain symmetry adapted combinations of p_z-like orbitals for use in the DMRG.

To obtain the optimized active space orbitals for the two lowest singlet states in the A_g symmetry a DMRG-SCF calculation was run. The DMRG piece was run using $M = 1000$ and $M = 2000$ for PPV-1 and PPV-2, respectively, and using a state-average to obtain the ground state and the lowest lying excited ^1A_g state. The DMRG-SCF calculation was converged such that norm of the gradient was less then 1.e-5. A similar calculation was run to obtain the two lowest lying states in the ^1B_u symmetry. Once the DMRG-SCF calculation was converged and the optimized active space orbitals were obtained, a final DMRG state-average calculation for each symmetry with fixed orbitals was run to obtain the active space correlation energy for each state. The final DMRG state-average calculations were run using $M = 2000$ and $M = 4000$ for PPV-1 and PPV-2, respectively. The final DMRG energies were converged to within 1 mH of the exact energy.

To obtain the dynamic correlation energy, a state-averaged strong contraction CT (SC-CT)[12] calculation was run for each symmetry to obtain the two lowest lying states in the ^1A_g and the ^1B_u symmetry.

After these calculations were completed, we also evaluated the CT density matrices for each state, as well as certain transition density matrices, using the techniques described in Sec. 6.2.

6.5 Results

Examining the excitation energies, we see that the effect of dynamic correlation is very significant. For example, the ordering of the B_u states is changed between DMRG-SCF and CT theory due to the dynamic correlation. Within a VB language, the $B_u(HL)$ state is a so-called ionic state, while the $B_u(W)$ state is a covalent state. It is commonly found that the CASSCF treatments place the ionic states too high in energy, and this is what we are seeing here also. In general, our results confirm the more recent theoretical investigations. The absolute excitation energies are still too high, however, especially for the $1B_u$ state. This is likely due to the fact that the CT calculations were carried out in a state-averaged manner.

Examining the natural occupancies allows us to identify the character of the states. For example, we see that in the DMRG-SCF, the $1B_u$ state has a significant number of orbitals with occupancies different from 0 and 2, and is consistent with a state that contains both $HOMO-1 \rightarrow LUMO$ and $HOMO \rightarrow LUMO+1$ excitations (i.e. $B_u(W)$) while the $2B_u$ state is primarily singly excited in character ($B_u(HL)$). The situation is reversed in the CT calculations. Relative to the DMRG-SCF calculations, the CT occupancies appears further away from 0 and 2, indicating the larger degree of correlation.

Table 6.2: Excitation energies for DMRG-SCF, CT, and experiment for PPV-1.

Basis	State	DMRG-SCF		CT		Experiment[1]
ANO-DZ	1^1A_g	-537.3905		-539.1204		n/a
	2^1A_g	4.71	$A_g(D)$	4.80	$A_g(D)$	
	1^1B_u	4.77	$B_u(W)$	4.61	$B_u(HL)$	$3.98, 4.22, \approx 4.0$
	2^1B_u	6.14	$B_u(HL)$	4.71	$B_u(W)$	≈ 4.6
ANO-TZ	1^1A_g	-537.4621		-539.4085		n/a
	2^1A_g	4.70	$A_g(D)$	4.78	$A_g(D)$	
	1^1B_u	4.76	$B_u(W)$	4.53	$B_u(HL)$	$3.98, 4.22, \approx 4.0$
	2^1B_u	6.11	$B_u(HL)$	4.70	$B_u(W)$	≈ 4.6

[1]The $2A_g$ and $1B_u$ excitation energies are from Table 2 in Ref. [2]; the $2B_u$ value is an estimate (see Ref. [5]) obtained as 0.6 eV + $1B_u$ excitation energy.

Table 6.3: Excitation energies for DMRG-SCF and CT for PPV-2.

Basis	State	DMRG-SCF	CT
ANO-DZ	1^1A_g	-843.9750	-846.6959
	2^1A_g	4.52	4.50
	1^1B_u	4.38	4.42
	2^1B_u	4.73	4.78

Table 6.4: Natural Occupancies of excited states of PPV-1 and PPV-2

Method/Molecule	State	HONO-1	HONO	LUNO	LUNO+1
DMRG-SCF / PPV-1 (ANO-TZ)	1^1B_u	1.75	1.54	0.52	0.25
	2^1B_u	1.91	1.06	0.95	0.09
DMRG-SCF / PPV-2	1^1B_u	1.85	1.48	0.55	0.15
CT / PPV-1 (ANO-TZ)	1^1B_u	1.85	1.05	0.94	0.12
	2^1B_u	1.70	1.50	0.54	0.28
CT / PPV-2	1^1B_u	1.80	1.45	0.56	0.18

6.6 Conclusions

The ability to correctly evaluate density matrices is an essential component of a practical correlation method. CT density matrices can be computed in a simple and efficient way analogous to the computation of the effective Hamiltonian in the theory. We demonstrated that the CT density matrices could be used to identify the character of an excited state with some simple applications on oligo-phenyvinylenes.

BIBLIOGRAPHY

[1] D. Ghosh, J. Hachmann, T. Yanai, and G. K. L. Chan, J. Chem. Phys. **128**, 144117 (2008).

[2] V. Molina, M. Merchán, and B. Roos, J. Phys. Chem. **101**, 3478 (1997).

[3] L. Gagliardi, G. Orlandi, V. Molina, P.-A. ke Malmqvist, and B. Roos, J. Phys. Chem. **106**, 7355 (2002).

[4] G. Hohlneicher, R. Wrzal, D. Lenoir, and R. Frank, J. Phys. Chem. **103**, 8969 (1999).

[5] C. Angeli, R. Improta, and F. Santoro, J. Chem. Phys. **130**, 174307 (2009).

[6] R. Improta, F. Santoro, C. Dietl, E. Papastathopoulos, and G. Gerber, Chem. Phys. Lett. **387**, 509 (2004).

[7] B. Saha, M. Ehara, and H. Nakatsuji, J. Phys. Chem. **111**, 5473 (2007).

[8] M. J. Frisch et al., GAUSSIAN 03, REVISION C.02, Gaussian, Inc., Wallingford CT, 2004, see http://www.gaussian.com/.

[9] P. Widmark, P. Malmqvist, and B. Roos.

[10] T. D. Crawford et al., PSI 3.2 (2003), see www.psicode.org.

[11] J. Pipek and P. Mezey, J. Chem. Phys. **90**, 4916 (1989).

[12] E. Neuscamman, T. Yanai, and G. K.-L. Chan, J. Chem. Phys. (2009), submitted.

CHAPTER 7

FUTURE DIRECTIONS

As we have described in previous chapters, the Density Matrix Renormalization Group (DMRG) is an excellent tool for obtaining the static electron correlation, and Canonical Transformation Theory (CT) is an excellent tool for obtaining the dynamic electron correlation. These two tools used in combination, produce results that can quantitatively be compared with experimental results. A natural next step, would be to determine the properties of the ground and excited states. Specifically, in this chapter, we describe two derivations of CT response theory that are useful for obtaining properties. The first part describes the response of a pure CT theory, and should only be used for systems that are single-reference. The second part describes the response of a combined DMRG and CT theory.

7.1 Canonical Transformation Theory - Response Theory

7.1.1 First Order Derivatives

The CT gradient theory is derived similarly to the gradient theory found in Coupled Cluster (CC) response theory[1–8]. Both theories are non-variational, and the corresponding Lagrangian introduces an extra set of parameters in addition to the amplitudes. In CC, this extra set of parameters is referred to as Λ, and as such we will also call this similar set of parameters in CT, Λ.

The energy for CT is given by the following equation

$$E =< \Psi_0|\overline{H}_{1,2}|\Psi_0 > \tag{7.1}$$

with the following constraints for solving for the amplitudes, A

$$0 =< \Psi_0|[\overline{H}_{1,2}, \hat{o}_i]_{1,2}|\Psi_0 > \tag{7.2}$$

As mentioned, CT theory is a non-variational theory, and therefore we cannot simply take the derivative of eqn. 7.1 with respect to an external perturbation χ. Instead, we must add a Lagrange multiplier to eqn. 7.1

$$L =< \Psi_0|\overline{H}_{1,2}|\Psi_0 > + < \Psi_0|[\overline{H}_{1,2}, \Lambda]_{1,2}|\Psi_0 > \tag{7.3}$$

where Λ is identical to A in eqn. 5.2, except that the coefficients of A are replaced with the coefficients of Λ

$$\Lambda = \Lambda_i^a(a_i^a - a_a^i) + \Lambda_{ij}^{ab}(a_{ij}^{ab} - a_{ab}^{ij}) + \Lambda_{ij}^{ak}(a_{ij}^{ak} - a_{ak}^{ij}) + \cdots \tag{7.4}$$

We notice that $L = E$, when the constraints of the Lagrangian are satisfied as in 7.2. The second term on the right-hand side of eqn. 7.3 equates to 0 based on eqn. 7.2. The Lagrangian in eqn. 7.3 doesn't yet have the property that it is stationary with respect to the variation of its components (A,Λ), and therefore doesn't satisfy the generalized Hellmann-Feynman theorem. We need to examine the derivatives of the components of the Lagrangian with respect to an external perturbation χ and set them equal to 0 as in the following set of equations

$$0 = \sum_i \frac{\partial \Lambda_i}{\partial \chi} < \Psi_0|[\overline{H}_{1,2}, \hat{o}_i]_{1,2}|\Psi_0 > \tag{7.5}$$

$$0 = \sum_i \frac{\partial A_i}{\partial \chi} \Big(< \Psi_0|\overline{H}_{1,2}^{A_i}|\Psi_0 > + < \Psi_0|[\overline{H}_{1,2}^{A_i}, \Lambda]_{1,2}|\Psi_0 > \Big) \tag{7.6}$$

where $\overline{H}_{1,2}^{A_i}$ is the derivative of the effective CT Hamiltonian with respect to each element of A, and $\hat{o}_i$ are the operators connected to the Λ coefficients in 7.4.

We first note that eqn. 7.5 is already satisfied based on eqn. 7.2. The generalized

Hellmann-Feynman theorem will be satisfied once eqn. 7.6 is satisfied. Therefore, we must solve for the coefficients of Λ utilizing the following equation

$$< \Psi_0|\overline{H}^{A_i}_{1,2}|\Psi_0 >= - < \Psi_0|[\overline{H}^{A_i}_{1,2}, \Lambda]_{1,2}|\Psi_0 > \tag{7.7}$$

Now that the generalized Hellmann-Feynman theorem is satisfied, we can formulate the first order response equation in CT

$$\frac{dE}{d\chi} = \sum_i \frac{\partial h_i}{\partial \chi} \Big(< \Psi_0|\overline{H}^{h_i}_{1,2}|\Psi_0 > + < \Psi_0|[\overline{H}^{h_i}_{1,2}, \Lambda]_{1,2}|\Psi_0 > \Big) \tag{7.8}$$

where $\overline{H}^{h_i}_{1,2}$ is the derivative of effective CT Hamiltonian with respect to each element of H.

7.1.2 Second Order Derivatives

The second order derivative is the derivative of the first order derivative with respect to an external perturbation φ

$$\begin{aligned} \frac{d^2E}{d\chi d\varphi} &= \sum_{i,j} \frac{\partial h_i}{\partial \chi}\frac{\partial h_j}{\partial \varphi} \Big(< \Psi_0|\overline{H}^{h_i h_j}_{1,2}|\Psi_0 > + < \Psi_0|[\overline{H}^{h_i h_j}_{1,2}, \Lambda]_{1,2}|\Psi_0 > \Big) + \\ &\quad \sum_{i,j} \frac{\partial h_i}{\partial \chi}\frac{\partial A_j}{\partial \varphi} \Big(< \Psi_0|\overline{H}^{h_i A_j}_{1,2}|\Psi_0 > + < \Psi_0|[\overline{H}^{h_i A_j}_{1,2}, \Lambda]_{1,2}|\Psi_0 > \Big) + \\ &\quad \sum_{i,j} \frac{\partial h_i}{\partial \chi}\frac{\partial \Lambda_j}{\partial \varphi} \Big(< \Psi_0|[\overline{H}^{h_i}_{1,2}, \hat{o}_j]_{1,2}|\Psi_0 > \Big) \end{aligned} \tag{7.9}$$

The first term on the right-hand side of eqn. 7.9 equates to 0. In the second term, the only unknown terms are $\frac{\partial A_j}{\partial \varphi}$. These unknown terms can be determined from the system of equations produced by taking the derivative of eqn. 7.2 with respect to an external perturbation φ

$$\sum_j \frac{\partial h_j}{\partial \varphi} < \Psi_0|[\overline{H}^{h_j}_{1,2}, \hat{o}_j]_{1,2}|\Psi_0 >= -\sum_j \frac{\partial A_j}{\partial \varphi} < \Psi_0|[\overline{H}^{A_j}_{1,2}, \hat{o}_j]_{1,2}|\Psi_0 > \tag{7.10}$$

Lastly, the only unknown terms in eqn. 7.9 are $\frac{\partial \Lambda_j}{\partial \varphi}$. We can solve for $\frac{\partial \Lambda_j}{\partial \varphi}$, directly by taking the derivative of eqn. 7.7 with respect to the external perturbation φ

$$\begin{aligned}
\sum_j \frac{\partial \Lambda_j}{\partial \varphi} \left(< \Psi_0 | [\overline{H}_{1,2}^{A_i}, \hat{o}_j]_{1,2} | \Psi_0 > \right) \quad = \\
- \sum_j \frac{\partial h_j}{\partial \varphi} \left(< \Psi_0 | \overline{H}_{1,2}^{A_i h_j} | \Psi_0 > + < \Psi_0 | [\overline{H}_{1,2}^{A_i h_j}, \Lambda]_{1,2} | \Psi_0 > \right) \\
- \sum_j \frac{\partial A_j}{\partial \varphi} \left(< \Psi_0 | \overline{H}_{1,2}^{A_i A_j} | \Psi_0 > + < \Psi_0 | [\overline{H}_{1,2}^{A_i A_j}, \Lambda]_{1,2} | \Psi_0 > \right) \qquad (7.11)
\end{aligned}$$

Using eqn. 7.11 and eqn. 7.10, we can substitute directly the unknown terms $\frac{\partial \Lambda_j}{\partial \varphi}$ and $\frac{\partial A_j}{\partial \varphi}$ into eqn. 7.9 to determine the second order derivative. This is useful when there are more derivatives with respect to χ, than there are derivatives with respect to φ (e.g. χ is nuclear coordinates, and φ is electric field). In the case of polarizability, where the number of derivatives with respect to χ is equal to the number of derivatives with respect to φ, there is more efficient method to solve for the second order derivative. For this choice we solve for $\frac{\partial \Lambda_j}{\partial \varphi}$ indirectly using a combination of the derivative of eqn. 7.7 with respect to φ and eqn. 7.10 to obtain

$$\begin{aligned}
\sum_{i,j} \frac{\partial h_i}{\partial \chi} \frac{\partial \Lambda_j}{\partial \varphi} \left(< \Psi_0 | [\overline{H}_{1,2}^{h_i}, \hat{o}_j]_{1,2} | \Psi_0 > \right) \quad = \\
\sum_{i,j} \frac{\partial h_i}{\partial \varphi} \frac{\partial A_j}{\partial \chi} \left(< \Psi_0 | \overline{H}_{1,2}^{h_i A_j} | \Psi_0 > + < \Psi_0 | [\overline{H}_{1,2}^{h_i A_j}, \Lambda]_{1,2} | \Psi_0 > \right) \\
+ \sum_{i,j} \frac{\partial A_i}{\partial \chi} \frac{\partial A_j}{\partial \varphi} \left(< \Psi_0 | \overline{H}_{1,2}^{A_i A_j} | \Psi_0 > + < \Psi_0 | [\overline{H}_{1,2}^{A_i A_j}, \Lambda]_{1,2} | \Psi_0 > \right) \qquad (7.12)
\end{aligned}$$

The term on the left hand side of eqn. 7.12 is the same as the third term in 7.9. An alternative form of the second order derivative in CT theory can now be

constructed by substituting eqn. 7.12 into eqn. 7.9

$$\begin{aligned}\frac{d^2E}{d\chi d\varphi} &= \sum_{i,j}\frac{\partial h_i}{\partial\chi}\frac{\partial A_j}{\partial\varphi}\Big(<\Psi_0|\overline{H}_{1,2}^{h_iA_j}|\Psi_0>+<\Psi_0|[\overline{H}_{1,2}^{h_iA_j},\Lambda]_{1,2}|\Psi_0>\Big)+\\ &\sum_{i,j}\frac{\partial h_i}{\partial\varphi}\frac{\partial A_j}{\partial\chi}\Big(<\Psi_0|\overline{H}_{1,2}^{h_iA_j}|\Psi_0>+<\Psi_0|[\overline{H}_{1,2}^{h_iA_j},\Lambda]_{1,2}|\Psi_0>\Big)+\\ &\sum_{i,j}\frac{\partial A_i}{\partial\chi}\frac{\partial A_j}{\partial\varphi}\Big(<\Psi_0|\overline{H}_{1,2}^{A_iA_j}|\Psi_0>+<\Psi_0|[\overline{H}_{1,2}^{A_iA_j},\Lambda]_{1,2}|\Psi_0>\Big)\end{aligned} \quad (7.13)$$

7.1.3 Correction for Strong-Contraction CT

In the previous section, we described how to solve for the amplitude A with respect to an external derivative. In chapter 5, we mentioned that eqn. 7.2 was an ill-defined equation due to the approximations of the effective Hamiltonian and the resulting numerical instabilities. This will affect how to solve for the unknown terms $\frac{\partial A_j}{\partial\varphi}$ in eqn. 7.10. As such, the modified equation to solve for the unknown terms $\frac{\partial A_j}{\partial\varphi}$ in the strong contraction is shown below

$$\begin{aligned}-\sum_j\frac{\partial A_j}{\partial\varphi}<\Psi_0|[\overline{H}_{1,2}^{A_j},\hat{o}_j]_{1,2}|\Psi_0> &= \sum_j\frac{\partial h_j}{\partial\varphi}<\Psi_0|[\overline{H}_{1,2}^{h_j},\hat{o}_j]_{1,2}|\Psi_0>\\ &+\sum_{ij}\frac{\partial h_i}{\partial\varphi}\frac{\partial\hat{o}_j}{\partial h_i}\frac{\partial}{\partial\hat{o}_j}<\Psi_0|[\overline{H}_{1,2}^{h_j},\hat{o}_j]_{1,2}|\Psi_0>\end{aligned} \quad (7.14)$$

7.2 DMRG + CT - Response Theory

7.2.1 First Order Derivatives

In section 7.2.1, we assumed that the static electron correlation of the chemical system could be described with a single determinant which doesn't respond to the perturbation. In this section, we will assume that static electron correlation is described by a multireference state which itself responds to the perturbation. We begin with the same Lagrangian as in the previous section plus an extra Lagrange multiplier

$$L =< \Psi_0|\overline{H}_{1,2}|\Psi_0 > + < \Psi_0|[\overline{H}_{1,2}, \Lambda]_{1,2}|\Psi_0 > + < \Psi_0|Z(H-E)|\Psi_0 > \quad (7.15)$$

where Z is a diagonal matrix, and E is the ground state energy from DMRG. Λ is identical to A in eqn. 5.2, except that the coefficients of A are replaced with the coefficients of Λ

$$\Lambda = \Lambda_i^a(a_i^a - a_a^i) + \Lambda_{ij}^{ab}(a_{ij}^{ab} - a_{ab}^{ij}) + \Lambda_{ij}^{ak}(a_{ij}^{ak} - a_{ak}^{ij}) + \cdots \quad (7.16)$$

As seen in the previous section, we will solve for Λ using the following equation

$$< \Psi_0|\overline{H}_{1,2}^{A_i}|\Psi_0 >= - < \Psi_0|[\overline{H}_{1,2}^{A_i}, \Lambda]_{1,2}|\Psi_0 > \quad (7.17)$$

We can solve for Z by taking the derivative of the Lagrangian with respect to the each element of the reference density matrix and setting the result equal to zero

$$< \Psi_0|Z(H-E)|\Psi_0 >^{\psi_i}= - < \Psi_0|\overline{H}_{1,2} + [\overline{H}_{1,2}, \Lambda]_{1,2}|\Psi_0 >^{\psi_i} \quad (7.18)$$

where $^{\psi_i}$ is the derivative with respect to each element of the reference wavefunction.

The combined DMRG+CT first order derivative will have the form

$$\frac{dE}{d\chi} = \sum_i \frac{\partial h_i}{\partial \chi}\left(< \Psi_0|\overline{H}^{h_i}_{1,2}|\Psi_0 > + < \Psi_0|[\overline{H}^{h_i}_{1,2}, \Lambda]_{1,2}|\Psi_0 > \right) + \sum_i \frac{\partial h_i}{\partial \chi}\left(< \Psi_0|ZH^{h_i}|\Psi_0 > \right) - < \Psi_0|Z\frac{\partial E}{\partial \chi}|\Psi_0 > \quad (7.19)$$

where $\overline{H}^{h_i}_{1,2}$ is the derivative of effective CT Hamiltonian with respect to each element of H, and H^{h_i} is the derivative of the Hamiltonian with respect to each element of H. $\frac{\partial E}{\partial \chi}$ is the first order change in energy from DMRG with respect to the external perturbation χ.

7.2.2 Second Order Derivatives

The second order derivative is the derivative of the first order derivative with respect to an external perturbation φ

$$\begin{aligned}
\frac{d^2E}{d\chi d\varphi} &= \sum_{i,j} \frac{\partial h_i}{\partial \chi}\frac{\partial \psi_j}{\partial \varphi}\left(< \Psi_0|\overline{H}^{h_i}_{1,2} + [\overline{H}^{h_i}_{1,2}, \Lambda]_{1,2}|\Psi_0 >^{\psi_j} \right) + \\
&\sum_{i,j} \frac{\partial h_i}{\partial \chi}\frac{\partial A_j}{\partial \varphi}\left(< \Psi_0|\overline{H}^{h_i A_j}_{1,2}| + [\overline{H}^{h_i A_j}_{1,2}, \Lambda]_{1,2}|\Psi_0 > \right) + \\
&\sum_{i,j} \frac{\partial h_i}{\partial \chi}\frac{\partial \Lambda_j}{\partial \varphi}\left(< \Psi_0|[\overline{H}^{h_i}_{1,2}, \hat{o}_j]_{1,2}|\Psi_0 > \right) + \\
&\sum_j \frac{\partial \psi_j}{\partial \varphi}\left(\sum_i \frac{\partial h_i}{\partial \chi} < \Psi_0|ZH^{h_i}|\Psi_0 >^{\psi_j} - < \Psi_0|Z\frac{\partial E}{\partial \chi}|\Psi_0 >^{\psi_j} \right) + \\
&\sum_j \frac{\partial z_j}{\partial \varphi}\left(\sum_i \frac{\partial h_i}{\partial \chi} < \Psi_0|Z^{z_j}H^{h_i}|\Psi_0 > - < \Psi_0|Z^{z_j}\frac{\partial E}{\partial \chi}|\Psi_0 > \right) \\
&- < \Psi_0|Z\frac{\partial^2 E}{\partial \chi \partial \varphi}|\Psi_0 > \quad (7.20)
\end{aligned}$$

The first unknown terms are $\frac{\partial A_j}{\partial \varphi}$. These terms can be determined from the system of equations given by taking the derivative of eqn. 7.2 with respect to an

external perturbation φ. This equation looks similar to eqn. 7.10, except that it has an extra term due to the perturbation of the reference density matrix

$$\begin{aligned}\sum_j \frac{\partial A_j}{\partial \varphi} < \Psi_0|[\overline{H}^{A_j}_{1,2}, \hat{o}_j]_{1,2}|\Psi_0 > &= -\sum_j \frac{\partial h_j}{\partial \varphi} < \Psi_0|[\overline{H}^{h_j}_{1,2}, \hat{o}_j]_{1,2}|\Psi_0 > \\ &\quad -\sum_j \frac{\partial \psi_j}{\partial \varphi} < \Psi_0|[\overline{H}_{1,2}, \hat{o}_j]_{1,2}|\Psi_0 >^{\psi_j}\end{aligned} \tag{7.21}$$

Before explaining how to solve for the remaining unknown terms in eqn. 7.20, we would like to interject with the modified equation for strong contraction CT. In section 7.1.3, we provided a modified equation for solving for the unknowns, $\frac{\partial A_j}{\partial \varphi}$, in single reference strong contraction CT response theory. We will now provide the analogous equations for multireference CT response theory

$$\begin{aligned}\sum_j \frac{\partial A_j}{\partial \varphi} < \Psi_0|[\overline{H}^{A_j}_{1,2}, \hat{o}_j]_{1,2}|\Psi_0 > &= -\sum_j \frac{\partial h_j}{\partial \varphi} < \Psi_0|[\overline{H}^{h_j}_{1,2}, \hat{o}_j]_{1,2}|\Psi_0 > \\ &\quad -\sum_j \frac{\partial \psi_j}{\partial \varphi} < \Psi_0|[\overline{H}_{1,2}, \hat{o}_j]_{1,2}|\Psi_0 >^{\psi_j} \\ &\quad -\sum_{ij} \frac{\partial h_i}{\partial \varphi}\frac{\partial \hat{o}_j}{\partial h_i}\frac{\partial}{\partial \hat{o}_j} < \Psi_0|[\overline{H}^{h_j}_{1,2}, \hat{o}_j]_{1,2}|\Psi_0 > \\ &\quad -\sum_{ij} \frac{\partial \psi_i}{\partial \varphi}\frac{\partial \hat{o}_j}{\partial \psi_i}\frac{\partial}{\partial \hat{o}_j} < \Psi_0|[\overline{H}^{h_j}_{1,2}, \hat{o}_j]_{1,2}|\Psi_0 >\end{aligned} \tag{7.22}$$

The next unknown terms in eqn. 7.20 are $\frac{\partial \Lambda_j}{\partial \varphi}$. In the previous section, we solved for $\frac{\partial \Lambda_j}{\partial \varphi}$, indirectly using a combination of the derivative of eqn. 7.17 with respect to φ and eqn. 7.21. In this section, we will solve for $\frac{\partial \Lambda_j}{\partial \varphi}$, directly by taking the

derivative of eqn. 7.17 with respect to φ

$$
\begin{aligned}
-\sum_j \frac{\partial \Lambda_j}{\partial \varphi} < \Psi_0 | [\overline{H}_{1,2}^{A_i}, \hat{o}_j]_{1,2} | \Psi_0 > = \\
\sum_j \frac{\partial h_j}{\partial \varphi} \left(< \Psi_0 | \overline{H}_{1,2}^{A_i h_j} + [\overline{H}_{1,2}^{A_i h_j}, \Lambda]_{1,2} | \Psi_0 > \right) + \\
\sum_j \frac{\partial A_j}{\partial \varphi} \left(< \Psi_0 | \overline{H}_{1,2}^{A_i A_j} + | [\overline{H}_{1,2}^{A_i A_j}, \Lambda]_{1,2} | \Psi_0 > \right) + \\
\sum_j \frac{\partial \psi_j}{\partial \varphi} \left(< \Psi_0 | \overline{H}_{1,2}^{A_i} + [\overline{H}_{1,2}^{A_i}, \Lambda]_{1,2} | \Psi_0 >^{\psi_j} \right)
\end{aligned}
\tag{7.23}
$$

Finally, the last unknown terms $\frac{\partial z_j}{\partial \varphi}$ can be solved for by taking the derivative of eqn. 7.18 with respect to φ

$$
\begin{aligned}
-\sum_j \frac{\partial z_j}{\partial \varphi} < \Psi_0 | Z^{z_j} (H - E) | \Psi_0 >^{\psi_i} = \\
\sum_j \frac{\partial \psi_j}{\partial \varphi} < \Psi_0 | Z (H - E) | \Psi_0 >^{\psi_i \psi_j} \\
\sum_j \frac{\partial h_j}{\partial \varphi} < \Psi_0 | Z H^{h_j} | \Psi_0 >^{\psi_i} - < \Psi_0 | Z \frac{\partial E}{\partial \varphi} | \Psi_0 >^{\psi_i} + \\
\sum_j \frac{\partial h_j}{\partial \varphi} < \Psi_0 | \overline{H}_{1,2}^{h_j} + [\overline{H}_{1,2}^{h_j}, \Lambda]_{1,2} | \Psi_0 >^{\psi_i} + \\
\sum_j \frac{\partial \psi_j}{\partial \varphi} < \Psi_0 | \overline{H}_{1,2} + [\overline{H}_{1,2}, \Lambda]_{1,2} | \Psi_0 >^{\psi_i \psi_j} + \\
\sum_j \frac{\partial A_j}{\partial \varphi} < \Psi_0 | \overline{H}_{1,2}^{A_j} + [\overline{H}_{1,2}^{A_j}, \Lambda]_{1,2} | \Psi_0 >^{\psi_i} + \\
\sum_j \frac{\partial \Lambda_j}{\partial \varphi} < \Psi_0 | [\overline{H}_{1,2}^{h_j}, \hat{o}_j]_{1,2} | \Psi_0 >^{\psi_i}
\end{aligned}
\tag{7.24}
$$

Using eqns. 7.24, 7.23, and 7.21, we can rewrite eqn. 7.20, so that we no longer need to solve for the unknowns $\frac{\partial \Lambda_j}{\partial \varphi}$ and $\frac{\partial Z_j}{\partial \varphi}$

$$
\begin{aligned}
\frac{d^2E}{d\chi d\varphi} &= \sum_{i,j} \frac{\partial h_i}{\partial \chi}\frac{\partial \psi_j}{\partial \varphi}\left(< \Psi_0|\overline{H}^{h_i}_{1,2} + [\overline{H}^{h_i}_{1,2}, \Lambda]_{1,2}|\Psi_0 >^{\psi_j}\right) + \\
&\sum_{i,j} \frac{\partial \psi_i}{\partial \chi}\frac{\partial h_j}{\partial \varphi}\left(< \Psi_0|\overline{H}^{h_j}_{1,2} + [\overline{H}^{h_j}_{1,2}, \Lambda]_{1,2}|\Psi_0 >^{\psi_i}\right) + \\
&\sum_{i,j} \frac{\partial h_i}{\partial \chi}\frac{\partial A_j}{\partial \varphi}\left(< \Psi_0|\overline{H}^{h_i A_j}_{1,2}| + [\overline{H}^{h_i A_j}_{1,2}, \Lambda]_{1,2}|\Psi_0 >\right) + \\
&\sum_{i,j} \frac{\partial A_i}{\partial \chi}\frac{\partial h_j}{\partial \varphi}\left(< \Psi_0|\overline{H}^{A_i h_j}_{1,2}| + [\overline{H}^{A_i h_j}_{1,2}, \Lambda]_{1,2}|\Psi_0 >\right) + \\
&\sum_{i,j} \frac{\partial A_i}{\partial \chi}\frac{\partial \psi_j}{\partial \varphi}\left(< \Psi_0|\overline{H}^{A_i}_{1,2} + [\overline{H}^{A_i}_{1,2}, \Lambda]_{1,2}|\Psi_0 >^{\psi_j}\right) + \\
&\sum_{i,j} \frac{\partial \psi_i}{\partial \chi}\frac{\partial A_j}{\partial \varphi}\left(< \Psi_0|\overline{H}^{A_j}_{1,2} + [\overline{H}^{A_j}_{1,2}, \Lambda]_{1,2}|\Psi_0 >^{\psi_i}\right) + \\
&\sum_{i,j} \frac{\partial \psi_i}{\partial \chi}\frac{\partial \psi_j}{\partial \varphi}\left(< \Psi_0|\overline{H}_{1,2} + [\overline{H}_{1,2}, \Lambda]_{1,2}|\Psi_0 >^{\psi_i\psi_j}\right) + \\
&\sum_{i,j} \frac{\partial A_i}{\partial \chi}\frac{\partial A_j}{\partial \varphi}\left(< \Psi_0|\overline{H}^{A_i A_j}_{1,2} + [\overline{H}^{A_i A_j}_{1,2}, \Lambda]_{1,2}|\Psi_0 >\right) + \\
&\sum_{j} \frac{\partial \psi_j}{\partial \varphi}\left(\sum_i \frac{\partial h_i}{\partial \chi} < \Psi_0|ZH^{h_i}|\Psi_0 >^{\psi_j} - < \Psi_0|Z\frac{\partial E}{\partial \chi}|\Psi_0 >^{\psi_j}\right) + \\
&\sum_{i} \frac{\partial \psi_i}{\partial \chi}\left(\sum_j \frac{\partial h_j}{\partial \varphi} < \Psi_0|ZH^{h_j}|\Psi_0 >^{\psi_i} - < \Psi_0|Z\frac{\partial E}{\partial \varphi}|\Psi_0 >^{\psi_i}\right) \\
&- < \Psi_0|Z\frac{\partial^2 E}{\partial \chi \partial \varphi}|\Psi_0 > \qquad (7.25)
\end{aligned}
$$

BIBLIOGRAPHY

[1] J. F. Stanton and J. Gauss, Theor. Chim. Acta **91**, 267 (1995).

[2] B. Datta, P. Sen, and D. Mukherjee, J. Phys. Chem. **99**, 6441 (1995).

[3] K. Hald et al., J. Chem. Phys. **118**, 2985 (2003).

[4] S. R. Gwaltney and R. J. Bartlett, J. Chem. Phys. **110**, 62 (1999).

[5] J. F. Stanton and R. J. Bartlett, J. Chem. Phys. **99**, 5178 (1993).

[6] O. Christiansen, A. Halkier, H. Koach, P. Jørgensen, and T. Helgaker, J. Chem. Phys. **108**, 2801 (1998).

[7] J. F. Stanton, J. Chem. Phys. **99**, 8840 (1993).

[8] O. Christiansen, P. Jørgensen, and C. Hättig, Int. J. Quantum Chem. **68**, 1 (1998).